الجمهورية الجزائرية الديمقراطية الشعبية
République Algérienne Démocratique et Populaire
وزارة التعليم العالي و البحث العلمي
Ministère de l'Enseignement Supérieur et de la Recherche Scientifique

المدرسة الوطنية المتعددة التقنيات
Ecole Nationale Polytechnique
Département Génie Civil
Centre National de Recherche Appliquée en Génie Parasismique

End-of-study project dissertation

for obtaining the State Engineer's degree in Civil Engineering

Seismic Vulnerability Study Incorporating Ambient Vibration-Based Dynamic Characterization : Case of a Reinforced Concrete Tower

Realized by :
Mr. Merouane CHAIRA
Mr. Ayoub CHEKKAL

Proposed by :
Dr. Assia BOUCHELOUH (CGS)

Supervised by :
Pr. Abdelkrim BOURZAM (ENP)
Dr. Assia BOUCHELOUH (CGS)

Publicly presented and defended on the 26^{th} *of June, 2024.*

Jury members :

President	Mr. Abdelmadjid TADJADIT	Doctor	ENP
Examiner	Mr. Nouredine BOURAHLA	Professor	ENP
Supervisor	Mr. Abdelkrim BOURZAM	Professor	ENP
Guest	Ms. Racha ZEGHMAR	Adjunct Teacher	ENP

ENP 2024

الجمهورية الجزائرية الديمقراطية الشعبية
République Algérienne Démocratique et Populaire
وزارة التعليم العالي و البحث العلمي
Ministère de l'Enseignement Supérieur et de la Recherche Scientifique

المدرسة الوطنية المتعددة التقنيات
Ecole Nationale Polytechnique
Département Génie Civil
Centre National de Recherche Appliquée en Génie Parasismique

End-of-study project dissertation

for obtaining the State Engineer's degree in Civil Engineering

Seismic Vulnerability Study Incorporating Ambient Vibration-Based Dynamic Characterization : Case of a Reinforced Concrete Tower

Realized by :
Mr. Merouane CHAIRA
Mr. Ayoub CHEKKAL

Proposed by :
Dr. Assia BOUCHELOUH (CGS)

Supervised by :
Pr. Abdelkrim BOURZAM (ENP)
Dr. Assia BOUCHELOUH (CGS)

Publicly presented and defended on the 26^{th} *of June, 2024.*

Jury members :

President	Mr. Abdelmadjid TADJADIT	Doctor	ENP
Examiner	Mr. Nouredine BOURAHLA	Professor	ENP
Supervisor	Mr. Abdelkrim BOURZAM	Professor	ENP
Guest	Ms. Racha ZEGHMAR	Adjunct Teacher	ENP

ENP 2024

الجمهورية الجزائرية الديمقراطية الشعبية
République Algérienne Démocratique et Populaire
وزارة التعليم العالي و البحث العلمي
Ministère de l'Enseignement Supérieur et de la Recherche Scientifique

المدرسة الوطنية المتعددة التقنيات
Ecole Nationale Polytechnique
Département Génie Civil
Centre National de Recherche Appliquée en Génie Parasismique

Mémoire de projet de fin d'étude

Pour l'obtention du diplôme d'Ingénieur d'État en Génie Civil

Prise en compte de la caractérisation dynamique par vibration ambiante dans l'étude de la vulnérabilité sismique : Cas d'une tour en béton armé

Réalisé par :
M. Merouane CHAIRA
M. Ayoub CHEKKAL

Proposé par :
Dr. Assia BOUCHELOUH (CGS)

Encadré par :
Pr. Abdelkrim BOURZAM (ENP)
Dr. Assia BOUCHELOUH (CGS)

Présenté publiquement et défendu le 26 Juin 2024.

Membres du jury :

Président	M. Abdelmadjid TADJADIT	Docteur	ENP
Examinateur	M. Nouredine BOURAHLA	Professeur	ENP
Encadrant	M. Abdelkrim BOURZAM	Professeur	ENP
Invitée	Mme. Racha ZEGHMAR	Enseignante Vacataire	ENP

ENP 2024

ملخص

يقيّم هذا المشروع في نهاية الدراسة مدى قابلية البرج الخرساني المسلح الذي يبلغ ارتفاعه 70 مترًا والواقع في المحمدية بالجزائر العاصمة والذي تستخدمه وزارة التجارة وترقية الصادرات. يقع البرج في منطقة ذات قدرة زلزالية عالية، لذا فقدرة البرج على تحمل الزلازل أمر بالغ الأهمية. تتضمن الدراسة تقييم الخصائص الديناميكية للبرج من خلال تحليل الاهتزازات المحيطة، وتطوير ومعايرة نموذج العناصر المحدودة في نظام ETABS، وإجراء تقييمات قابلية التأثر بالزلازل باستخدام كل من الطرق الخطية وغير الخطية وفقًا للوائح الزلازل الجزائرية (RPA 2003/99) والمقياس الأوروبي للزلازل الكبرى (EMS-98). تم جمع بيانات الاهتزازات المحيطة وتحليلها لتحديد الترددات الطبيعية وأشكال الأنماط ونسب التخميد. استُفيد من هذه البيانات في معايرة النموذج العددي الذي مثّل السلوك الديناميكي المرصود بدقة. كشفت التقييمات الزلزالية، بما في ذلك تحليل الدفع، أن البرج يفي بمعايير الأداء المطلوبة، مع وجود تعزيزات محسوبة ومحدودة تجتاز عتبات القبول الخاصة بمعايير تقييم الزلازل. أشار تقييم (EMS-98) إلى وجود درجة ضرر معقولة، مما يؤكد مرونة البرج. تسلط هذه الدراسة الضوء على أهمية معايرة النموذج لإجراء تقييم زلزالي دقيق وتقترح تحسينات على تقييم الأداء الزلزالي RPA لإجراء تقييم أكثر تفصيلاً للأداء، مما يضمن السلامة الهيكلية للبرج ومرونة البرج الزلزالية.

الكلمات المفتاحية: الهشاشة الزلزالية، تحليل الاهتزازات المحيطة، القوانين الزلزالية الجزائرية (RPA 2003/99)، معايرة النموذج، تحليل التحميل التدريجي.

Resumé

Ce projet de fin d'études évalue la vulnérabilité sismique d'une tour en béton armé de 70 mètres de haut située à El Mohammadia, Alger, utilisée par le Ministère du Commerce et de la Promotion des Exportations. Située dans une région à forte sismicité, la capacité de la tour à résister aux tremblements de terre est d'une importance cruciale. L'étude implique l'évaluation des propriétés dynamiques de la tour par l'analyse des vibrations ambiantes, le développement et la calibration d'un modèle par éléments finis dans ETABS, ainsi que la réalisation d'évaluations de la vulnérabilité sismique en utilisant des méthodes linéaires et non linéaires conformément aux Règlements Parasismiques Algériens (RPA 99/2003) et à l'Échelle Macrosismique Européenne (EMS-98). Les données de vibrations ambiantes ont été collectées et analysées pour déterminer les fréquences naturelles, les formes modales et les ratios d'amortissement. Ces données ont permis la calibration du modèle numérique, qui représentait fidèlement le comportement dynamique observé. Les évaluations sismiques, y compris l'analyse poussée, ont révélé que la tour répond aux critères de performance requis, les renforcements calculés et minimaux passant les seuils d'acceptation du RPA. L'évaluation selon l'EMS-98 a indiqué un degré de dommage raisonnable, validant la résilience de la tour. Cette étude souligne l'importance de la calibration du modèle pour une évaluation sismique précise et suggère des améliorations au RPA pour une évaluation plus détaillée de la performance, garantissant l'intégrité structurelle et la résilience sismique de la tour.

Mots-clés: Vulnérabilité sismique, Analyse des vibrations ambiantes, Règlement parasismique algérien (RPA 99/2003), Calibration de modèle, Analyse pushover.

Abstract

This end-of-study project assesses the seismic vulnerability of a 70-meter-tall reinforced concrete tower located in El Mohammadia, Algiers, used by the Ministry of Trade and Export Promotion. Situated in a high seismicity region, the tower's ability to withstand earthquakes is critically important. The study involves evaluating the tower's dynamic properties through ambient vibration analysis, developing and calibrating a finite element model in ETABS, and conducting seismic vulnerability assessments using both linear and nonlinear methods per the Algerian Seismic Regulations (RPA 99/2003) and the European Macroseismic Scale (EMS-98). Ambient vibration data was collected and analyzed to determine natural frequencies, mode shapes, and damping ratios. This data informed the calibration of the numerical model, which accurately represented the observed dynamic behavior. Seismic assessments, including pushover analysis, revealed that the tower meets the required performance criteria, with calculated and minimal reinforcements passing the RPA's acceptance thresholds. The EMS-98 assessment indicated a reasonable damage degree, validating the tower's resilience. This study highlights the importance of model calibration for accurate seismic assessment and suggests enhancements to RPA for more detailed performance evaluation, ensuring the tower's structural integrity and seismic resilience.

Keywords: Seismic vulnerability, Ambient vibration analysis, Algerian Seismic Regulations (RPA 99/2003), Model calibration, Pushover analysis.

Dedications

“

I dedicate this work to

***My moms**, who have been my primary source of support after Allah. Their unwavering efforts in raising, guiding, and assisting me have paved the way for my achievements.*

***My beloved sister and brothers** have also supported me, celebrated my accomplishments, and offered moral support.*

***My friends**, words alone cannot express my gratitude to each and every one of them. However, I would like to acknowledge a few individuals here to convey my profound thanks and love. I am particularly grateful to **THE BOYS**. May they all be blessed and protected by Allah.*

*A heartfelt thank you to **Dr. Aghiles Nekmouche**, without whom this project would not have been executed flawlessly.*

*My great partner, **Chaira Merouane**, your collaboration has been invaluable.*

Lastly, I sincerely thank all those who have directly or indirectly contributed to the realization of this project.

Thank you sincerely to everyone.

”

- Ayoub -

“

I dedicate this modest work to those I appreciate:

To my dear ***parents****, whose unwavering support has been the cornerstone of my achievements. I owe everything to you.*

To my ***brothers*** *and* ***sisters****, for their constant encouragement and support.*

To my project collaborator, ***Chekkal Ayoub****, I truly appreciated working with you on this project. Your unwavering support and encouragement have been a constant source of motivation and strength.*

To ***Dr. Nekmouche Aghiles****, for his invaluable support and guidance. Your encouragement and assistance have been crucial to my success.*

To my dear friend, ***Benmoussa Mohammed****, for your steadfast support and friendship. Your encouragement has been invaluable throughout this journey.*

To my childhood friends, ***Laouar Abdelwaheb*** *and* ***Khebri Dirar****, for your lifelong friendship and support. You have been a vital part of my journey.*

To my ***colleagues*** *from university and high school, with whom I have shared unforgettable memories. Your camaraderie and support have enriched my life and academic journey.*

To everyone who has contributed to my success, your invaluable support and encouragement have been crucial throughout this journey.

Thank you all from the bottom of my heart.

”

- Merouane -

Acknowledgments

First and foremost, we thank Almighty Allah for giving us the strength and patience to complete this work.

We would like to express our special gratitude to our supervisor, Dr. BOUCHELOUH Assia, who trusted us and provided unwavering support and guidance throughout the completion of this thesis. We are grateful for her competent assistance, patience, and encouragement. Her critical eye has been invaluable in structuring the work and improving the quality of its various sections. We extend our sincerest thanks to you.

We are immensely grateful to Pr. BOURZAM Abdelkrim and Dr. NEKMOUCHE Aghiles for their support and guidance during this project. Their valuable insights and feedback were crucial to the successful completion of this work.

We would like to extend our heartfelt gratitude to PhD cand. HANNACHI Abdalatif for his invaluable support and the precious information he shared with us.

We also want to extend our sincere thanks to the jury members for taking the time to read and evaluate our work. Your recognition is truly an honor to us.

We would also like to express our appreciation to the educational and administrative team at ENP, particularly the civil engineering teachers, for their dedication in providing us with an excellent education.

Furthermore, we would like to express our deepest gratitude to our parents for their support and encouragement throughout these years. We send them all our love and gratitude.

Lastly, we want to acknowledge and thank everyone who has directly or indirectly contributed to the completion of this work.

Contents

List of Figures . . . .

List of Tables . . . .

Acronyms . . . .

Key Variables . . . .

Greneral Introduction **19**

I Ambient Vibration Analysis and Seismic Risk: Theoretical Foundations **23**

I.1 Ambient Vibrations and Modal Analysis 23

I.1.1 Historical Context 23

I.1.2 Definitions and Concepts 24

I.1.3 Comparison with Seismic Vibrations 24

I.1.4 Origin and Nature of Ambient Vibrations in Structures . . 25

I.1.5 Applications in Civil Engineering 26

I.1.6 Recording and Treating Ambient Vibrations in Structures 28

I.1.7 Modal Analysis 33

I.2 Seismic Risk 35

I.2.1 Seismic Events 36

I.2.2 Seismic Vulnerability 39

I.2.3 Evaluation of Seismic Vulnerability: Nonlinear Methods and Pushover Analysis 40

I.3 Conclusion: 51

II Characterizing Tower Structural Properties through Ambient Vibration Experiment **53**

II.1 Introduction 53

II.2 Sensors Placement and Data Recording 53

II.3 Results and Interpretation 54

II.3.1 Frequency 54

II.3.2 Mode shapes 61

II.3.3 Damping 61

II.4 Conclusion 64

III Modeling and Numerical Analysis **66**

III.1 Introduction . . . 66
III.2 Tower Description . . . 66
III.2.1 Introduction . . . 66
III.2.2 Site Location . . . 67
III.2.3 Building Presentation . . . 68
III.2.4 Current Use . . . 69
III.2.5 Material Characteristics . . . 70
III.3 Modeling . . . 73
III.3.1 Material Characterization . . . 73
III.3.2 Reinforcement Rebars . . . 75
III.3.3 Element Sections . . . 78
III.3.4 Definition of Static Loads G and Q . . . 78
III.3.5 Definition of Mass Source . . . 79
III.4 Results and Interpretation . . . 79
III.4.1 Modal Analysis . . . 79
III.5 Direct Natural Frequency Comparison . . . 81
Direct Natural Frequency Comparison . . . 81
III.5.1 Comparison Between Experimental and Numerical Frequencies . . . 82
III.6 Calibration of the Numerical Model . . . 83
III.6.1 Results . . . 83
III.6.2 Interpretation: . . . 84
III.7 Conclusion . . . 85

IV Vulnerability Study . . . 87
IV.1 Introduction . . . 87
IV.2 Elastic Linear Analysis . . . 87
IV.2.1 Introduction . . . 87
IV.2.2 Seismic Analysis . . . 87
IV.2.3 Response Spectrum . . . 92
IV.2.4 Verification of Total Static Force . . . 93
IV.2.5 Verification of the maximum story drift . . . 94
IV.2.6 Conclusion . . . 95
IV.3 Nonlinear Analysis . . . 95
IV.3.1 Introduction . . . 95
IV.3.2 Nonlinear Behavior of Construction Materials . . . 96
IV.3.3 Implementation of Nonlinear Behavior in Structural Elements Using ETABS (Plastic Hinges) . . . 97
IV.3.4 Elastic Spectrum . . . 98
IV.3.5 Lateral Load Distribution . . . 98
IV.3.6 Pushover Analysis Results . . . 99
IV.4 Vulnerability Evaluation per EMS98: . . . 113
IV.5 Conclusion . . . 114

Greneral Conclusion . . . 116

Bibliography **118**

Webography **120**

Appendices **122**

List of Figures

1.1 Example of ambient vibrations sources in a building 26
1.2 Example of sensors placement in a bridge for health monitoring . 27
1.3 Half-Power Bandwidth Method illustrating Fourier spectrum amplitude and corresponding frequencies f_1 and f_2. 32
1.4 Flowchart of Signal Processing Techniques in GEOPSY 33
1.5 Example of a Detailed Stick Model Representation of a Five-Story Structure for Dynamic Analysis 34
1.6 Exemple of mode Shapes and Modal Decomposition of a Five-Story Structure 34
1.7 Earthquake,Focus and Epicenter, Magnitude and Intensity 36
1.8 Illustration of Pushover Analysis for Determining Structural Capacity Curve 42
1.9 Illustration of Load Distribution Schemes 43

2.1 Sensor placement for monitoring EW (T) and NS (L) directions. . 54
2.2 FDD method: Time-domain data (top) transformed into frequency-domain for L (bottom left) and T (bottom right) directions. . . . 55
2.3 Amplitude vs. Frequency for Longitudinal Direction. 56
2.4 Amplitude vs. Frequency for Transversal Direction. 56
2.5 Modal shapes of the first three modes in both longitudinal and transversal directions. 61
2.6 Illustration of the application of the Random Decrement Technique and the resulting damping coefficients for the first mode L (top) and T (bottom) directions. 62

3.1 Seismic Classification of the Provinces of Algeria 67
3.2 Overview of the site of the Ministry of Trade and Export Promotion 68
3.3 Ministry Of Trade Tower 69
3.4 Representation of concentric struts in compression. 71
3.5 Dimensions of the Equivalent Diagonal Strut Model for Masonry Infill Walls. 72
3.6 First longitudinal mode (Mode 1). 80
3.7 First transversal mode (Mode 2). 80
3.8 Second longitudinal mode (Mode 4). 81
3.9 Second transversal mode (Mode 6). 81
3.10 Third longitudinal mode (Mode 7). 81
3.11 Third transversal mode (Mode 9). 81
3.12 Masonry wall distribution from base to 14th story. 84

3.13 Masonry wall distribution on the 15th story. 84

4.1 Response Spectrum 93
4.2 Maximum Story Drifts for X and Y directions. 95
4.3 concrete behavior 96
4.4 Stress-Strain Relationship for Rebar 97
4.5 Elastic Spectrum 98
4.6 Seismic Force Distribution Patterns: Uniform and Modal 99
4.7 Capacity Curves Under Fundamental Mode Loading in the X-Direction 100
4.8 Capacity Curves Under Fundamental Mode Loading in the Y-Direction 100
4.9 Performance points Under Fundamental Mode Loading in the X-Direction 102
4.10 Performance points Under Fundamental Mode Loading in the Y-Direction 103
4.11 Maximum Story Drift Under Fundamental Mode Loading in the X-Direction 105
4.12 Maximum Story Drift Under Fundamental Mode Loading in the Y-Direction 105
4.13 Capacity Curves Under Uniform Loading in the X-Direction . . . 106
4.14 Capacity Curves Under Uniform Loading in the Y-Direction . . . 107
4.15 Performance points Under Uniform Loading in the X-Direction . 108
4.16 Performance point Under Uniform Loading in the Y-Direction of Minimal reinforcement 109
4.17 Maximum Story Drift Capacity Curve Under Uniform Loading in the X-Direction 111
4.18 Maximum Story Drift Under Uniform Loading in the Y-Direction 111
4.19 Capacity Curve with Damage Levels and Performance Analysis . 114
4.20 Data extracted from treating the Ambient Vibration signals. . . . 122
4.21 Extracted peaks and natural frequencies L direction. 124
4.22 Extracted peaks and natural frequencies T direction. 125
4.23 Elements sections. 126

List of Tables

1.1 Richter Magnitude Scale 37
1.2 EMS 98 Intensity Scale 38
1.3 Degrees of Seismic Damage and Ranges According to EMS 40

2.1 Natural frequencies recorded at the 15th floor. 57
2.2 Values of C_T for different bracing systems 58
2.3 Comparison of empirical and experimental fundamental frequencies. 59
2.4 Frequency ratios of the second and third modes relative to the first mode frequency. 60
2.5 Damping values obtained using the random decrement technique and the half-power bandwidth method. 63

3.1 Zone Acceleration Coefficient A According to RPA 69
3.2 Reinforcement Area Calculation for Structural Elements Based on SOCOTEC Analysis and RPA Standards. 77
3.3 Estimation of additional permanent loads and operational live loads 78
3.4 Mass Participation Ratios of the Structure in Longitudinal and Transversal Directions. 79
3.5 Comparison between experimental and numerical frequencies. . . 82
3.6 Comparison of experimental and numerical frequencies after calibration. 84
3.7 Comparison of experimental and numerical frequencies of the 1^{st} mode before and after calibration. 85

4.1 Seismic weights of the structure. 89
4.2 Seismic parameters used in the analysis. 91
4.3 Verification of the Resultant Seismic Forces at the Base 101
4.4 Comparison of Reinforcement Types Overstregth Under Fundamental Mode Loading 104
4.5 Verification of the Resultant Seismic Forces at the Base 108
4.6 Comparison of Reinforcement Types Overstregth Under Uniform Loading 110
4.7 Comparison of Base Shear and Target Displacement for Minimal and Calculated Reinforcement 112
4.8 geometric characteristics of the equivalent strut. 122

Acronyms

RPA : Regulation Paraseismique Algerien

ENP : École Nationale Polytechnique

CGS : Centre National de Recherche Appliquée en Génie Parasismique

FDD : Frequency Domain Decomposition

RDT : Random Decrement Technique

SHM : Structural Health Monitoring

FEM : Finite Element Model

MPA : Modal Pushover Analysis

AMPA : Adaptive Modal Pushover Analysis

ETABS : Extended Three Dimensional Analysis of Building Systems

PSD : Power Spectral Density

FFT : Fast Fourier Transform

SVD : Singular Value Decomposition

RDS : Random Decrement Signature

UBC : Uniform Building Code

EMS : European Macroseismic Scale

OMA : Operational Modal Analysis

HPBW : Half-Power Bandwidth Method

CSM : Capacity Spectrum Method

N2 Method : Eurocode 8 N2 Method

ASCE : American Society of Civil Engineers

Gadd : Additional Dead Loads

Key Variables

.

ξ: Damping ratio

T: Period

m: Mass

k: Stiffness

$u(t)$: Displacement as a function of time

$\dot{u}(t)$: Velocity as a function of time

$\ddot{u}(t)$: Acceleration as a function of time

ϕ: Phase angle

Δf: Bandwidth

f_r: Resonance frequency

f_i: Frequency of mode i

$\Sigma(f)$: Diagonal matrix containing singular values

$U(f)$: Unitary matrix from Singular Value Decomposition (SVD)

$V(f)$: Unitary matrix from Singular Value Decomposition (SVD)

$S(f)$: Spectral density matrix

$PSD(f)$: Power Spectral Density function

$RDS(t)$: Random Decrement Signature

γ: Volumetric weight

E_{ij}: Linear elasticity modulus

f_{c28}: Compressive strength at 28 days

L_p: Hinge length

ϕ_i: Mode shape at frequency i

C_T: Coefficient depending on the bracing system and type of infill

Key Variables

h_N: Height measured from the base to the top level

w_{ds}: Width of the equivalent strut

Θ: Angle of the strut

L_{ds}: Diagonal length of the infill panel

δ_t: Target displacement

C_0: Coefficient relating spectral displacement of an SDOF system to probable roof displacement of an MDOF system

C_1: Coefficient relating maximum inelastic displacement to elastic displacement calculated by an elastic response

C_2: Coefficient representing the effect of hysteresis shape on maximum displacement

C_3: Coefficient representing the P-Δ effect due to dynamic behavior

S_a: Spectral acceleration

T_e: Effective fundamental period of the building

Γ: Modal participation factor

D: Dynamic amplification factor

η: Damping correction factor

f_{exp}: Experimental frequency

f_{num}: Numerical frequency

f_{num2}: Secondary numerical frequency

Q: Quality Factor

A: Zone Acceleration Coefficient

R: Structural Behavior Coefficient

W: Seismic Weight

T_1: Characteristic Period 1

T_2: Characteristic Period 2

T_x: Fundamental Period (X-axis)

T_y: Fundamental Period (Y-axis)

D_x: Dynamic Amplification Factor (X-axis)

D_y: Dynamic Amplification Factor (Y-axis)

Greneral Introduction

Greneral Introduction

Ensuring the structural integrity and seismic resilience of buildings is of paramount importance, particularly in regions prone to earthquakes. Algeria, situated on the edge of the African and Eurasian tectonic plates, is one such region that frequently experiences seismic activities. Earthquakes pose a significant threat to life, property, and economic stability, making the need for robust and comprehensive seismic assessments essential. Historically, many structures may not have been designed to withstand the forces generated by significant seismic events, particularly older buildings that predate modern seismic design codes and regulations.

In Algeria, the risk of earthquakes is exacerbated by its complex tectonic setting. The country is divided into several seismic zones, with the northern part, including Algiers, being particularly susceptible to seismic activity. The frequent seismic occurrences necessitate a proactive approach to assessing and mitigating seismic risks. Buildings that serve critical functions, such as administrative offices, hospitals, and schools, must be evaluated to ensure they can withstand seismic forces without compromising their structural integrity.

In this context, our study focuses on a reinforced concrete tower located in El Mohammadia, Algiers. This administrative building, used by the Ministry of Trade and Export Promotion, holds significant functional importance. Ensuring its ability to withstand seismic events is crucial, particularly as the structure is situated in a high seismicity region according to the Algerian Seismic Regulations RPA 99/2003.

Problematic

The primary challenge addressed in this study is the potential seismic vulnerability of the tower. The tower, located in a high seismicity region, has vital importance due to its administrative function and its significant height of approximately 70 meters, which is considerably taller compared to typical constructions in Algeria. This is the first case of its kind in the country, presenting unique challenges in ensuring its seismic resilience. Given the building's height and the number of floors, it is crucial to assess whether its response will be sufficient to withstand the seismic hazards prevalent in Algeria.

Additionally, as buildings age, their materials can deteriorate, leading to reduced structural capacity and increased vulnerability to seismic forces. Despite

the use of reinforced concrete and a central core for bracing, there is a need to understand how the building will respond to seismic forces in its current state. Traditional methods of seismic assessment might not be sufficient to capture the nuanced behavior of the structure under dynamic loads, especially without causing disruptions to its current use.

Objective

The objective of this study is to perform a comprehensive seismic vulnerability assessment of the tower. This involves:

- **Evaluating the Dynamic Properties**: Determine the natural frequencies, mode shapes, and damping ratios of the tower using ambient vibration analysis.
- **Developing and Calibrating a Numerical Model**: Create a finite element model in ETABS and calibrate it to accurately reflect the observed dynamic properties from the ambient vibration data.
- **Assessing Seismic Vulnerability Using RPA Methods**: Conduct seismic vulnerability assessments using the static equivalent and modal spectral methods as presented in the Algerian Seismic Regulations (RPA 99/2003).
- **Evaluating Seismic Vulnerability Using Pushover Analysis**: Perform pushover analysis and ensure that the analysis satisfies the limits set by the RPA to evaluate the building's capacity to withstand seismic forces.
- **Assessing Vulnerability Using EMS 98 Code**: Utilize the European Macroseismic Scale 1998 (EMS-98) to further evaluate the seismic vulnerability of the tower and provide a comprehensive assessment of its seismic performance.

Outline of the Dissertation

The dissertation begins with **Theoretical Foundations for Ambient Vibrations and Seismic Analysis**, which covers the theoretical principles of ambient vibrations, modal analysis, and seismic risk assessment. This chapter introduces the concepts, historical context, and applications in civil engineering, and it provides a comprehensive overview of the methods used for recording and analyzing ambient vibrations in structures.

Next, **Characterizing Tower Structural Properties through Ambient Vibration Experiments** focuses on the ambient vibration experiments conducted to capture the tower's dynamic properties. This chapter includes the methodology, results, and interpretation of frequency, damping, and mode shapes derived from the ambient vibration data.

Modeling and Numerical Analysis is the subsequent chapter that details the development and calibration of the finite element model in ETABS. It covers the description of the tower, site location, material characteristics, and the steps involved in creating and validating the numerical model using the data obtained from ambient vibration analysis.

The **Vulnerability Study** chapter presents the seismic vulnerability assessment of the tower. It includes linear elastic analysis using static equivalent and modal spectral methods as per the RPA 99/2003 guidelines. The chapter also covers nonlinear analysis using pushover methods, discussing load distribution, capacity curves, and performance points. Additionally, it integrates an assessment of seismic vulnerability using the European Macroseismic Scale 1998 (EMS-98) to provide a comprehensive evaluation of the building's performance under seismic loading.

Finally, the dissertation concludes with the **General Conclusion**, summarizing the findings of the study, discussing the implications for seismic resilience, and offering recommendations for future research and practical applications.

Chapter 1

Ambient Vibration Analysis and Seismic Risk: Theoretical Foundations

Ambient Vibration Analysis and Seismic Risk: Theoretical Foundations

I.1 Ambient Vibrations and Modal Analysis

I.1.1 Historical Context

The investigation of ambient vibrations in civil engineering has a rich history spanning over a century. The initial forays into this field were marked by the pioneering work of Japanese seismologist Fusakichi Omori in the early 1900s. Omori's contributions laid the groundwork for understanding how natural environmental forces like wind, traffic, and micro-seismic activities induce vibrations in buildings and other structures. This era marked the beginning of using ambient vibrations to gain insights into the dynamic properties of structures.

As technology advanced, so did the methods for studying these vibrations. The mid-20th century saw significant developments with the advent of more sensitive and precise instrumentation, allowing for detailed measurements of ambient vibrations. Studies like those by Michel et al. (2008)[1] underscore the evolution of this field, highlighting the transition from basic observational techniques to sophisticated analytical methods that incorporate ambient vibration data for seismic vulnerability assessments.

One of the key milestones in the history of ambient vibration studies was the integration of Operational Modal Analysis (OMA) techniques. These techniques enabled engineers to extract modal parameters from ambient vibration data without requiring artificial excitation. This development was crucial for practical applications in structural health monitoring, as it allowed for non-invasive and continuous assessment of structures. The work by Michel and colleagues[1] illustrates how these techniques have been applied to evaluate the seismic performance of buildings in moderate seismic hazard regions.

In recent decades, the focus has increasingly shifted towards real-time monitor-

ing and predictive maintenance of structures using ambient vibrations. The proliferation of digital sensors and advancements in data processing algorithms have made it possible to deploy extensive monitoring networks. These networks provide continuous data streams that can be analyzed in real-time to detect changes in structural behavior, potentially indicating damage or degradation. Such advancements reflect the growing importance of ambient vibration studies in ensuring the safety and longevity of civil infrastructure.

I.1.2 Definitions and Concepts

- **Ambient Vibrations**: Naturally occurring, low-level oscillations in structures caused by environmental sources such as wind, traffic, and microseismic activities. Unlike forced vibrations, which are induced deliberately using external equipment (e.g., shakers or impact hammers), ambient vibrations occur continuously and ubiquitously. They provide a non-intrusive means to gather data on the dynamic behavior of structures over time.

- **Modal Analysis**: The study of the inherent dynamic properties of structures, including their natural frequencies, mode shapes, and damping ratios. Modal analysis is a critical tool in structural dynamics, as it helps engineers understand how structures respond to various excitations. Techniques such as Operational Modal Analysis (OMA) and Frequency Domain Decomposition (FDD) are commonly used to extract modal parameters from

- **Forced Vibrations**: Oscillations introduced deliberately into a structure through the application of external forces. This is typically done using equipment such as shakers, impact hammers, or vibrators to simulate dynamic loading conditions. Forced vibration testing is valuable for controlled experiments to study speambient vibration data [1].cific responses of structures but is less practical for continuous monitoring.

Understanding these fundamental concepts is crucial for leveraging ambient vibration data effectively. As highlighted by Michel et al. (2008)[1], ambient vibrations, despite their naturally low amplitude, provide a rich source of information about the dynamic characteristics of structures. They offer a practical and non-invasive means of assessing the health and integrity of buildings, bridges, and other infrastructure. This is particularly important in the context of seismic vulnerability assessments, where traditional forced vibration methods may be impractical or too invasive.

I.1.3 Comparison with Seismic Vibrations

While ambient vibrations are generally of lower intensity than seismic vibrations, they share similar characteristics that make them valuable for structural analysis. Both types of vibrations can excite the natural frequencies of a structure, allowing

engineers to study its dynamic properties. For instance, ambient vibrations typically have amplitudes of 10^{-6} to 10^{-4} g, whereas seismic vibrations can exceed 1 g during a strong earthquake.

Ambient vibrations do not cause damage and can be measured frequently without disrupting the structure's operation. Seismic vibrations, on the other hand, involve significant, potentially damaging energy inputs. For example, the 2003 Boumerdès earthquake in Algeria produced peak ground accelerations exceeding 0.5 g, providing a real-world test of a structure's performance during such events.

By analyzing ambient vibrations, engineers can predict how a structure might respond to seismic events. Studies have shown that buildings with natural frequencies between 0.1 and 5 Hz are particularly susceptible to earthquake damage. Understanding these frequencies through ambient vibration analysis aids in the design of earthquake-resistant buildings, enhancing their safety and resilience.

I.1.4 Origin and Nature of Ambient Vibrations in Structures

Ambient vibrations in structures originate from diverse sources, each contributing to the dynamic behavior of buildings and infrastructure. Understanding the origins and characteristics of these vibrations is crucial for accurately interpreting measurement data and assessing structural health.

- **Environmental Factors:** Wind blowing against a building, vehicular traffic on nearby roads, and micro-seismic activities (small ground movements) all contribute to ambient vibrations.
- **Human Activities:** Everyday activities such as walking, operating machinery, and even conversations can introduce vibrations into a structure.
- **Geological Conditions:** The geological characteristics of the ground on which a structure is built can affect its vibration response. For example, structures on soft soils may experience different vibration patterns than those on bedrock.

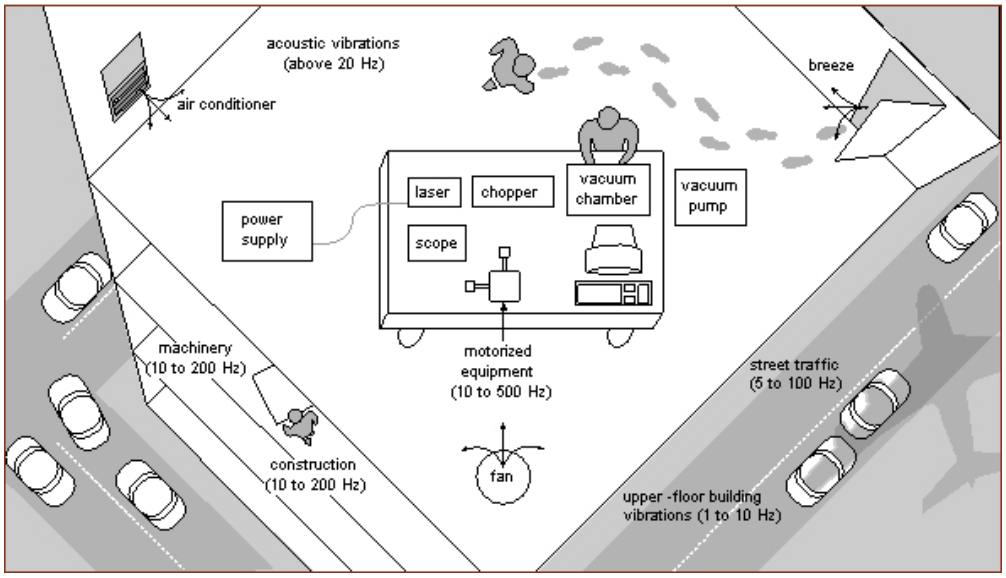

Figure 1.1: Example of ambient vibrations sources in a building

These vibrations typically cover a wide range of frequencies and are characterized by their random nature. Despite their low amplitude, ambient vibrations are valuable for studying the dynamic behavior of structures.

I.1.5 Applications in Civil Engineering

Ambient vibration measurements are increasingly utilized in civil engineering due to their non-invasive nature and the valuable insights they provide into structural dynamics. Here, we discuss several critical applications in greater detail, along with references to seminal studies and recent advancements in the field.

I.1.5.1 Structural Health Monitoring (SHM)

Structural Health Monitoring (SHM) involves the continuous or periodic assessment of a structure's condition to detect damage, degradation, or other changes over time. Ambient vibration measurements are critical for SHM because they allow for continuous structure monitoring without disrupting its normal use.

- **Long-term Monitoring:** Continuous ambient vibration monitoring can identify gradual changes in a structure's dynamic properties, signaling potential issues before they become critical. De Roeck et al. (2000)[2] demonstrated how long-term monitoring of bridges using ambient vibrations could detect early signs of damage, allowing for timely maintenance interventions.
- **Damage Detection:** Engineers can detect deviations that may indicate damage by comparing current vibration data with baseline measurements. Peeters and De Roeck (2001)[3] used ambient vibration data to identify

structural changes due to damage in the Z24 Bridge in Switzerland, illustrating the effectiveness of this method for damage detection.

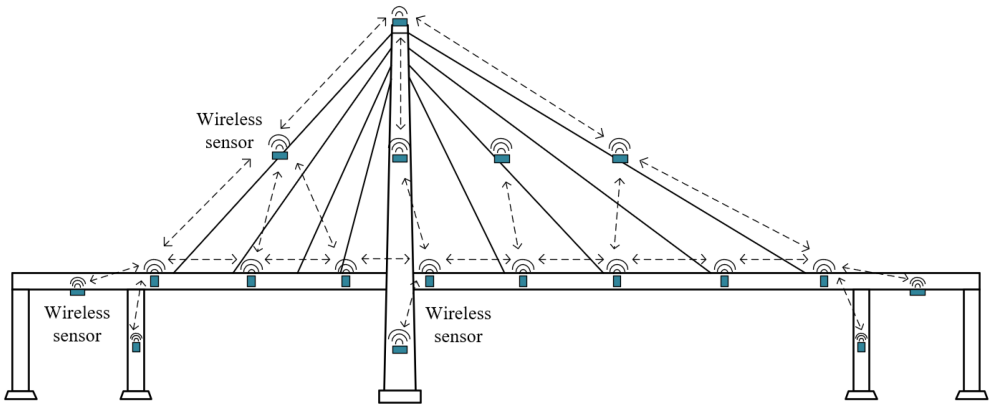

Figure 1.2: Example of sensors placement in a bridge for health monitoring

I.1.5.2 Model Calibration and Validation

Finite Element Models (FEM) are essential for predicting the behavior of structures under various loads. However, these models must be calibrated and validated against real-world data to ensure their accuracy.

- **Model Updating:** Ambient vibration data are used to update and refine FEM by adjusting parameters until the model accurately reflects the observed behavior. Ren et al. (2004)[4] demonstrated the effectiveness of using ambient vibration measurements to update the FEM of a large bridge, resulting in improved predictive accuracy.
- **Validation of Seismic Models:** In seismic engineering, validated models are crucial for designing earthquake-resistant structures. Clinton et al. (2006)[5] used ambient vibration data to validate models of buildings in California, enhancing their reliability for seismic performance assessment.

I.1.5.3 Post-Earthquake Assessments

After an earthquake, it is crucial to assess the integrity of affected structures to determine their safety and necessary repairs. Ambient vibration measurements provide a rapid, non-destructive means of assessment.

- **Rapid Damage Assessment:** Ambient vibration measurements can quickly identify changes in dynamic properties that indicate structural damage. Celebi (1996)[6] utilized ambient vibrations to assess the condition of buildings following the 1994 Northridge earthquake, providing valuable information for emergency response.

- **Rehabilitation Planning:** Detailed modal analysis helps in planning the rehabilitation of damaged structures by identifying specific areas that require strengthening. Studies like those by Çelebi and Sanli (2002)[7] have shown how ambient vibration data guide the planning and execution of rehabilitation efforts.

I.1.5.4 Retrofitting and Strengthening

Retrofitting involves upgrading existing structures to improve their performance under seismic or other loads. Ambient vibration measurements inform these processes by providing detailed insights into the structure's current state.

- **Guiding Retrofitting Designs:** Ambient vibration data help engineers design effective retrofitting measures by accurately characterizing the existing dynamic behavior of the structure. Saito et al. (2008)[8] used ambient vibration analysis to design retrofitting strategies for historical buildings in Japan.
- **Evaluating Retrofitting Effectiveness:** After retrofitting, ambient vibration measurements can determine the effectiveness of the interventions. For example, Çelebi (2006)[9] measured the changes in dynamic properties of retrofitted buildings to ensure the desired improvements were achieved.

I.1.5.5 Uncertainties in Modal Parameters

Uncertainties in modal parameters arise from various sources, including:

- **Measurement Noise:** External factors such as environmental noise and instrument sensitivity can introduce variability in the recorded data.
- **Environmental Conditions:** Changes in temperature, humidity, and other environmental factors can affect the structure's dynamic properties.
- **Data Processing:** The techniques used to process and analyze the data can introduce errors, particularly in the estimation of damping ratios and mode shapes.

Understanding and quantifying these uncertainties are crucial for reliable structural health monitoring and assessment. Engineers use statistical methods and repeated measurements to mitigate and account for these uncertainties, ensuring robust and accurate modal analysis.

I.1.6 Recording and Treating Ambient Vibrations in Structures

Recording and treating ambient vibrations in structures is a critical process in structural health monitoring and dynamic analysis. It involves the strategic place-

ment of sensitive instruments to capture vibration data, advanced data acquisition systems to store this information, and sophisticated signal processing techniques to extract meaningful insights. This process aims to identify key dynamic properties such as natural frequencies, damping ratios, and mode shapes, which are essential for understanding structural behavior and ensuring safety and integrity.

I.1.6.1 Ambient Vibration Measurement: Tools and Techniques

- **Sensors (Accelerometers/Velocimeters):** The 2s Velocity Sensor, or velocimeter, measures the velocity of structural vibrations with high accuracy and a wide frequency range. It is durable, designed to withstand harsh conditions, and compact for easy installation. Additionally, its low-noise design ensures high-quality data collection. Together, these devices provide a comprehensive solution for monitoring and analyzing structural vibrations.
- **Data Acquisition System:** The City Shark II Station is a high-performance data acquisition system for recording and analyzing vibration data in seismic studies and structural health monitoring. It features high sensitivity, multi-channel capability, substantial data storage, a user-friendly interface, and real-time data processing for immediate analysis and visualization of vibrations.
- **Supporting Equipment:** Cables and connectors link the sensors to the data acquisition system, ensuring seamless data transfer. A reliable power supply is crucial to ensure continuous operation of the equipment. Additionally, a computer with analysis software is essential for processing and analyzing the collected data, facilitating detailed structural assessments.

I.1.6.2 Procedure for Ambient Vibration Experimentation

- **Sensor Placement** The first phase of ambient vibration measurement involves defining the objectives and scope to understand the specific data required and how it will be used. After setting clear objectives, measurement points, which are strategic locations within the structure, are identified to provide comprehensive coverage of the structure's dynamic behavior. Sensors are then installed at these strategic points, such as floors, roofs, and structural joints, ensuring they are securely fixed, properly oriented (often aligned to the north), and protected from environmental factors to avoid data loss or corruption.
- **Data Recording** The data acquisition system is activated to begin recording ambient vibrations. Continuous monitoring ensures accurate and uninterrupted data collection. For towers, extending the recording duration under normal environmental conditions is crucial for accurately measuring damping. Tall buildings exhibit low-frequency vibrations and complex dynamic behaviors that require extended measurement periods to capture the subtle oscillations necessary for precise damping assessment.

- **Signal Processing** After the data recording phase, the recorded data are transferred to a computer for analysis. Specialized software, such as Geopsy, is used to process the raw vibration data. Techniques such as Fast Fourier Transform (FFT) are applied to identify key dynamic properties. The data is further analyzed to determine damping ratios and mode shapes, which are critical for understanding the structural behavior.

I.1.6.3 Ambient Vibration and Damping Calculation with Geopsy

Geopsy is specialized software for analyzing ambient vibration data to determine the dynamic properties of structures, including natural frequencies, mode shapes, and damping ratios. Essential in structural engineering, Geopsy is a tool that helps us assess seismic performance and structural health by employing advanced methods such as Frequency Domain Decomposition (FDD), the Random Decrement Technique (RDT), and the Half-Power Bandwidth Method. These sophisticated techniques enable precise evaluation of a structure's dynamic behavior, ensuring safety and resilience against seismic events.

I.1.6.3.1 Frequency Domain Decomposition (FDD)

Frequency Domain Decomposition (FDD) is a robust and widely adopted technique for modal analysis. It works by analyzing the frequency content of vibration data to identify natural frequencies and mode shapes.

- **Spectral Analysis:** The power spectral density (PSD) function is calculated using the Fast Fourier Transform (FFT) from the time-domain vibration signals:

$$PSD(f) = \left| \frac{1}{N} \sum_{n=0}^{N-1} x(n) e^{-j2\pi fn/N} \right|^2$$

  where $x(n)$ is the vibration signal, N is the number of data points, and f is the frequency.

- **Singular Value Decomposition (SVD):** The spectral density matrix $S(f)$ is decomposed using SVD:

$$S(f) = U(f)\Sigma(f)V^H(f)$$

  where $U(f)$ and $V(f)$ are unitary matrices, and $\Sigma(f)$ is a diagonal matrix containing singular values.

- **Mode Shape Estimation:** The peaks of the singular values correspond to natural frequencies. The mode shapes are derived from the corresponding columns of the $U(f)$ matrix at these frequencies:

$$\phi_i = U(f_i)$$

  where ϕ_i is the mode shape at frequency f_i.

- **Close Mode Separation:** The FDD method is particularly effective in distinguishing close modes by analyzing multiple singular values and their associated mode shapes.

I.1.6.3.2 Random Decrement Technique (RDT)

The Random Decrement Technique (RDT) is an effective method for estimating damping from ambient vibration data. It involves:

- **Triggering:** Identifying instances where the vibration signal exceeds a predefined threshold, triggering segments of the signal for analysis.

$$x(t) > \text{threshold}$$

- **Averaging:** The triggered segments are averaged to produce a decay signature, known as the Random Decrement Signature (RDS). This signature represents the free decay response of the structure.

$$\text{RDS}(t) = \frac{1}{N} \sum_{i=1}^{N} x_i(t)$$

where $x_i(t)$ are the triggered segments and N is the number of segments.

- **Damping Estimation:** The damping ratio is estimated from the RDS by fitting an exponential decay function to the signature.

$$\text{RDS}(t) = Ae^{-\xi_n t} \cos(_d t + \phi)$$

where A is the amplitude, ξ is the damping ratio, $_n$ is the natural frequency, $_d$ is the damped natural frequency, and ϕ is the phase angle. The damping ratio (ξ) is then calculated using:

$$\xi = \frac{1}{2\pi f} \ln \left(\frac{x(t)}{x(t + \Delta t)} \right)$$

where f is the natural frequency, and $x(t)$ and $x(t + \Delta t)$ are the amplitudes of the decay signature at times t and $t + \Delta t$, respectively.

I.1.6.3.3 Half-Power Bandwidth Method

The Half-Power Bandwidth Method is a widely used technique for estimating damping ratios from frequency response functions. It involves:

- **Identifying Resonance Peaks:** Determining the resonance frequency (f_r) from the Power Spectral Density (PSD) plot.

- **Calculating Bandwidth:** Measuring the bandwidth (Δf) by identifying the frequencies at which the amplitude is equal to the maximum amplitude at the resonance frequency divided by $\sqrt{2}$. These frequencies are known as the half-power points.

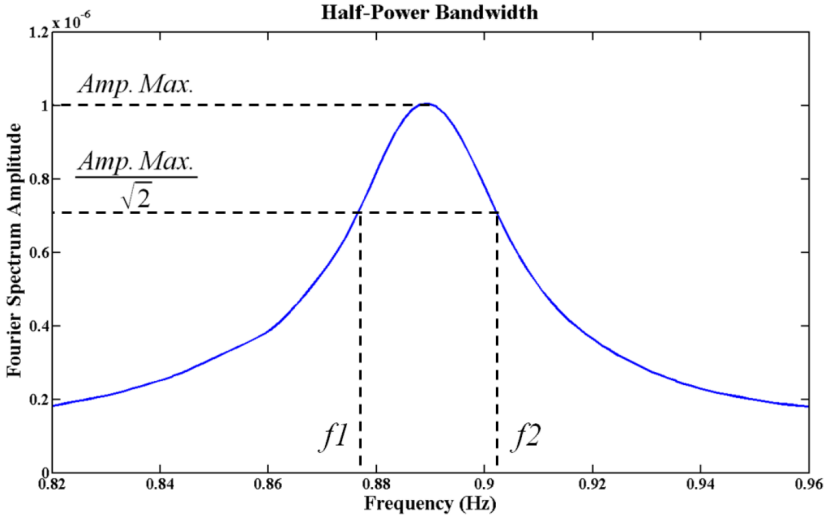

Figure 1.3: Half-Power Bandwidth Method illustrating Fourier spectrum amplitude and corresponding frequencies f_1 and f_2.

The damping ratio (ξ) is then calculated using the formula:

$$\xi = \frac{\Delta f}{2 f_r}$$

where Δf is the bandwidth and f_r is the resonance frequency.

This method provides a straightforward approach to estimating damping, based on the width of the resonance peak in the frequency domain. It is particularly useful for quick assessments and validating other damping estimation methods [10].

The diagram below provides an overview of the processing workflow used in GEOPSY for analyzing recorded signals. It illustrates the transition from input to output, highlighting key methodologies applied during the processing phase. The recorded signal undergoes several processing techniques, including Fast Fourier Transform (FFT), Frequency Domain Decomposition (FDD), and Random Decrement Technique (RDT), to extract essential dynamic characteristics such as natural frequencies, mode shapes, and damping ratios. This workflow summarizes the procedures discussed in the previous sections, emphasizing the importance of each step in the dynamic characterization of structures.

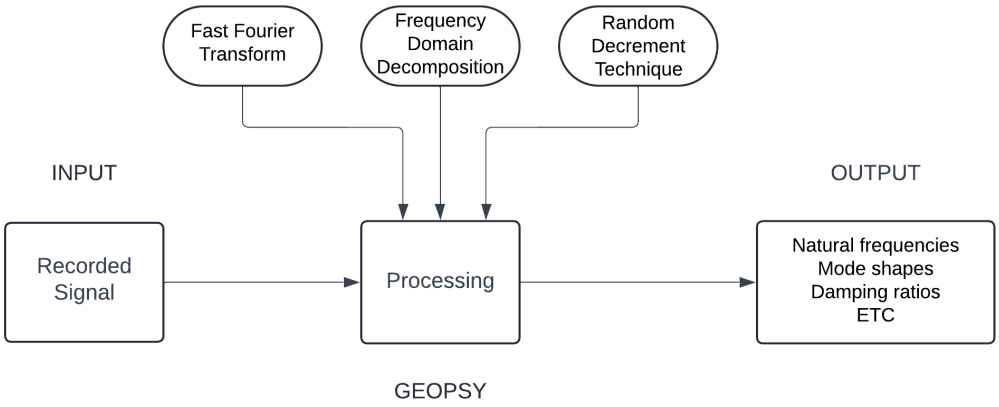

Figure 1.4: Flowchart of Signal Processing Techniques in GEOPSY

I.1.7 Modal Analysis

I.1.7.1 Decomposition of Structural Motion and Linear Approximation

Modal analysis is a powerful tool in structural dynamics that involves decomposing the complex motion of a structure into simpler, independent mode shapes. This process is based on the principle that any complex vibration pattern can be represented as a combination of simpler vibrational modes, each with its own natural frequency and mode shape. Key aspects include:

- **The stick model:** Is a simplified approach used in modal analysis to represent the dynamic behavior of tall buildings. It treats the building as a series of masses connected by springs and dampers, analogous to a skewer with pieces on it. The building is divided into discrete segments, each represented as a lumped mass, capturing the effect of different floors on the building's overall inertia. Springs and dampers between the masses represent the stiffness and damping properties, allowing for the simulation of both elastic and inelastic behaviors under dynamic loading.

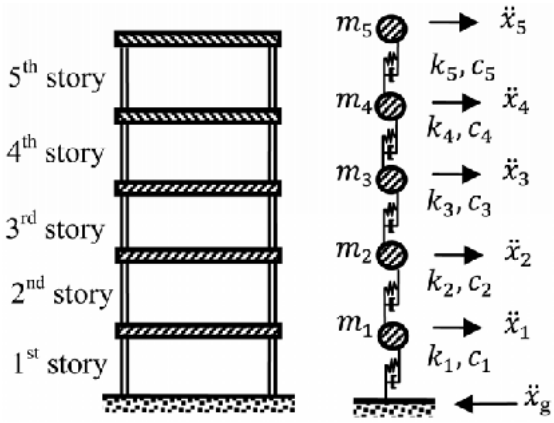

Figure 1.5: Example of a Detailed Stick Model Representation of a Five-Story Structure for Dynamic Analysis

- **Linear Approximation:** Modal analysis typically assumes a linear response, where the relationship between applied forces (P) and resulting displacements (U) is proportional. This assumption simplifies the analysis and is valid for small to moderate vibration amplitudes.

$$P = KU$$

- **Mode Shapes:** These are the specific patterns of deformation that a structure undergoes at its natural frequencies. Each mode shape corresponds to a particular frequency at which the structure tends to vibrate naturally. The overall behavior of a structure under dynamic loading, such as an earthquake, can be represented by summing these mode shapes. This approach involves decomposing a Multi-Degree-of-Freedom System (MDOF) into several Single-Degree-of-Freedom Systems (SDOF). The responses of these different modes are then combined using methods such as the Absolute Method (ABS), Square Root of the Sum of the Squares (SRSS), and Complete Quadratic Combination (CQC) to obtain the average maximum structural response.

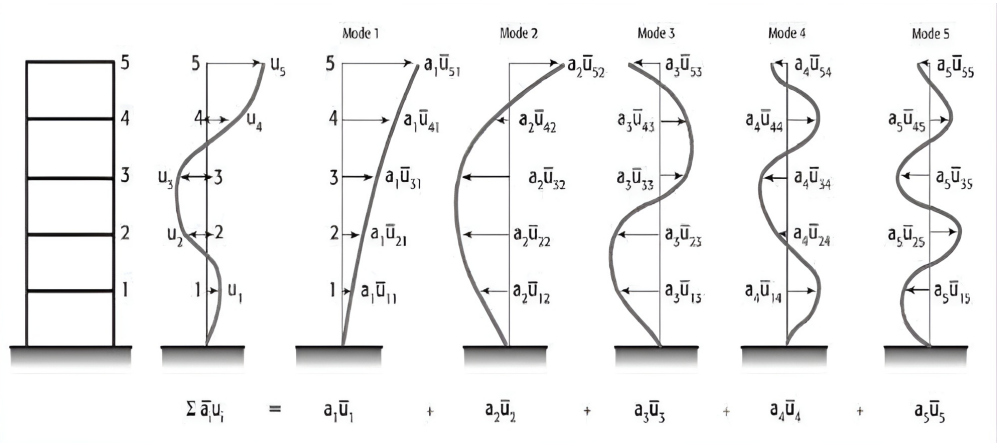

Figure 1.6: Exemple of mode Shapes and Modal Decomposition of a Five-Story Structure

By understanding these fundamental modes, engineers can gain insights into the overall dynamic behavior of the structure.

I.2 Seismic Risk

Seismic hazard can be defined based on the classical terms defined by the United Nations [11] by coupling various parameters such as hazard, vulnerability, and the exposed values to the considered risk, according to the equation:

$$\text{Risk} = \text{Hazard X Vulnerability X Value}$$

Where the terms are defined as follows:

- **Risk:** A probabilistic measure of impacts that can affect a system; it represents the mathematical expectation of losses over a reference period for a given site or region.
- **Hazard:** The probability of occurrence of an event in terms of intensity; evaluating the hazard involves calculating, for a given site, the distribution function of the characteristic parameters of the event, which are the intensity (on a given scale) and the probability of occurrence.
- **Vulnerability:** The degree of damage for different events, depending on the physical and geometric characteristics of the buildings.
- **Value:** The exposed socio-economic value of the system to the considered risk.

More precisely, risk can be expressed as the product of the probability of occurrence of a seismic event, the probability of reaching a given damage level, and the exposed values, which include buildings, their occupants, their contents, and the economic activities they house [PELI_04]. When the system is exposed to multiple potential hazards, the total risk is defined as the sum of the risks causing a loss of value. For seismic events:

$$R = \sum R_i$$

Where R_i represents the risk corresponding to an earthquake of intensity i.

Value losses can be classified into different categories:

- **Property losses:** Directly related to the damage sustained and consequently to the physical vulnerability.
- **Human losses:** Related to the damage, the building's capacity, the occupancy rate, and the quality of emergency services.

- **Indirect losses:** Related to the context in which the building is located, particularly the activities it houses.

We will now specify the evaluation of the different parameters, particularly focusing on vulnerability, which plays a central role as it causes the damage that, in turn, leads to the losses sustained.

I.2.1 Seismic Events

A seismic event can be defined as a movement, more or less violent, of the ground, which can be artificially decomposed into three directions: north-south, east-west, and vertical. The vertical (Z) component of the movement is generally weaker than the horizontal components and is often neglected. The frequency range of a seismic shock is between 0 and 35 Hz. Each shock can be characterized by its focus (the point where the fault rupture occurs), its epicenter (the point on the surface directly above the focus), its magnitude, and its intensity.

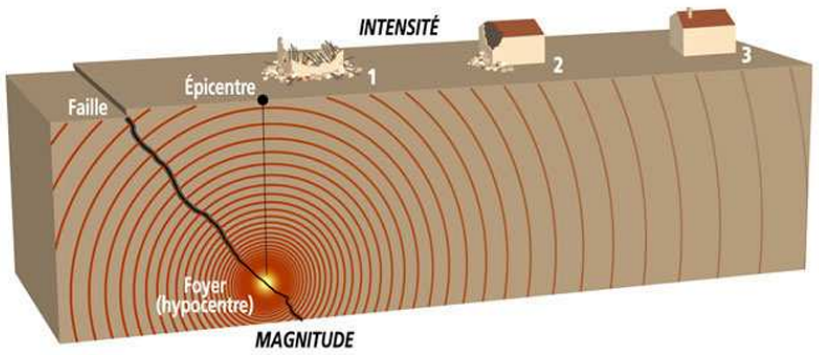

Figure 1.7: Earthquake,Focus and Epicenter, Magnitude and Intensity

I.2.1.1 Magnitude

To estimate earthquakes' power, seismologist Charles F. Richter introduced the concept of magnitude, which corresponds to the energy released at the earthquake's source and depends on the length of the activated fault and the extent of displacement. Richter's quantification [RICH_58], expressed in degrees (Table below), is considered open-ended as it has no maximum value; the strongest recorded earthquake to date is 9.5 degrees (Chile, 1960).

Magnitude	Earthquake Effects
< 3.5	Not felt, but recorded by seismographs.
3.5 - 5.4	Often felt, but rarely causes damage.
5.4 - 6	May cause slight damage to well-built buildings but can cause significant damage to poorly constructed buildings.
6.1 - 6.9	Can be destructive within a radius of 100 km.
7 - 7.9	Major earthquake. Can cause serious damage over a large area.
> 8	Great earthquake, capable of causing severe damage over several hundred kilometers.

Table 1.1: Richter Magnitude Scale

I.2.1.2 Intensity

Expressed in Roman numerals (with an upper limit of XII), intensity translates the effects produced on the surface by an earthquake at a given location. The MSK intensity scale (Medvedev-Sponheuer-Karnik), created in 1964, has been replaced since January 1, 2000, by the European Macroseismic Scale EMS 98 [12], as shown in Table below. These seismic scales allow the assessment of an earthquake's consequences through observations of damage to buildings and testimonies from people.

Intensity EMS	Definition	Typical Effects Observed
I	Not felt	Not felt.
II	Rarely felt	Felt only by a few people at rest indoors.
III	Weak	Felt indoors by a few people. Resting people feel a vibration or slight tremor.
IV	Largely observed	Felt indoors by many, outdoors by few. Some people are awakened. Windows, doors, and dishes rattle.
V	Strong	Felt indoors by most, outdoors by few. Many sleepers awaken. Some people are frightened. Buildings shake in their entirety. Hanging objects swing strongly. Small objects are moved. Doors and windows open or close.
VI	Slight damage	Many people are frightened and run outdoors. Objects fall. Many homes experience non-structural damage like fine cracks and small pieces of plaster falling.
VII	Damage	Most people are frightened and run outdoors. Furniture moves, and many objects fall from shelves. Many well-built ordinary buildings sustain moderate damage: small cracks in walls, plaster falls, and parts of chimneys fall. Older buildings may have large cracks in walls and failure of partition walls.
VIII	Significant damage	Many people have difficulty standing. Many homes have large cracks in walls. Some well-built ordinary buildings have serious wall failures, while poorly built older structures may collapse.
IX	Destructive	General panic. Many poorly built structures collapse. Even well-built buildings suffer severe damage: serious wall failures and partial structural collapse.
X	Very destructive	Many well-built buildings collapse.
XI	Catastrophe	Most well-built buildings collapse, even those with good seismic design are destroyed.
XII	Total catastrophe	Practically all buildings are destroyed.

Table 1.2: EMS 98 Intensity Scale

I.2.1.3 Relationship between Magnitude, Intensity, and Rock Response Spectra

Magnitude and intensity are two distinct measures characterizing a seismic event. Magnitude is based on numerical data, while intensity is based on qualitative data and often subjective testimonies. However, these testimonies, representing human memory, are the only data available over long periods. Therefore, intensity is naturally used to determine the probabilities of seismic events. Compiling past earthquake data makes it possible to deduce a return period for each intensity class associated with an "exhaustiveness date," from which the event sample can be considered complete [SECA_06]. If the number of felt events for a given intensity is low, the return period will have significant uncertainty.

I.2.2 Seismic Vulnerability

I.2.2.1 The Concept of Vulnerability

Human structures, such as buildings, equipment, and facilities, cannot fully absorb and dissipate the forces transmitted by seismic waves without sustaining damage. The extent of this damage depends on the structure's nature and design, making them more or less vulnerable to seismic stresses. Seismic vulnerability is thus defined as the relationship between the levels of consequential damage and the degrees of seismic aggression experienced.

While vulnerability is often discussed in the context of buildings, it is a concept that can be applied to other structures such as bridges, roads, industrial installations, gas distribution networks, and electrical networks. Beyond these "physical" vulnerabilities, there are also human, functional, economic, and social vulnerabilities. These aspects contribute to a comprehensive understanding of vulnerability, independent of the geographic location. For example, a building may be vulnerable but not present a risk if it is located in an area without seismic danger.

More precisely, seismic vulnerability is the probability of a system sustaining a certain level of damage during an earthquake. This probability is determined by defining the damage as a continuous variable (D), ranging from 0 (no damage) to 1 (complete ruin), linked to a specific indicator. For practical decision-making, the damage variable is categorized into "degrees" of damage.

we utilize the European Macroseismic Scale (EMS 98), which serves as a reference in Europe and categorizes damage into five degrees. Additionally, we incorporate the concept of Spectral Displacement as an indicator for determining the damage degree, based on the study by Kahil et al. (2010) [13] on the state of damage in reinforced concrete structures.

Degree	Damage Description	Damage Range	Spectral Displacement
DG 1	Negligible to light damage	$0 \leq D < 0.2$	$S_d = 0.4S_{dy}$
DG 2	Moderate damage	$0.2 \leq D < 0.4$	$S_d = 0.8S_{dy}$
DG 3	Significant to considerable damage	$0.4 \leq D < 0.6$	$S_d = S_{dy}+0.25(S_{du}-S_{dy})$
DG 4	Very significant damage	$0.6 \leq D < 0.8$	$S_d = 0.75S_{du}$
DG 5	Partial or total collapse (destruction)	$0.8 \leq D \leq 1$	$S_d = S_{du}$

Table 1.3: Degrees of Seismic Damage and Ranges According to EMS

I.2.3 Evaluation of Seismic Vulnerability: Nonlinear Methods and Pushover Analysis

I.2.3.1 Introduction

Evaluating the seismic vulnerability of existing buildings is a critical aspect of civil engineering, particularly in earthquake-prone regions. Nonlinear analysis methods provide detailed insights into the complex inelastic behavior of structures under seismic loading, allowing engineers to predict potential failure mechanisms and assess overall structural performance accurately. These methods are indispensable for understanding the dynamic response of buildings, identifying weak points, and designing effective retrofit strategies to enhance seismic resilience. This section focuses on the methodology for assessing seismic vulnerability using nonlinear analysis.

I.2.3.2 Nonlinear Analysis

The advent of computational tools has revolutionized structural engineering practices, enabling the implementation of advanced analytical methods. Two crucial types of nonlinear analysis procedures are used to assess structures' seismic performance.

- **Nonlinear dynamic time history analysis:** involves simulating the detailed response of a structure to recorded or synthetic earthquake ground motions over time, providing precise estimates of seismic demands.

- **Pushover analysis:** it's a nonlinear static method that incrementally applies lateral loads to estimate a building's capacity and identify potential failure mechanisms.

I.2.3.3 Nonlinear Static Analysis Procedures (Pushover Analysis)

I.2.3.3.1 Review and Developments in Pushover Analysis

The development of nonlinear static analysis, or pushover analysis, can be traced back to the work of Gulkan and Sozen (1974) [14], who proposed a method for representing a multi-degree-of-freedom system as an equivalent single-degree-of-freedom system. Over the last two decades, significant advancements in pushover analysis have been made, including the development of adaptive and modal pushover methods [15]. These advancements account for higher mode effects and provide more accurate seismic demand estimates for tall buildings and structures with complex dynamic behavior. Notable contributions include the Modal Pushover Analysis (MPA) by Chopra and Goel (2002)[15] and the Adaptive Modal Pushover Analysis (AMPA) by Gupta and Kunnath (2000)[16].

Pushover analysis has evolved from a simple heuristic method to a robust and comprehensive analytical tool. Initially, the method involved applying a monotonically increasing lateral load pattern until a target displacement was reached, capturing the global behavior of structures. However, traditional pushover analysis primarily considered the fundamental mode, neglecting higher mode effects and dynamic characteristics. This limitation led to modal pushover analysis (MPA), which integrates multiple mode shapes to represent the dynamic response of structures better.

Adaptive pushover methods have further refined the technique by adjusting the load patterns based on the changing stiffness and mass distribution during the analysis. These advancements ensure that the analysis remains relevant throughout the loading process, improving the accuracy of predicted seismic demands. The combination of these methods has made pushover analysis a powerful tool for performance-based seismic design, capable of providing detailed insights into potential failure mechanisms and overall structural performance.

I.2.3.3.2 Conventional Pushover Analysis Formulation

Conventional pushover analysis is an incremental-iterative nonlinear solution of the equilibrium equation ($\boldsymbol{KU = P}$) in a finite element formulation. Here, K is the nonlinear stiffness matrix, U is the displacement vector, and P is a predefined lateral load vector applied incrementally. The process continues until a target displacement or structural collapse is reached. The aim is to estimate global lateral strength, ductility, displacement, and failure mechanisms under applied lateral forces.

This method involves creating a detailed finite element model of the structure,

incorporating nonlinear material properties and geometric configurations. The lateral loads are applied step-by-step, with each increment representing a fraction of the total expected seismic force. At each step, the analysis updates the stiffness and strength properties of the structural elements to reflect the accumulation of damage and inelastic behavior.

The primary outputs of a conventional pushover analysis include the capacity curve, which plots the base shear versus roof displacement, and the sequence of plastic hinge formations [17]. These results help engineers understand the progressive failure mechanisms and the overall ductility of the structure. The capacity curve provides critical information on the initial stiffness, yield strength, and ultimate load-carrying capacity, essential for evaluating buildings' seismic resilience.

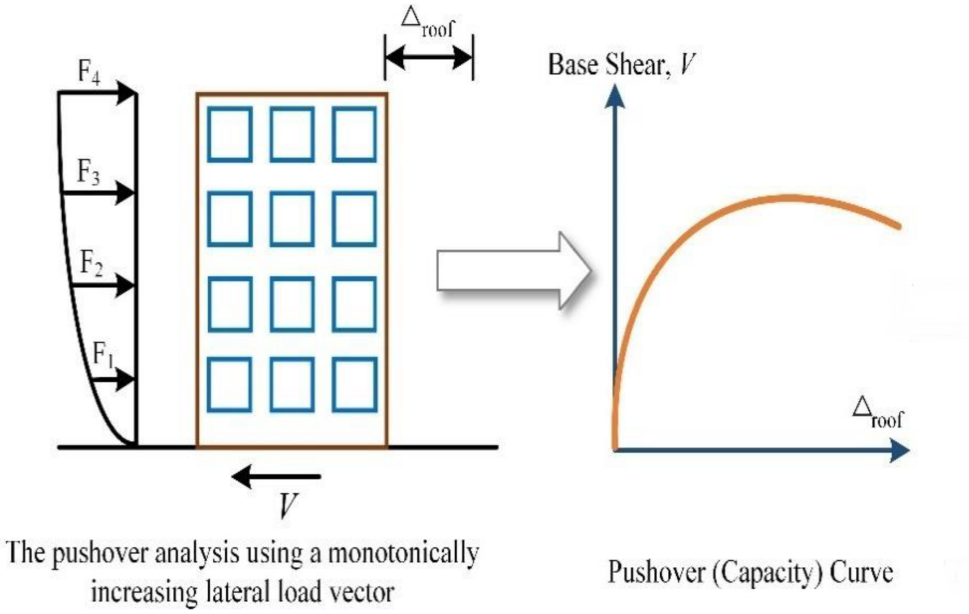

Figure 1.8: Illustration of Pushover Analysis for Determining Structural Capacity Curve

I.2.3.3.3 Load Distribution Schemes

Several load distribution schemes are used in pushover analysis, each with specific applications and advantages:

- **Uniform Distribution:** Forces are distributed uniformly across the building's height, favoring shear forces over overturning moments. This distribution is simple to apply and is often used for preliminary assessments. However, it may not accurately represent the actual dynamic behavior of tall buildings, where higher mode effects are significant.

- **Fundamental Mode Distribution:** Forces are distributed according to the building's fundamental mode shape, used when the fundamental mode's

mass participation exceeds 75%. This method provides a better approximation of the building's response, especially for low-rise structures where the fundamental mode dominates the seismic response.

- **Code-Based Modal Distribution (FEMA-356):** Forces are distributed based on code specifications, often requiring a uniform distribution as a secondary measure. FEMA-356 recommends specific load patterns that account for the contributions of multiple modes, providing a more comprehensive assessment of seismic demands.

- **Triangular Distribution:** Forces follow a triangular shape, providing better estimates of building responses compared to uniform and modal distributions in some cases. This distribution is beneficial for buildings with a significant height where the lateral force distribution varies linearly with height, capturing the effects of both shear and flexural behavior.

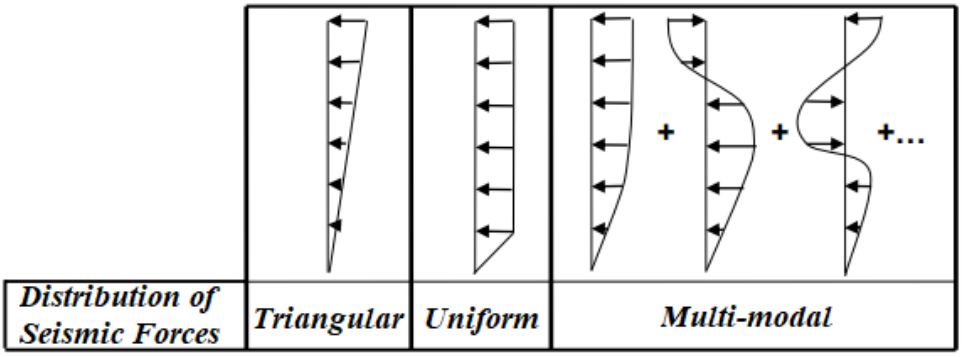

Figure 1.9: Illustration of Load Distribution Schemes

I.2.3.3.4 Key Parameters in Pushover Analysis

A. Capacity Curve

The capacity curve is a fundamental component in pushover analysis. It plots the base shear force against the roof displacement, illustrating the transition from elastic to inelastic behavior. This curve helps identify the building's initial stiffness, yield capacity, and ultimate strength. The performance points on the capacity curve indicate the building's capacity to withstand lateral forces without significant loss of structural integrity [17].

The capacity curve provides critical insights into the structural behavior under increasing lateral loads. Key points on the curve include:

- **Elastic Region:** The initial linear portion of the curve represents the elastic behavior of the structure, where deformations are proportional to applied forces.

- **Yield Point:** This point marks the onset of inelastic behavior, indicating that the structure has reached its yield capacity and plastic deformations have begun to occur.
- **Post-Yield Region:** The nonlinear portion beyond the yield point represents the inelastic behavior, where the structure undergoes significant plastic deformations while sustaining additional loads.
- **Ultimate Capacity:** The peak of the curve indicates the maximum load-carrying capacity of the structure. Beyond this point, any additional loading leads to rapid degradation and potential collapse.

B. Nonlinear Modeling of Structures

Nonlinear modeling involves representing the material and geometric nonlinearity of structural elements. This can be achieved through concentrated plasticity models, where plastic hinges form at specific locations, or distributed plasticity models, which spread the inelastic behavior along the length of the element. These models capture the progressive stiffness degradation and strength deterioration of structural components under cyclic loading.

Concentrated plasticity models, or plastic hinge models, are commonly used due to their simplicity and efficiency. These models assume that inelastic deformations are concentrated at specific points (hinges) along the structural members while the rest of the members remain elastic. Plastic hinges are typically placed at locations where moments are expected to be highest, such as beam-column joints.

Distributed plasticity models, on the other hand, provide a more detailed representation of inelastic behavior by distributing plastic deformations along the length of the structural elements. This approach requires more computational effort but offers a more accurate depiction of the stress-strain relationships and damage progression within the structure [17].

C. Hinge Types and Properties According to ASCE 41-13

ASCE 41-13, titled "Seismic Evaluation and Retrofit of Existing Buildings," is a standard developed by the American Society of Civil Engineers (ASCE). This standard provides comprehensive guidelines for the seismic assessment and retrofitting of existing buildings to improve their performance during earthquakes. Here are some key aspects of ASCE 41-13:

- **Flexural Hinge (M3):** This type of hinge models the flexural behavior of structural elements like beams and columns under bending moments. The M3 hinge is defined based on moment-rotation relationships, which capture the inelastic rotation capacity of the element.
- **Axial-Flexural Hinge (P-M2-M3):** This hinge type accounts for the interaction between axial force (P) and moments about both the major (M2)

and minor (M3) axes. It is typically used for columns, where the combined effects of axial load and bending are significant. This hinge type captures the axial-flexural interaction and provides a comprehensive representation of the inelastic behavior under combined loading conditions.

- **Shear Hinge:** Although not as commonly used as flexural and axial-flexural hinges, shear hinges model the inelastic behavior of elements subjected to shear forces. These are particularly relevant for elements like shear walls and certain types of beams.

- **Auto Hinges:** ASCE 41-13 provides specifications for automatic hinge generation in structural analysis software like ETABS. Auto hinges use predefined parameters and empirical relationships to define the hinge properties based on the material, cross-sectional dimensions, and expected loading conditions. This ensures consistency and reliability in the modeling process.

- **Fiber Hinges:** Fiber hinges model the inelastic behavior of structural elements by dividing the cross-section into multiple fibers, each with its own stress-strain relationship. This approach allows for a more detailed and accurate representation of the element's behavior under axial forces and bending moments. Fiber hinges are particularly useful for modeling complex interactions in reinforced concrete and composite sections, capturing the progressive stiffness degradation and strength deterioration of the material. They are commonly used for shear walls and columns, where detailed modeling of inelastic behavior is required.

D. Key Aspects of Hinge Properties

- **Moment-Rotation Curves:** The standard provides tables and guidelines for defining moment-rotation curves for flexural hinges. These curves are based on empirical data and experimental studies detailing the relationship between applied moments and resulting rotations at the hinge location.

- **Acceptance Criteria:** ASCE 41-13 establishes acceptance criteria for different performance levels, such as Immediate Occupancy, Life Safety, and Collapse Prevention. These criteria evaluate whether the hinge rotations and overall structural response meet the desired performance objectives under seismic loading.

- **Hinge Length:** The hinge length (L_p) is typically a fraction of the member's depth or width for flexural hinges. For example, the hinge length for columns might be set to 0.5 [17] times the column width to accurately capture the inelastic rotation capacity. Empirical formulas estimate the hinge length, accurately representing the inelastic behavior. This method effectively simulates structural members' progressive stiffness degradation and strength deterioration under cyclic loading, providing a robust framework for seismic performance assessment.

E. Presentation of Existing Generalized Law Models

Several models are used to calculate the generalized stress-strain relationships of structural components in pushover analysis [17]. These include:

- **Biskinis et al. Model:** This model focuses on the deformation capacity of reinforced concrete elements under monotonic and cyclic loading. It provides detailed formulations for predicting the inelastic behavior and ductility of concrete members, considering the effects of axial load, shear, and confinement.
- **Lopez et al. Model:** Evaluates ductility demands for single-degree-of-freedom systems subjected to short-duration earthquake ground motions. This model addresses the influence of ground motion characteristics on the inelastic deformation demands of structural components.
- **FEMA-356 Model:** This model provides guidelines for the nonlinear modeling of structures for seismic rehabilitation. It includes comprehensive recommendations for defining plastic hinge properties, material models, and load patterns for pushover analysis.
- **Response-2000 Model:** Software-based model for detailed nonlinear analysis of reinforced concrete elements. Response-2000 incorporates advanced material models and nonlinear analysis techniques to simulate the behavior of concrete members under seismic loading.
- **ETABS-SD Model:** An integrated model within the ETABS software for performing detailed pushover analysis. The ETABS-SD model offers a user-friendly interface and powerful analysis capabilities for evaluating the seismic performance of buildings.

I.2.3.3.5 Performance Point Estimation Methods

The performance point is the specific point on the capacity curve where the structure's capacity to resist seismic forces intersects with the demand imposed by a seismic event. At this point, the structure's predicted displacement and force levels align with the seismic demand, indicating the expected level of performance during an earthquake. The performance point provides critical insights into how much displacement a structure can endure and the corresponding force levels, thereby guiding design decisions to ensure safety and resilience against seismic forces [17].

Performance point estimation methods are crucial for determining the expected performance of a structure under seismic loading. These methods help in identifying the displacement demand that a structure can safely withstand during an earthquake.

A. Capacity Spectrum Method (CSM)

The Capacity Spectrum Method (CSM) involves plotting the capacity curve and demand spectrum on the same graph to identify the performance point where the structure's capacity meets the seismic demand. This method provides a visual and analytical approach to performance-based seismic design. Improvements proposed in FEMA-440 enhance the accuracy of CSM by incorporating modifications to the demand spectrum and capacity curve adjustment procedures.

The CSM method integrates the capacity curve with the demand spectrum, which represents the seismic demands imposed on the structure. The intersection of these two curves, known as the performance point, indicates the expected displacement and force levels that the structure can withstand during an earthquake. The method involves several steps:

1. **Develop Capacity Curve:** Perform pushover analysis to generate the capacity curve, plotting base shear against roof displacement.

2. **Construct Demand Spectrum:** Convert the elastic response spectrum to the inelastic demand spectrum, considering factors such as damping and ductility.

3. **Find Performance Point:** Plot the capacity curve and demand spectrum on the same graph and identify their intersection point. This point represents the expected performance level of the structure.

B. Coefficients Method

The Coefficients Method, also improved in FEMA-440, uses predefined coefficients to estimate the performance point based on the building's fundamental period and ductility. This method simplifies the performance point estimation process by applying modification factors to linear elastic response values. It is widely used in practice due to its straightforward implementation and reasonable accuracy.

The Coefficients Method involves the following steps:

1. **Determine Elastic Response:** Calculate the elastic displacement response using the response spectrum for the given seismic hazard.

2. **Apply Modification Factors:** Use predefined coefficients to adjust the elastic response values, accounting for factors such as structural period, damping, and ductility. These coefficients are derived from empirical data and experimental studies.

3. **Estimate Performance Point:** Combine the modified response values to estimate the expected displacement and force levels that the structure can withstand during an earthquake.

The Coefficients Method provides a practical approach for estimating performance points without the need for complex nonlinear analysis. It is particularly useful for preliminary assessments and for structures with well-defined dynamic properties.

C. N2 Method

As presented in Eurocode 8, the N2 Method combines the capacity and inelastic demand spectrum to determine the performance point. It provides a straightforward approach to estimate the displacement demands of structures subjected to seismic loading. The method integrates the nonlinear characteristics of the capacity curve with the elastic response spectrum, resulting in a bilinear representation of structural performance.

The N2 Method involves the following steps:

1. **Generate Capacity Curve:** Perform pushover analysis to develop the capacity curve, representing the relationship between base shear and roof displacement.
2. **Convert Demand Spectrum:** Use the elastic response spectrum to generate the inelastic demand spectrum, considering factors such as damping and ductility.
3. **Determine Performance Point:** Plot the capacity curve and inelastic demand spectrum on the same graph and identify their intersection point. This point represents the expected performance level of the structure.

The N2 Method provides a clear and concise framework for performance-based seismic design, enabling engineers to evaluate the seismic performance of structures and develop appropriate retrofit strategies.

I.2.3.4 Coefficients Method

I.2.3.4.1 Overview

The Coefficients Method, initially presented in American guides such as ATC-40 [18], FEMA-273, and FEMA-356, serves as a simplified method for estimating the target displacement of structures during seismic events. This method has been refined in subsequent guidelines, notably FEMA-440 and ASCE 41-13, to improve accuracy. It is widely adopted in practice due to its straightforward implementation and reasonable accuracy for various building types.

I.2.3.4.2 Principle

The Coefficients Method uses a series of predefined coefficients to convert the maximum displacement of a linear single-degree-of-freedom (SDOF) system into a maximum nonlinear displacement, which serves as the target displacement for pushover analysis. These coefficients are derived from the parameters of the idealized nonlinear pushover curve [17].

I.2.3.4.3 Key Equations

The target displacement (δ_t) is estimated using the following equation:

$$\delta_t = C_0 C_1 C_2 C_3 S_a \frac{T_e^2}{4\pi^2 g}$$

Where:

- $\mathbf{C_0}$: Coefficient relating the spectral displacement of an SDOF system to the probable roof displacement of a multi-degree-of-freedom (MDOF) system.
- $\mathbf{C_1}$: Coefficient relating the maximum inelastic displacement to the elastic displacement calculated by an elastic response.
- $\mathbf{C_2}$: Coefficient representing the effect of hysteresis shape on the maximum displacement.
- $\mathbf{C_3}$: Coefficient representing the P-Δ effect due to dynamic behavior.
- $\mathbf{S_a}$: Spectral acceleration corresponding to the fundamental period and damping of the building.
- $\mathbf{T_e}$: Effective fundamental period of the building in the considered direction.

I.2.3.4.4 Estimation of Coefficients

1. C_0 **Coefficient:** Calculated from the modal mass participation factor of the fundamental mode using the following equations:

$$C_0 = \phi_{1,r}\Gamma_1 = \phi_{1,r}\frac{\{\phi_1\}^T[M]\{1\}}{\{\phi_1\}^T[M]\{\phi_1\}}$$

$$C_0 = \phi_{1,r}\frac{\sum_{i=1}^{N} m_i\phi_{i,n}}{\sum_{i=1}^{N} m_i\phi_{i,n}^2}$$

Where $\phi_{1,r}$ is the coordinate of the fundamental mode at the roof, and $[M]$ is the mass matrix.

2. C_1 **Coefficient:** Calculated based on the effective period (T_e) of the building relative to the characteristic period (T_0) of the response spectrum:

$$C_1 = 1.0 \quad \text{if} \quad T_e \geq T_0$$

$$C_1 = \left[1.0 + \frac{(R-1)T_0}{T_e}\right] R \quad \text{if} \quad T_e < T_0$$

Where R is a coefficient related to the spectral acceleration (S_a) and the yield limit (V_y).

3. C_2 **Coefficient:** Represents the degradation of stiffness and strength due to hysteretic behavior, with values provided in FEMA guidelines.

4. C_3 **Coefficient:** Accounts for P-Δ effects and dynamic instability, calculated as follows:

$$C_3 = 1.0 + \frac{|\alpha|(R-1)^{3/2}}{T_e}$$

Where α is the post-elastic slope of the capacity curve.

5. **Effective Period (T_e):** The effective period is calculated using the fundamental period and the lateral stiffness of the building:

$$T_e = T_i \sqrt{\frac{K_i}{K_e}}$$

Where T_i is the fundamental period, K_i is the effective elastic stiffness, and K_e is the effective plastic stiffness.

I.2.3.4.5 Application

The Coefficients Method is particularly suitable for practical engineering applications due to its simplicity and direct numerical procedure. It avoids the iterative graphical process required by the Capacity Spectrum Method and provides a reliable means of estimating the seismic demand for building structures [17].

I.3 Conclusion:

This chapter introduces essential scientific concepts and methodologies related to ambient vibration analysis, modal analysis, and seismic vulnerability assessment. By establishing the theoretical foundation and presenting the necessary data for the study, it ensures a thorough understanding of the project's framework and the dynamic behavior of the structure under seismic loads.

Chapter 2

Characterizing Tower Structural Properties through Ambient Vibration Experiment

Characterizing Tower Structural Properties through Ambient Vibration Experiment

II.1 Introduction

In this chapter, we characterize the tower's structural properties through ambient vibration experiments. By evaluating dynamic properties such as natural frequencies, mode shapes, and damping ratios, we gain insights into the tower's seismic behavior. Our analysis of the vibration data provides a critical understanding of the tower's dynamic characteristics, which is essential for accurate seismic vulnerability assessment.

II.2 Sensors Placement and Data Recording

The tower is a reinforced concrete structure, standing at 69.64 meters with 15 floors and a basement, featuring a central reinforced concrete core. The building was instrumented using a City Shark I station equipped with a Lennartz 2s sensor with two horizontal and one vertical components. The horizontal components were studied along the building's two principal directions:

$$East - West(EW) \equiv Transverse(T)$$
$$North - South(NS) \equiv Longitudinal(L).$$

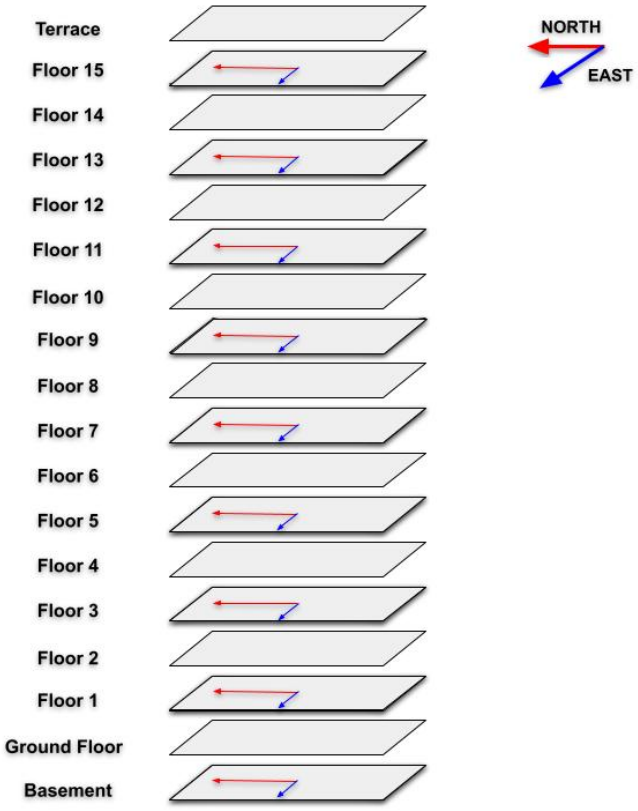

Figure 2.1: Sensor placement for monitoring EW (T) and NS (L) directions.

Recordings were conducted in one day. Only the odd-numbered floors were recorded, one by one. Sensors were placed in the center of each instrumented floor. Due to the terrace's inaccessibility, instrumentation was installed from the 15th floor down to the basement, floor by floor, according to the experimental scheme. This setup allowed us to obtain 15-minute ambient noise recordings. The sampling frequency was 200 Hz.

For processing the recordings, we used the following coefficients: $Lta = 30s$, $Sta = 1s$, min $Sta/Lta = 0.3$, max $Sta/Lta = 2$. The processing windows were 40 seconds long, and an anti-trigger algorithm was used for their selection with a 5% overlap. Spectrum smoothing (Konno and Ohmachi, $b = 40$) [19] and 5% cosine tapering were applied to each side of the selected windows.

II.3 Results and Interpretation

II.3.1 Frequency

The FDD method operates by decomposing the recorded vibration data, initially in the form of amplitude-time graphs, into its constituent frequency components. This decomposition is achieved by converting the time-domain data into the frequency domain. Each segment of the recorded vibration is analyzed to identify consistent frequencies, and these segments are color-coded to represent different

frequencies. This visual representation, as shown in **Figure 2.2**, allows for an intuitive understanding of how the structure responds to various vibrational stimuli over time.

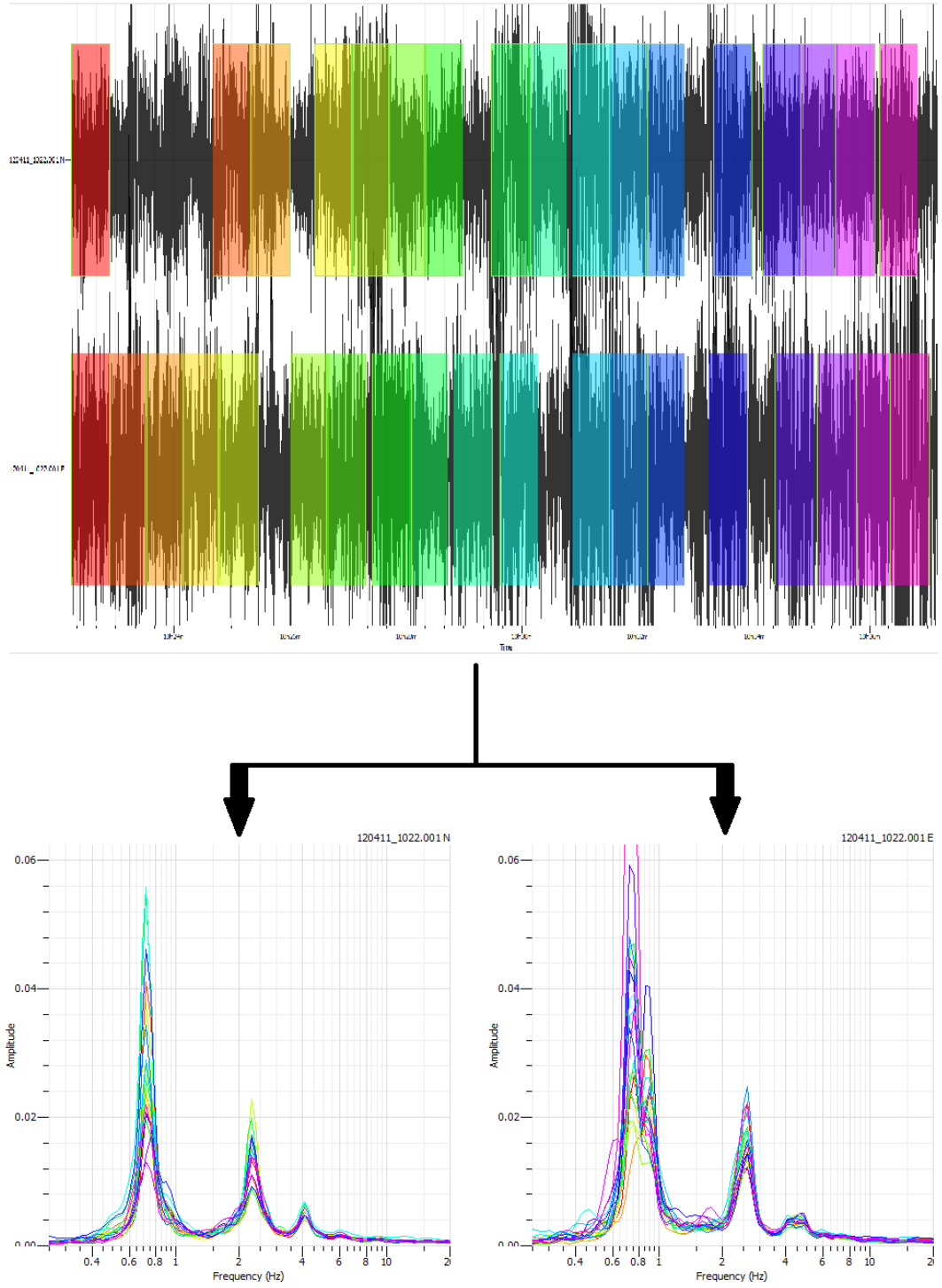

Figure 2.2: FDD method: Time-domain data (top) transformed into frequency-domain for L (bottom left) and T (bottom right) directions.

After treating and filtering the data, we obtained the average curves for both longitudinal (L) and transverse (T) directions. These curves helped us identify

three natural frequencies (peaks) for each direction (check Appendices **Figures 4. 21 and 4.22**), resulting in a total of six modes, as represented in the following figures

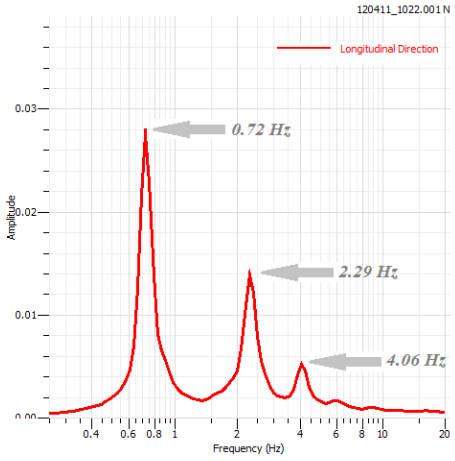

Figure 2.3: Amplitude vs. Frequency for Longitudinal Direction.

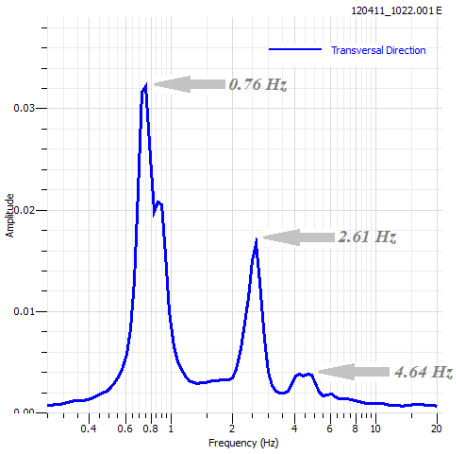

Figure 2.4: Amplitude vs. Frequency for Transversal Direction.

Longitudinal Direction (Figure 2.3):

- **First Peak at 0.72 Hz:** This peak represents the fundamental natural frequency of the structure in the longitudinal direction. The high amplitude indicates a significant response, which is characteristic of the primary mode of vibration.
- **Second Peak at 2.29 Hz:** This peak is the first higher-order mode in the longitudinal direction. It indicates a secondary mode of vibration that is less dominant but still significant.
- **Third Peak at 4.06 Hz:** This peak represents another higher-order mode, showing further vibrational characteristics of the structure at a higher frequency.

Transversal Direction (Figure 2.4):

- **First Peak at 0.76 Hz:** Similar to the longitudinal direction, this peak represents the fundamental natural frequency of the structure in the transverse direction. The slight difference in frequency (compared to the longitudinal direction) is due to different stiffness and mass distribution in this direction. The small peak that is hanging on the fundamental frequency peak might represent a coupled mode (translational + torsional). To confirm this suggestion, we should perform another ambient vibration experiment with different sensor disposition (at the extremities of the floors) to capture the torsional mode.

- **Second Peak at 2.61 Hz:** This peak indicates the first higher-order mode in the transverse direction. It shows additional vibrational characteristics of the structure.
- **Third Peak at 4.64 Hz:** This higher-order mode indicates complex vibrational behavior at a higher frequency. The equal doubled peak observed around 4-5 Hz in the transversal direction suggests the presence of closely spaced higher-order modes. These could be due to degenerate modes or coupled translational and rotational movements.

Note: *Degenerate modes are a phenomenon in structural dynamics where two or more vibrational modes have nearly the same natural frequency but different mode shapes. This often occurs in structures with a high degree of symmetry [20].*

The sensor on the 15th floor recorded the most significant amplitude (check appendices **Figure 4.20**); it clearly represents the tower's fundamental frequency. The following table presents the natural frequencies recorded at this floor.

Direction	Mode 1 Frequency (Hz)	Mode 2 Frequency (Hz)	Mode 3 Frequency (Hz)
Longitudinal	0.723261	2.28611	4.06441
Transversale	0.755994	2.61075	4.64159

Table 2.1: Natural frequencies recorded at the 15th floor.

The slight differences between the frequencies in both directions indicate that the structure predominantly exhibits translational modes rather than torsional modes [21]. None of the observed frequencies match exactly in both the longitudinal and transverse directions, which means we cannot confirm the presence of dominant torsional modes based on the current sensor placement.

For a more definitive identification of torsional modes, sensors would need to be optimally placed at the corners or along the periphery of the structure. However, due to the constraints of our testing setup, where sensors were placed at the center of the floors, we could not capture the torsional behavior effectively.

Given the restricted access to the tower, preventing further tests and sensor adjustments, we will proceed under the assumption that all the obtained frequencies represent translational modes. This approach is necessary for using these frequencies in the calibration process described in the next chapter. Therefore, for the purposes of our work, we conclude that the building primarily exhibits translational movements along the longitudinal and transverse axes, as indicated by the current data.

This finding allows us to utilize the obtained frequencies for model calibration, ensuring that our subsequent analysis remains consistent and valid within the constraints of the available data.

To validate our results, we estimated the fundamental frequency using formulas mentioned in various codes.

II.3.1.1 Estimation of the Fundamental Frequency

The value of the fundamental frequency of the structure can be estimated using empirical formulas or calculated through analytical or numerical methods.

II.3.1.1.1 RPA 99/2003

The empirical formula to use in all cases listed in [**Table 2.2**] is:

$$f = \frac{1}{C_T h_N^{3/4}}$$

where:

- h_N: Height measured in meters from the base of the structure to the top level (N)
- C_T: Coefficient, depending on the bracing system and type of infill, given by the table below:

Case No.	Bracing System	C_T
1	Self-supporting reinforced concrete frame without masonry infill	0.075
2	Self-supporting steel frame without masonry infill	0.085
3	Self-supporting reinforced concrete or steel frame with masonry infill	0.05
4	Bracing ensured partially or completely by concrete shear walls, braced frames, and masonry walls	0.05

Table 2.2: Values of C_T for different bracing systems

II.3.1.1.2 RPA 88

The following formula can determine the frequency f:

$$f = \frac{10}{N}$$

where N is the number of stories of the building.

II.3.1.1.3 UBC 88

$$f = \frac{\sqrt{L_{x,y}}}{0.09h}$$

where h is the height of the building, and $L_{x,y}$ is the dimension of the building in the considered direction.

Note: *In this scenario, the larger of the two values provided by* ***RPA99/2003*** *[22] and* ***UBC 88*** *[23] should be retained in each considered direction.*

.	f_{RPA88} **(Hz)**	$f_{UBC88}L$ **(Hz)**	$f_{UBC88}T$ **(Hz)**	f_{RPA99} **(Hz)**
Empirical Fundamental Frequency	0.59	0.75	0.66	0.83
Experimental Fundamental Frequency	0.72	0.72	0.76	0.72

Table 2.3: Comparison of empirical and experimental fundamental frequencies.

The comparison between empirical and experimental frequencies shows some variation, indicating that empirical models may not always accurately capture the building's actual dynamic behavior. The experimental results generally show higher frequencies, suggesting greater stiffness than the empirical models predict. The close match for the second code (UBC) indicates that some empirical models can accurately represent certain aspects of the building's behavior, while others may need adjustments.

These discrepancies underscore the importance of experimental validation in seismic performance assessments. empirical models provide useful estimates, but experimental data is crucial for accurately understanding the building's response to seismic forces and ensuring its structural integrity.

To assess the behavior of our structure, we calculated the frequency ratios of the second and third modes relative to the first mode frequency. The results of these calculations are presented in the Table below.

Mode i	**Direction**	**Frequency (Hz)**	$\mathbf{f_i/f_1}$	**The Reference Ratio of the Shear Beam Model** [24]
1	L	0.72	1	1
1	T	0.76	1	1
2	L	2.29	3.16	3
2	T	2.61	3.45	3
3	L	4.06	5.62	5
3	T	4.64	6.14	5

Table 2.4: Frequency ratios of the second and third modes relative to the first mode frequency.

The frequency ratios obtained align with those expected for a shear beam. This model assumes that the floors act as diaphragms with infinite rigidity compared to the bracing elements, meaning there is no moment transfer between consecutive floors. These results provide critical insights into the dynamic behavior of the structure, supporting the assumption of rigid diaphragms in the floors and ensuring accurate representation of the shear behavior.

II.3.2 Mode shapes

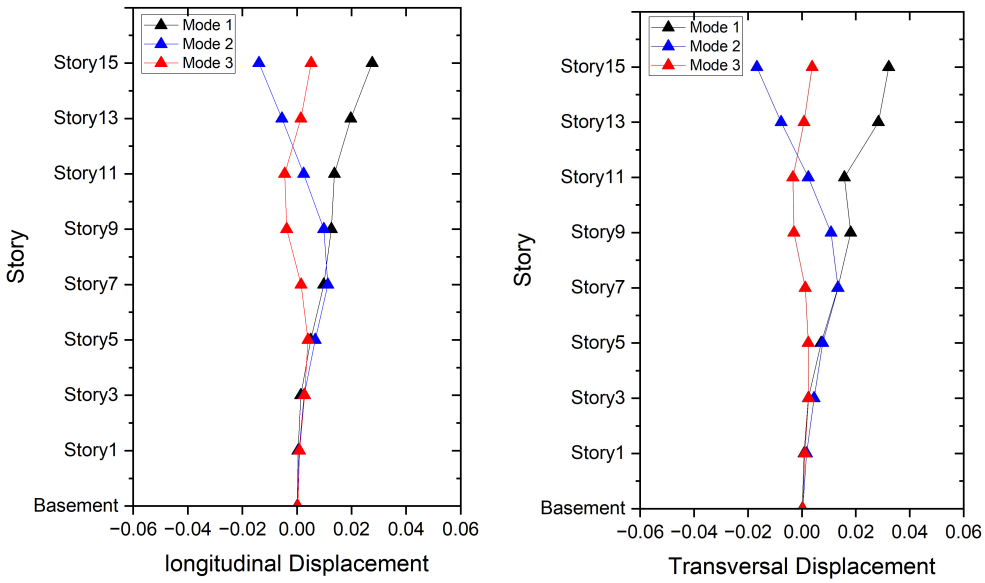

Figure 2.5: Modal shapes of the first three modes in both longitudinal and transversal directions.

The mode shapes depicted in the graphs align well with the frequency ratios presented in the **Table 2.3**. The fundamental mode (Mode 1) for both longitudinal (L) and transversal (T) directions shows the largest displacements at the top stories, which is consistent with the observed fundamental frequencies of 0.72 Hz and 0.76 Hz, respectively. As the modes progress to Mode 2 and Mode 3, the increasing complexity in the vibration patterns, with nodes indicating changes in displacement direction, matches the higher frequency ratios (e.g., 3.16 and 3.45 for Mode 2, and 5.62 and 6.14 for Mode 3).

These results confirm the theoretical model that assumes floors act as diaphragms with infinite rigidity compared to the bracing elements, leading to no moment transfer between consecutive floors. The alignment of the obtained frequency ratios with the expected values for a shear beam model [24] provides critical insights into the dynamic behavior of the structure, supporting the assumption of rigid diaphragms and ensuring an accurate representation of the shear behavior.

II.3.3 Damping

The analysis was conducted using the software GeoPsy, employing the Random Decrement Technique to calculate the damping coefficient. This method involves isolating and filtering each natural frequency using the Butterworth filter, which allows for the separation of different modes and the determination of their respective damping coefficients. The figures below illustrate the application of this technique and the resulting damping coefficients for the first mode.

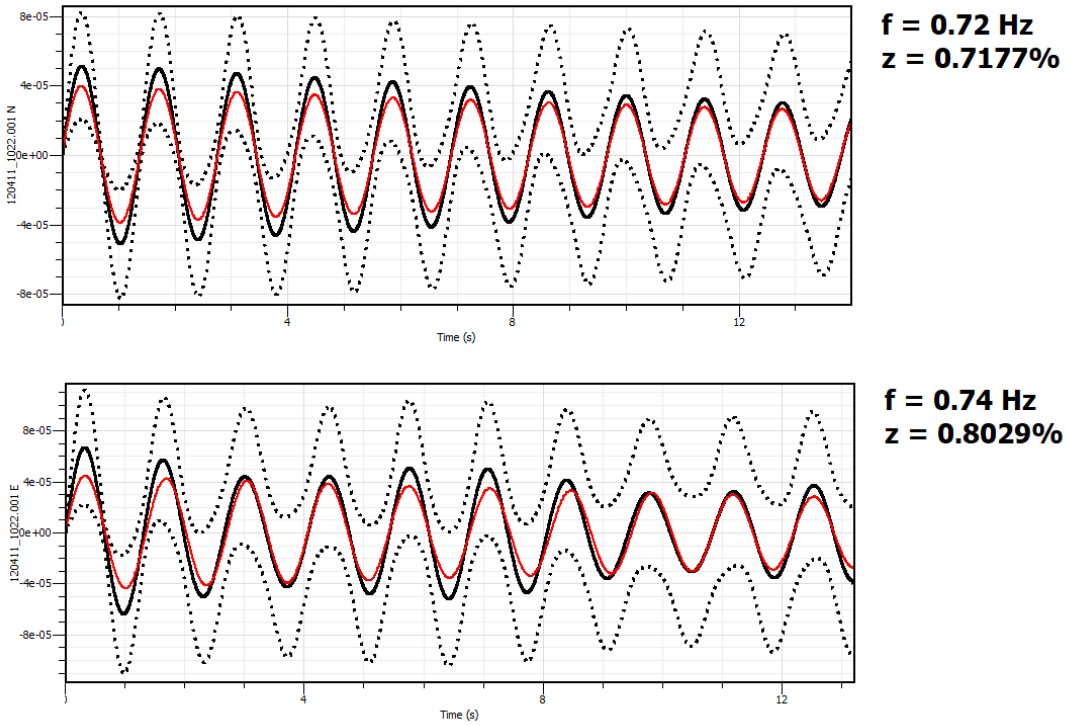

Figure 2.6: Illustration of the application of the Random Decrement Technique and the resulting damping coefficients for the first mode L (top) and T (bottom) directions.

we also used the Half Power Band Width Method to determine the damping coefficients. This method involves analyzing the frequency response function and applying the equation mentioned in **paragraph 1.2.6.3.3**, to calculate the damping.

The following table presents the damping values obtained using the random decrement technique and the half-power bandwidth method for various stories and directions of the building.

Story	Direction	Random decrement			Half-power bandwidth		
		$\xi_1(\%)$	$\xi_2(\%)$	$\xi_3(\%)$	$\xi_1(\%)$	$\xi_2(\%)$	$\xi_3(\%)$
Basement	L	6.50	8.53	4.21	21.35	24.05	26.27
	T	2.84	3.46	6.15	8.86	11.34	41.16
1	L	0.98	1.14	1.39	6.79	6.79	6.50
	T	0.67	0.62	2.06	4.43	4.43	6.50
3	L	0.73	0.79	1.17	6.79	6.79	6.79
	T	0.84	0.78	1.86	6.50	4.43	6.79
5	L	0.70	0.85	1.23	6.79	6.79	6.79
	T	1.16	0.61	1.69	6.50	4.43	8.86
7	L	0.71	0.88	2.06	4.43	6.79	8.48
	T	0.89	0.83	1.84	6.50	4.43	8.86
9	L	0.66	1.00	1.00	4.43	6.79	4.43
	T	1.10	0.76	1.44	6.50	4.43	4.43
11	L	0.69	1.43	1.01	4.43	13.92	6.79
	T	1.10	1.18	1.44	4.43	6.50	4.43
13	L	0.74	0.82	1.50	4.43	6.79	6.79
	T	0.76	0.71	1.70	6.50	4.43	6.50
15	L	0.72	0.80	1.21	4.43	6.79	6.79
	T	0.80	1.05	3.78	13.92	6.50	12.74

Table 2.5: Damping values obtained using the random decrement technique and the half-power bandwidth method.

The damping values obtained for our structure exhibit distinct trends when analyzed using the Random Decrement Technique (RDT) [25] and the Half-Power Bandwidth Method (HPBM) [10]. The basement and lower stories show relatively higher damping values in both longitudinal (L) and transverse (T) directions, indicating that the foundation and lower parts of the building exhibit more significant energy dissipation, likely due to interaction with the soil and inherent structural characteristics. This trend is consistent with expectations as lower stories often experience more pronounced damping effects due to their direct connection with the ground.

As we move up the structure, the damping values tend to decrease, reflecting the reduced interaction with the ground and potentially stiffer structural behavior

at higher levels. Interestingly, the HPBM results show generally higher damping values compared to RDT, especially at the basement level, which may be attributed to the HPBM's sensitivity to noise and signal variations. This sensitivity leads to higher damping estimates, highlighting the need for a careful interpretation of the results obtained from different methods.

Moreover, the relatively lower damping values observed with RDT across most stories suggest that this method may be less influenced by external noise and more stable in estimating the structure's inherent damping properties. These findings indicate that while HPBM can provide a broader range of damping estimates, RDT offers a more conservative and consistent assessment of the building's dynamic behavior.

The variations in damping values across different floors and between the two methods underscore the importance of using multiple techniques for a comprehensive evaluation of structural damping. Understanding these damping characteristics is crucial for accurate seismic vulnerability assessment and for designing appropriate retrofitting measures to enhance the building's seismic performance.

II.4 Conclusion

This chapter presents the results of ambient vibration experiments, revealing the tower's natural frequencies and mode shapes. The consistency between experimental and empirical data confirms the reliability of ambient vibration analysis. The detailed characterization of structural properties serves as a crucial step in validating the numerical model and enhances our understanding of the building's dynamic behavior.

Chapter 3

Modeling and Numerical Analysis

Modeling and Numerical Analysis

III.1 Introduction

In this chapter, we develop and calibrate a finite element model of the tower using ETABS 18. The focus is on accurately representing the material characteristics, defining the structural elements, and applying both static and dynamic loads. Through detailed modal analysis, we obtain the natural frequencies and vibration modes of the structure. This chapter also addresses discrepancies between experimental and numerical frequencies, which are resolved through a meticulous calibration process. The final model serves as a reliable basis for further seismic performance assessments.

III.2 Tower Description

III.2.1 Introduction

This work aims to study an emblematic structure located in the commune of El Mohammadia, in the wilaya of Algiers. This location is approximately 12 km east of the center of Algiers, in the heart of the Bay of Algiers. In terms of seismic regulations, the Tower is located in a high seismicity zone, specifically classified as Zone III, in accordance with the Algerian Seismic Regulations RPA 99/ V2003 [22].

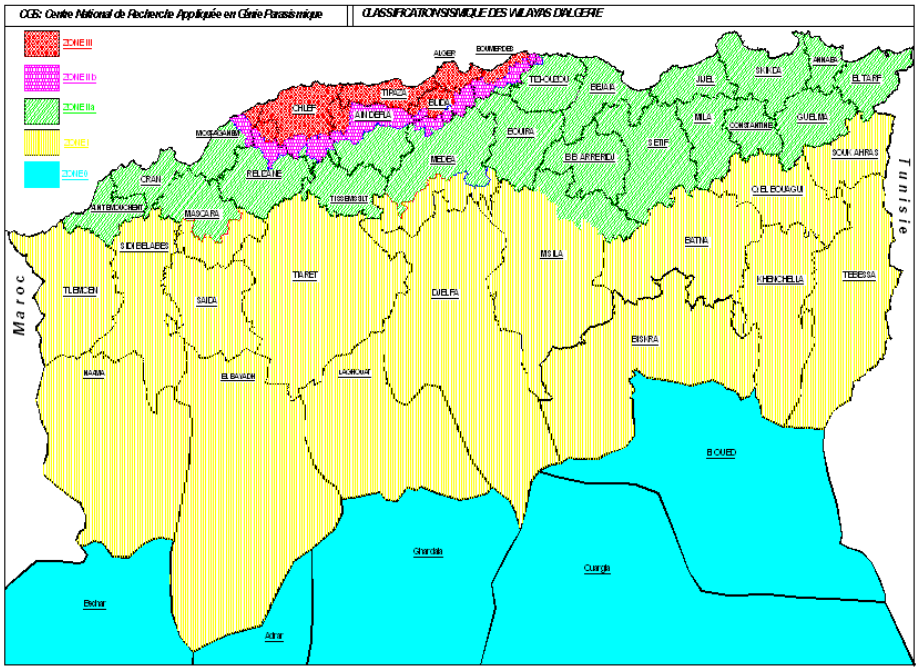

Figure 3.1: Seismic Classification of the Provinces of Algeria

III.2.2 Site Location

The structure is located in the commune of El Mohammadia, in the Bananiers neighborhood, wilaya of Algiers. The Middle School M'hamed Yazid borders it to the north, the Résidence Araucaria to the east, and the national road N11 to the south. Based on previous studies, the site soil is classified as S2 according to the RPA. The map below illustrates the main boundaries and location of the Tower.

Figure 3.2: Overview of the site of the Ministry of Trade and Export Promotion

III.2.3 Building Presentation

The Tower is a civil engineering structure primarily constructed of reinforced concrete, currently used as an administrative office. Designed and built with high-quality construction materials under the supervision of a respected study and execution office, the Tower, constructed in the year 2000, stands at a height of 69.64 meters with a North-South orientation. It consists of 15 floors, in addition to a basement. The bracing of the Tower, ensuring its structural stability, is provided by a central core made of reinforced concrete with a thickness of 40 cm, which means that the behavior coefficient of the structure according to the Algerian seismic regulation is R=3.5. This type of bracing is commonly used in the construction of tower buildings due to its effectiveness in ensuring the stability of structures, particularly in buildings used for residential and office purposes. The bracing core is generally located in the central part of the building to optimize its performance.

Figure 3.3: Ministry Of Trade Tower

III.2.4 Current Use

Currently, the Tower houses the Ministry of Trade and Export Promotion. This usage underscores its central role in the country's public administration, which justifies the choice of usage group 1A according to the Algerian seismic regulation. Using the previously mentioned data and per the provided RPA table, the zone acceleration coefficient is equal to A=0.4.

Groupe	**Zone**			
	I	**IIa**	**IIb**	**III**
1A	0.15	0.25	0.30	0.40
1B	0.12	0.20	0.25	0.30
2	0.10	0.15	0.20	0.25
3	0.07	0.10	0.14	0.18

Table 3.1: Zone Acceleration Coefficient A According to RPA

III.2.5 Material Characteristics

III.2.5.1 Concrete

Concrete is the primary material constituting the structure in this study. Due to the lack of detailed data on its specific properties and current quality, we used the minimum resistance values in accordance with Algerian regulations (RPA) [22] to represent the most unfavorable scenario. Considering the many severe and challenging earthquakes the region has experienced, we have taken into account the potential degradation of materials. The concrete properties used are detailed below.

III.2.5.1.1 Compressive Strength at 28 Days (f_{c28})

To simulate the most unfavorable conditions, the compressive strength at 28 days was defined as follows:

$$f_{c28} = 20 \text{ MPa}$$

III.2.5.1.2 Linear Elasticity Modulus (E_{ij})

The linear elasticity modulus was calculated using the revised BAEL 91 formula:

$$E_{ij} = 11000\sqrt{f_{cj}} = 11000\sqrt{20} = 29858.6 \text{ MPa}$$

This method allows for determining the stiffness of the concrete based on its compressive strength.

III.2.5.1.3 Volumetric Weight (γ)

The volumetric weight of the concrete was defined according to a standard value commonly used in civil engineering calculations:

$$\gamma = 25 \text{ kN/m}^3$$

III.2.5.2 Steel

Due to the lack of specific data on the characteristics of the rebars used in the construction of the building, we have chosen to use Fe500-grade steel for our analysis. Fe500 is a commonly used grade of steel reinforcement with a characteristic yield strength of 500 MPa. Additionally, the modulus of elasticity of the steel is considered to be $E_s = 210,000$ MPa, which is a standard value for structural steel.

III.2.5.3 Identification of Characteristics of Masonry Infill Walls

We lack specific data on the characteristics of masonry infill walls, such as thickness, constitutive material (brick, concrete block, etc.), and compressive strength. In the absence of this information, we adopt the equivalent diagonal strut method according to FEMA guidelines [26].

III.2.5.3.1 Principle

The concept of the equivalent diagonal strut aims to simplify the modeling of masonry infill walls by representing them as simpler and easier-to-analyze structural elements. Concretely, this involves considering the infill wall as a diagonal compression element (strut) connecting adjacent structural elements (beams, columns, etc.) and capable of transferring seismic forces.

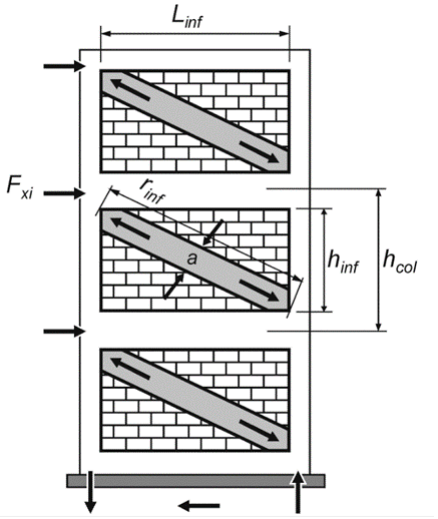

Figure 3.4: Representation of concentric struts in compression.

III.2.5.3.2 Methodology of the Equivalent Strut

According to FEMA recommendations [27], the equivalent diagonal strut represents the action of the infill wall through the introduction of diagonal compression struts. We can calculate the compressive strength of the masonry and the elasticity modulus of the masonry as follows:

$$f_m = 0.433 f_b^{0.64} f_{mo}^{0.36}$$

$$E_m = 550 f_m$$

With:

- $\mathbf{f_b}$: compressive strength of the brick in MPa

- $\mathbf{f_{mo}}$: compressive strength of the mortar in MPa
- $\mathbf{f_m}$: compressive strength of the masonry in MPa
- $\mathbf{E_m}$: elasticity modulus of the masonry in MPa

III.2.5.3.3 Calculation of the Strut Width

The width of the strut is determined based on the mechanical and geometric properties of the infill walls, taking into account the elasticity moduli of the concrete and masonry, the height and diagonal length of the infill panel, as well as the thickness and angle of the strut.

$$w_{ds} = 0.175\alpha_h^{-0.4} L_{ds}$$

With:

$$\alpha_h = h\left(\sqrt{\frac{E_m t \sin^2\theta}{4E_f I_c h}}\right)$$

Where:

- **h**: height of the infill panel
- $\mathbf{E_f}$: expected elasticity modulus of the concrete
- $\mathbf{E_m}$: elasticity modulus of the masonry
- $\mathbf{I_c}$: moment of inertia of the column
- $\mathbf{L_{ds}}$: diagonal length of the infill panel
- $\boldsymbol{\theta}$: angle of the strut

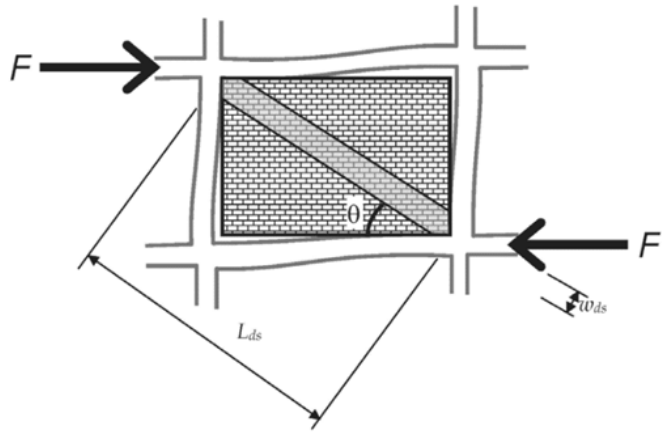

Figure 3.5: Dimensions of the Equivalent Diagonal Strut Model for Masonry Infill Walls.

These formulas allow for determining the necessary properties for accurate modeling of masonry infill walls.

III.3 Modeling

III.3.1 Material Characterization

III.3.1.1 Concrete

The concrete characteristics are defined as determined earlier in **paragraph III.2.5.1**. The results are presented as follows:

- **28-day Compressive Strength**: $f_{c28} = 20$ MPa
- **Linear Elasticity Modulus**: $E_{ij} = 29858.6$ MPa
- **Volumetric Weight**: $\gamma = 25$ kN/m^3

III.3.1.2 Steel

The steel characteristics are defined as determined earlier in **paragraph III.2.5.2**. The results are presented as follows:

- **Characteristic Yield Strength**: $f_y = 500$ MPa
- **Modulus of Elasticity**: $E_s = 210,000$ MPa

III.3.1.3 Characterisation of the Equivalent Strut of Infill Walls

In Algeria, clay bricks with eight holes (100 × 200 × 300 mm) have a compressive strength ranging from 10 to 15 MPa, according to Algerian standards NA 5023 and NA 5024 [28]. In this study, a double-layer infill wall was used, making the wall thickness 200 mm. In the absence of specific data on the characteristics of the infill walls, an average value of 12 MPa for compressive strength has been adopted.

The mortar, composed of a mixture of cement and sand in a 1:3 ratio, has a compressive strength of approximately 15 MPa, in accordance with local standards NA 5084-4.

The compressive strength of the masonry will be calculated using the following equation from **paragraph III.2.5.3.2**:

$$f_m = 0.433\,(12^{0.64}\ 15^{0.36}) = 5.63 \text{ MPa}$$

Therefore:

$$E_m = 550\ (5.63) = 3096.5\ \text{MPa}$$

Using these results in an Excel spreadsheet, it is possible to determine the geometric characteristics of the equivalent strut, as illustrated in **Table 4.8**.

The table below shows the width of the equivalent strut (w_{ds}) for different bay lengths (short (S) and long (L)) across various stories in both X and Y directions. The thickness of the infill panel and the equivalent strut is 200 mm.

bay length	Story	$w_{ds}(m)$
	X-axis	
L	Base - 3rd	0.76
S	Base - 3rd	0.74
L	4th - 8th	0.69
S	4th - 8th	0.68
L	9th - 13th	0.64
S	9th - 13th	0.62
L	14th	0.57
S	14th	0.56
L	15th	0.57
S	15th	0.56
	Y-axis	
S	Base - 3rd	0.77
L	Base - 3rd	1.08
S	4th - 8th	0.71
L	4th - 8th	1.02
S	9th - 13th	0.65
L	9th - 13th	0.93
S	14th	0.57
L	14th	0.82
S	15th	0.59
L	15th	0.82

With:

- w_{ds}**:** the width of the equivalent strut (m)
- t**:** the thickness of the infill panel and the equivalent strut, taken as 200 mm
- **S:** represents a short bay length equal to 4.35 m in the X direction and 4.85 m in the Y direction.
- **L:** represents a long bay length equal to 4.5 m in the X direction and 7.4 m in the Y direction.

III.3.2 Reinforcement Rebars

Rebar reinforcement is pivotal in the tower's structural integrity and seismic performance. This section will delve into the critical aspects of rebar reinforcement, highlighting its importance in enhancing the structure's ductility, strength, and overall resilience during seismic events. Understanding and accurately modeling the reinforcement details are essential for predicting the tower's behavior under lateral loads, which is the primary focus of the vulnerability study.

However, due to our structure's lack of detailed rebar drawings, we will conduct the pushover analysis using two different reinforcement drawings. One plan will be based on the minimum reinforcement requirements specified by the Algerian Seismic Regulation (RPA). At the same time, the other will be calculated using SOCOTEC software after extracting the necessary efforts from the ETABS model.

III.3.2.1 Minimum Reinforcement Specifications According to RPA99

The Algerian seismic regulation RPA99 provides specific guidelines for calculating the minimum reinforcement rebar for different structural elements. These guidelines ensure that the structures have adequate ductility, strength, and overall resilience during seismic events. The specifications are as follows:

- **Beams:** The minimum total percentage of longitudinal reinforcement must be 0.5% of the concrete section along the entire length of the beam.
- **Columns:** The longitudinal reinforcement must have high adhesion and be straight without hooks. In Seismic Zone III, the minimum percentage of longitudinal reinforcement must be 0.9% of the concrete section.
- **Shear Walls:** The minimum vertical and horizontal reinforcement percentage must be 0.15% of the concrete section. The spacing of the horizontal and vertical bars must be less than the smaller of 1.5 times the thickness of the wall or 30 cm.

III.3.2.2 Calculated Reinforcement Rebar

Using SOCOTEC software, based on BAEL91, after extracting the necessary efforts from the ETABS model. This approach involves determining the required

reinforcement by analyzing the structural response to applied loads, ensuring that the reinforcement is optimized for the actual demands on the structure. By doing so, we can achieve a more precise and reliable reinforcement scheme that reflects the specific conditions and requirements of the building.

The following table exhibits the rebar section results for each element according to Minimum Reinforcement Specifications and the calculated reinforcement:

Dimensions (cm)	Min. Required Reinforcement Area (cm²)	Calculated Reinforcement Area (cm²)	Status	Adjusted Reinforcement Area (cm²)
Columns				
100 X 100	90	71.44	Not Verified	90
80 X 80	57.6	44.71	Not Verified	57.6
60 X 60	32.4	19.64	Not Verified	32.4
40 X 40	14.4	50.26	Verified	50.26
80 X 60	24	40.1	Verified	40.1
Beams				
80 X 50	20	37.48	Verified	37.48
80 X 40	16	24.7	Verified	24.7
80 X 30	12	67.44	Verified	67.44
60 X 60	18	67.76	Verified	67.76
60 X 50	15	51.6	Verified	51.6
60 X 40	12	8.88	Not Verified	12
40 X 40	8	46.18	Verified	46.18
Shear Walls				
400 X 40	42.8	87.92	Verified	87.92
170 X 40	18.19	43.26	Verified	43.26

Table 3.2: Reinforcement Area Calculation for Structural Elements Based on SOCOTEC Analysis and RPA Standards.

III.3.3 Element Sections

Columns, beams, floors, stairs, shear walls

To accurately simulate the structural behavior of our building, we defined specific dimensions for various structural elements based on the architectural plans, including Columns, principal beams, secondary beams, floors, stairs, shear walls, and parapets. For further details on these sections, please check the appendices **Figure 4.23**.

III.3.4 Definition of Static Loads G and Q

When modeling the structural elements (columns, beams, shear walls, floors, etc.), which are made of concrete, the software calculates the self-weight of these elements using the weight per unit volume of concrete. We introduce additional permanent loads and live loads (G_{add} and Q) due to floors, masonry partition walls, and elevators.

For the estimation of additional permanent loads and operational live loads, the values considered are shown in the following table:

Element	**Additional Dead Loads (G_{add}) (KN/m²)**	**Live Loads (Q) (KN/m²)**	**Source**
Standard floor	1.8	2.5	DTR B.C 22 [29]
Inaccessible terrace	3.07	1.5	DTR B.C 22 [29]
Elevator slab	12.66	4.22	Standard elevator technical sheet
Masonry partition walls	1	/	DTR B.C 22 [29]
Curtain walls	0.868 m	/	Standard curtain wall technical sheet

Table 3.3: Estimation of additional permanent loads and operational live loads

Note: *The curtain wall is distributed along the perimeter of the structure, and its linear load is 0.868 kN/m. This value represents the additional dead load applied uniformly along the structure's edge.*

III.3.5 Definition of Mass Source

In Mass Source, permanent and operating loads to be considered for dynamic analysis are defined. According to RPA 99/V2003 [22], the loads are taken as follows:

$$G + \beta Q$$

Where:

$$G = G_{\text{self-weight}} + G_{add}$$

With β, the weighting coefficient is taken as 0.2 for our building, which is used as an administrative office.

III.4 Results and Interpretation

III.4.1 Modal Analysis

The following table presents the mass participation ratios of the structure with calculated reinforcement in both longitudinal and transversal directions, highlighting the contribution of different modes to the overall dynamic behavior of the structure.

Mode	Frequency (Hz)	Period (s)	UX (%)	UY (%)	SumUX (%)	SumUY (%)
Longitudinal						
1	0.643	1.555	69.11	0.0005543	69.11	0.000005543
4	1.78	0.562	15.16	0.00009616	84.27	0.000101703
7	3.194	0.313	5.81	0	90.08	0.000101703
Transversal						
2	0.743	1.347	0.001072	65.95	0.001072	65.95
6	2.186	0.457	0.00007448	17.62	0.00114648	83.57
9	4.141	0.242	0	6.75	0.00114648	90.32

Table 3.4: Mass Participation Ratios of the Structure in Longitudinal and Transversal Directions.

The table above indicates that the first mode has more than 65% mass participation ratio, which is expected as it represents the dominant mode of the structure's dynamic response. Additionally, the sum of the mass participation ratios in the longitudinal direction (X Direction) exceeds 90% within the first three modes, as required by the RPA regulations [22]. The same can be said about the transversal direction. This compliance ensures that the dynamic behavior of the

structure is adequately captured within the first few modes, which is essential for accurate seismic design and analysis.

The following figures illustrate the mode shapes corresponding to the significant vibration modes of the structure. These visual representations provide a clearer understanding of how the structure deforms under each mode.

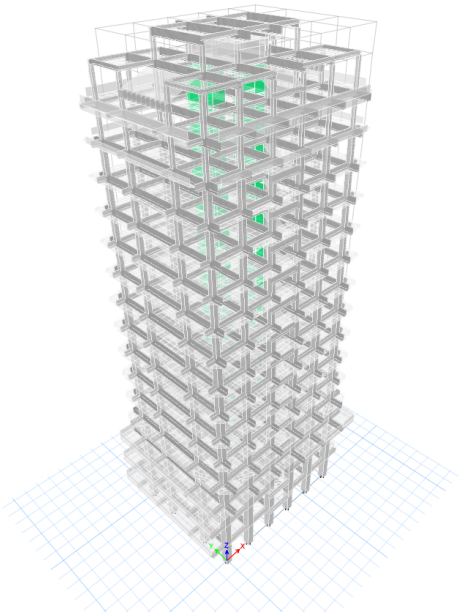

Figure 3.6: First longitudinal mode (Mode 1).

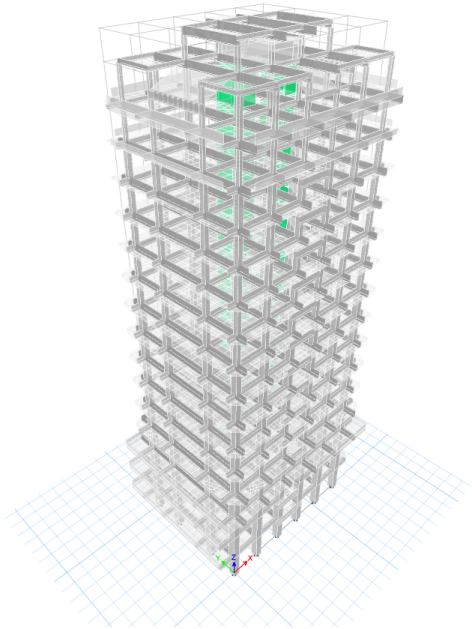

Figure 3.7: First transversal mode (Mode 2).

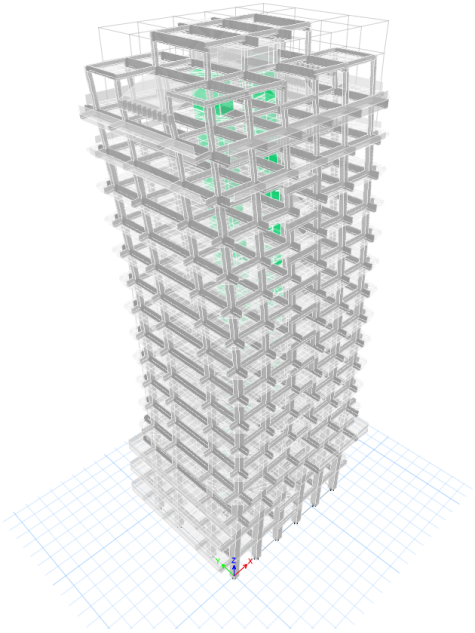

Figure 3.8: Second longitudinal mode (Mode 4).

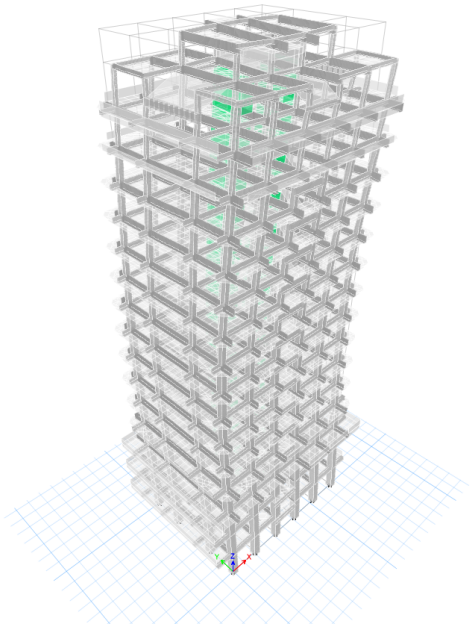

Figure 3.9: Second transversal mode (Mode 6).

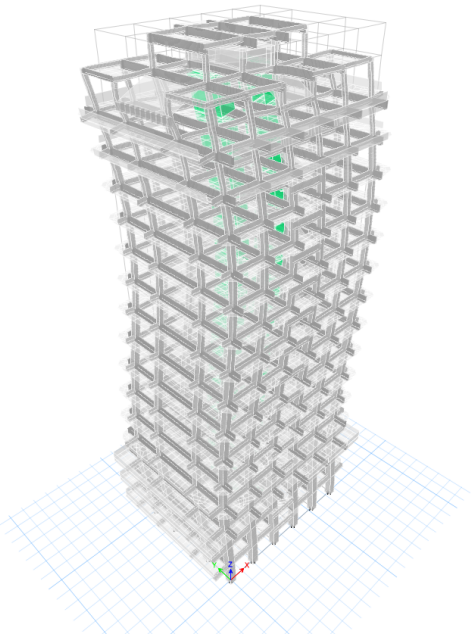

Figure 3.10: Third longitudinal mode (Mode 7).

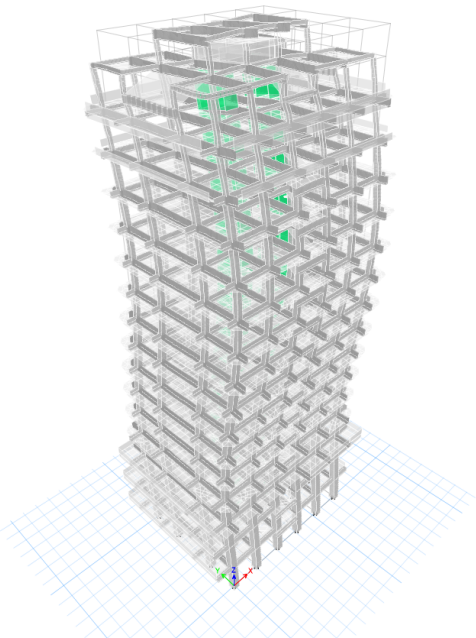

Figure 3.11: Third transversal mode (Mode 9).

III.5 Direct Natural Frequency Comparison

The most common and straightforward approach correlating two modal models is directly comparing natural frequencies. This method involves comparing the

experimental and numerical modal frequencies directly. If the experimental and numerical values overlap significantly, the data is considered perfectly correlated.

Methodology

The percentage error for each mode can be defined as:

$$\epsilon_i = \left| \frac{f_{exp}i - f_{num}i}{f_{exp}i} \right| 100$$

Where:

- $f_{exp}i$ is the experimental frequency for mode i
- $f_{num}i$ is the numerical frequency for mode i

Additionally, a global frequency dispersion indicator can be used to measure the overall accuracy:

$$\phi_A = \left[\frac{\sum_{i=1}^{L} (f_{exp}i - f_{num}i)^2}{\sum_{i=1}^{L} f_{exp}i^2} \right]^{1/2} 100$$

Where:

- L is the number of measured natural frequencies or modal shapes within the range of interest.

III.5.1 Comparison Between Experimental and Numerical Frequencies

For the Comparison, we only used the first mode of the 15th floor, as it has the highest mass participation ratio. This ensures that the structure's most significant dynamic behavior is considered.

Mode	Direction	Experimental Frequencies (Hz)	Numerical Frequencies (Hz)	Error (%)
1	L	0.72	0.643	11.10
1	T	0.76	0.743	1.72

Table 3.5: Comparison between experimental and numerical frequencies.

The results show that the initial numerical analysis has an error of 11.10% in the longitudinal direction (L) and 1.72% in the transversal direction (T). These

discrepancies may be attributed to the sensitivity of the ambient vibration method, which often overestimates the stiffness of structures due to the nature of the low-amplitude vibrations recorded.

To confirm this hypothesis and improve the accuracy of the numerical model, we proceed to the calibration part.

III.6 Calibration of the Numerical Model

The calibration process involves adjusting the model parameters to better match the experimental frequencies, thereby reducing errors and ensuring a more accurate representation of the structure's dynamic behavior. This is achieved by comparing the structure's frequency to the ambient vibration frequency and finding a reasonable configuration for masonry walls that minimizes the error. An iterative procedure was employed to find the optimal configuration, adjusting parameters and re-evaluating the model until the discrepancies between the experimental and numerical frequencies were minimized.

The reasons for choosing the masonry walls as a parameter in the calibration process are twofold:

- **Overestimation of Stiffness:** Ambient vibrations tend to overestimate the structure's stiffness by considering the stiffness of non-structural elements. Including masonry walls helps account for this effect and provides a more realistic representation of the structure's stiffness.

- **Lack of Exact Data:** There was a lack of data on the exact positioning of masonry walls in the tower. Therefore, an iterative process was necessary to determine a reasonable configuration that accurately represents the building's dynamic behavior.

A crucial factor in this process was the positioning of the masonry walls. A layout based on general construction practices and the intended use as office spaces was suggested. The walls were arranged symmetrically to avoid torsional effects, ensuring structural stability and functionality. This approach helped achieve a more accurate and practical representation of the building's dynamic behavior.

III.6.1 Results

The positioning of the masonry walls is consistent from the base to the 14th story, while the 15th story has a different distribution due to specific design requirements, as illustrated in the figures below.

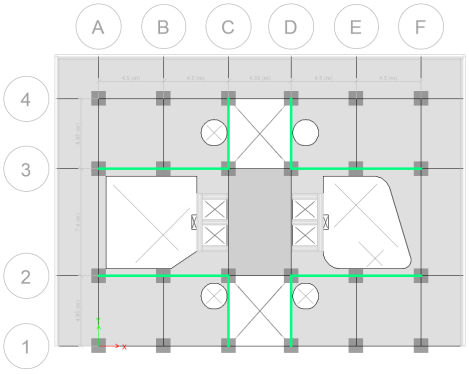

Figure 3.12: Masonry wall distribution from base to 14th story.

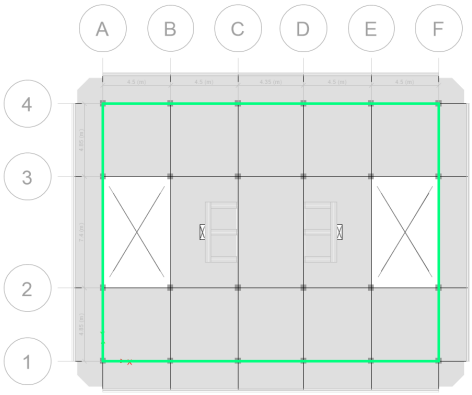

Figure 3.13: Masonry wall distribution on the 15th story.

The table below compares the experimental frequencies obtained from ambient vibration measurements with the numerical frequencies calculated using ETABS for the first mode after calibration.

Mode	Direction	Experimental Frequencies (Hz)	Numerical Frequencies (Hz)	Error (%)
1	L	0.72	0.69	4.60
1	T	0.76	0.754	0.26

Table 3.6: Comparison of experimental and numerical frequencies after calibration.

III.6.2 Interpretation:

The error of 4.60% in the longitudinal direction shows that the numerical model closely approximates the structure's actual dynamic behavior, making it reliable for further analysis and design. In the transversal direction, the very small error of 0.26% indicates an excellent match, suggesting that the calibrated model accurately captures the first mode's frequency. This near-perfect correlation implies that the model's assumptions and parameters are well-aligned with the building's actual dynamic characteristics, providing high reliability and precision in predictions.

Direction	Exp (Hz)	Num (Hz)	Num2 (Hz)	Err (%)	Err2 (%)
L	0.72	0.643	0.69	11.10	4.60
T	0.76	0.743	0.754	1.72	0.26

Table 3.7: Comparison of experimental and numerical frequencies of the 1^{st} mode before and after calibration.

The calibrated results demonstrate that the numerical model accurately represents the dynamic behavior of the Ministry of Trading building in both the longitudinal and transversal directions. The errors in both directions are within acceptable limits, confirming the model's effectiveness and reliability. This accuracy provides confidence in the model's use for seismic performance assessments and structural analysis, ensuring the safety and reliability of the building design.

III.7 Conclusion

This chapter has detailed the comprehensive process of modeling and numerical analysis conducted for the Ministry of Trading building. Initially, the material characterization was established using concrete and masonry properties according to Algerian regulations. The structural elements, including columns, beams, and shear walls, were modeled, and both static and dynamic loads were defined.

The modal analysis provided insights into the natural frequencies and vibration modes, revealing the structure's dominant dynamic responses. Comparing experimental and numerical frequencies highlighted initial discrepancies, which were addressed through a meticulous calibration process. By iteratively adjusting the model parameters, particularly the configuration of masonry walls, we significantly reduced the errors.

The final calibrated model demonstrated a close approximation of the building's dynamic behavior, with errors within acceptable limits for engineering applications. This validation ensures the model's reliability for further seismic performance assessments and structural analysis.

Chapter 4

Vulnerability Study

Vulnerability Study

IV.1 Introduction

In this chapter, we conduct a seismic vulnerability assessment of the tower. Starting with an elastic linear analysis, we use static equivalent and modal spectral methods per RPA99/2003 guidelines to establish a baseline. We then perform a nonlinear pushover analysis to evaluate the structure's performance beyond the elastic range, identifying potential weaknesses and assessing reinforcement strategies. Finally, we use the European Macroseismic Scale 1998 (EMS-98) to provide a comprehensive understanding of the tower's seismic performance.

IV.2 Elastic Linear Analysis

IV.2.1 Introduction

The primary goal of this study is to assess the seismic vulnerability of our structure. By analyzing the seismic characteristics, such as seismic responses (deformations, displacements, internal forces), frequencies, and natural vibration modes, we can evaluate its behavior under seismic events. This information is crucial for ensuring the building's stability, resistance to dynamic loads, and the safety of its occupants. The seismic analysis and verification of results are carried out in accordance with RPA99/2003 regulations [22] to provide a comprehensive assessment of the building's seismic performance.

IV.2.2 Seismic Analysis

the RPA99/2003 regulations propose three methods, each with specific conditions for application. The methods are as follows:

- Equivalent static method

- Modal spectral analysis method
- Dynamic analysis method using accelerograms

In this chapter, we will focus on the equivalent static method and the modal spectral analysis method.

IV.2.2.1 Equivalent Static Method

The principle of this method is to replace the real dynamic forces with a system of fictitious static forces applied in two main directions of the structure if certain conditions are met. One of the main conditions that is not met for the studied building is its height, which exceeds 30 meters, the maximum height in a high seismicity zone (RPA99/2003) [22].

IV.2.2.1.1 Calculation of Seismic Force

In this method, the effective intensity of the total seismic force V applied at the base of the structure must be calculated successively in both orthogonal horizontal directions as the maximum shear force using the following formula:

$$V = \frac{A\ D\ Q}{R}\ W$$

- **A**: Zone Acceleration Coefficient
- $\mathbf{D_x}$: Dynamic Amplification Factor
- **Q**: Quality Factor
- **R**: Behavior Coefficient
- **W**: Seismic Weight

A. Total Weight of the Structure (W)

The total weight is the sum of the weights W_i calculated at each level i:

$$W = \sum_{i=1}^{n} W_i \quad \text{with} \quad W_i = W_{Gi} + \beta W_{Qi}$$

Where:

- W_{Gi}: Weight due to permanent loads
- W_{Qi}: Live loads

- β: Weighting coefficient (0.2 for residential buildings, offices or similar [22])

Story	Weight (kN)
Top	1324.392594
Terrace	4625.575959
Story 15	6725.28289
Story 14	6692.374813
Story 13	6861.162852
Story 12	6858.810825
Story 11	6861.162852
Story 10	6858.810825
Story 9	7516.108112
Story 8	7858.82817
Story 7	7858.82817
Story 6	7858.82817
Story 5	7858.82817
Story 4	9070.398982
Story 3	11623.97003
Story 2	10513.97777
Story 1	10053.22095
Base	1926.080977
Total weight	**128946.6431**

Table 4.1: Seismic weights of the structure.

B. Fundamental Period

The value of the fundamental period (T) of the structure can be estimated using empirical formulas or calculated through analytical or numerical methods. According to paragraph 4.2.4 of RPA99 version 2003, the empirical formula to be used is given as follows (formula 4.6 of RPA99 version 2003) [22]:

$$T_{\text{empirical}} = C_T h_N^{3/4}$$

Where:

- h_N is the height measured in meters from the structure's base to the top level (N): 69.64 m.

- C_T is a coefficient depending on the bracing system and the type of infill, as given in **Table 2.2** of RPA99 version 2003 [22].

In case numbers 3 and 4, the following formula can also be used:

$$T = \frac{0.09 h_N}{\sqrt{D}}$$

Where:

- D is the dimension of the building measured at its base in the direction considered.

In this case, the smallest of the two values given should be retained for each direction considered.

The bracing of the structure is provided by a central core made of reinforced concrete shear walls, giving a coefficient C_T of 0.05.

Given that the total height of the structure is 69.64 meters, we can conclude:

$$T_{\text{empirical}} = 0.05\ (69.64^{3/4}) = 1.21 \text{ s}$$

The calculation is then performed according to **UBC 88 formula** in the X and Y directions, resulting in:

$$L_x = 22.35 \text{ m} \quad \Rightarrow \quad T_{Dx} = 1.33 \text{ s}$$
$$L_y = 17.1 \text{ m} \quad \Rightarrow \quad T_{Dy} = 1.52 \text{ s}$$

The Empirical periods to be considered will be the minimum calculated between the two formulas, giving:

$$T_x = 1.21 \text{ s}$$
$$T_y = 1.21 \text{ s}$$

As for the numerical periods, they are obtained from the finite element model using the ETABS 18 software:

$$T_{\text{numerical\_x}} = 1.45 \text{ s}$$
$$T_{\text{numerical\_y}} = 1.33 \text{ s}$$

After performing the calculations for the numerical and Empirical periods, it remains to verify if the condition required by RPA [22] is satisfied or not:

$$T_{\text{numerical}} < 1.3\ T_{\text{Empirical}} \quad \Rightarrow \quad 1.39 \text{ s} < 1.3\ (1.21) = 1.573 \text{ s}$$
$$\Rightarrow \text{Thus, the condition is satisfied.}$$

Since the condition is satisfied, the periods retained for calculating the dynamic amplification factor D for the X and Y axes are the numerical periods:

$$T_x = 1.45 \text{ s}$$

$$T_y = 1.33 \text{ s}$$

C. Dynamic Amplification Factor

The parameter D depends on the site category, the damping correction factor η, and the fundamental period of the structure T. The dynamic behavior of the structure, influenced by these factors, is expressed by the following piecewise function:

$$D = \begin{cases} 2.5\eta & 0 \leq T \leq T_1 \\ 2.5\eta \left(\frac{T_2}{T}\right)^{\frac{2}{3}} & T_2 \leq T \leq 3s \\ 2.5\eta \left(\frac{T_2}{3}\right)^{\frac{2}{3}} \left(\frac{3}{T}\right)^{\frac{5}{3}} & T \geq 3s \end{cases}$$

After performing the necessary calculations for the seismic parameters, the resulting coefficients are presented in the table below. These coefficients will be used in the calculation of the Total Static Force.

Parameter	**Symbol**	**Value**
Zone Acceleration Coefficient	A	0.40
Quality Factor	Q	1.25
Structural Behavior Coefficient	R	3.5
Characteristic Period 1	T_1	0.15 s
Characteristic Period 2	T_2	0.40 s
Fundamental Period (X-axis)	T_x	1.45 s
Fundamental Period (Y-axis)	T_y	1.33 s
Dynamic Amplification Factor (X-axis)	D_x	0.756
Dynamic Amplification Factor (Y-axis)	D_y	0.789
Percentage of Critical Damping	ξ	10%
Damping Correction Factor	η	0.76

Table 4.2: Seismic parameters used in the analysis.

Based on the provided results of the seismic parameters, we obtained the following seismic forces in both X and Y directions:

X Direction:

$$V_x = \frac{A\ D_x\ Q}{R}\ W = 13925.24 \text{ kN}$$

Y Direction:

$$V_y = \frac{A\ D_y\ Q}{R}\ W = 14518.77 \text{ kN}$$

IV.2.3 Response Spectrum

The Algerian seismic code RPA99 version 2003 [22] specifies a response spectrum used to determine the spectral acceleration as a function of the system's period, which is used to evaluate the elastic response of the structure under seismic loads.

- **Response Spectrum Formula**

$$\frac{S_a}{g} = \begin{cases} 1.25A\left(1 + \frac{T}{T_1}\left(2.5\eta\frac{Q}{R} - 1\right)\right) & 0 \le T \le T_1 \\ 1.25A\left(2.5\eta\frac{Q}{R}\right) & T_1 \le T \le T_2 \\ 1.25A\left(2.5\eta\frac{Q}{R}\right)\left(\frac{T_2}{T}\right)^{\frac{2}{3}} & T \ge T_2 \end{cases}$$

Where :

- **A**: Zone acceleration coefficient
- $\boldsymbol{\eta}$: Damping correction factor
- **R**: Structural behavior coefficient
- $\mathbf{T_1}, \mathbf{T_2}$: Characteristic periods associated with the site category
- **Q**: Quality factor defined as $Q = 1 + \sum P_q$, where P_q are the penalty factors

To calculate the response spectrum, we used the RPA99 software, which allowed us to input the necessary parameters for our specific structural and seismic conditions. By implementing these parameters, we were able to generate the response spectrum as shown in **Figure 4.1**. This response spectrum illustrates the relationship between acceleration and the period, providing critical insights into the dynamic response of the structure under seismic loading conditions.

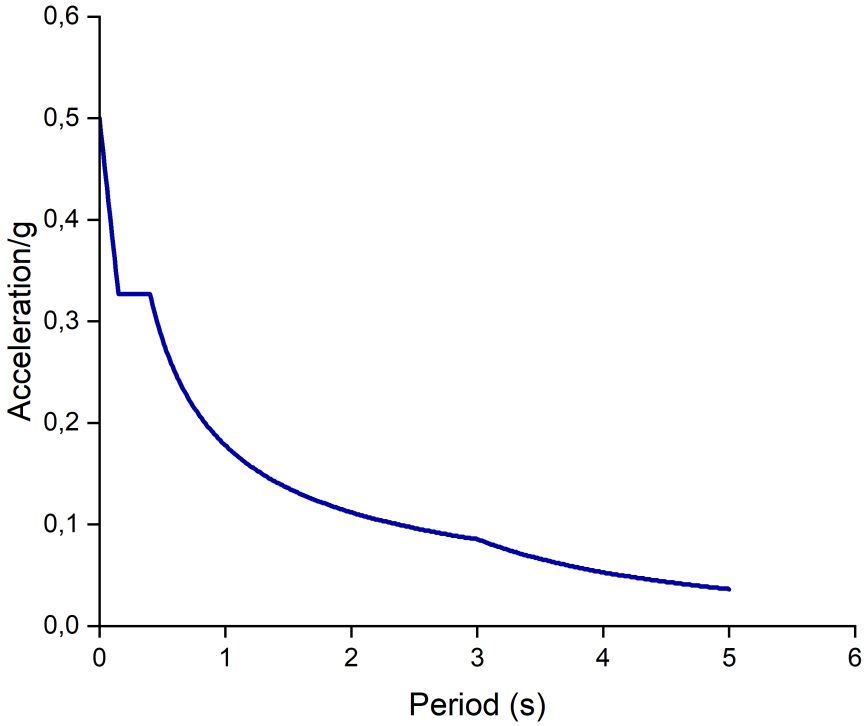

Figure 4.1: Response Spectrum

IV.2.4 Verification of Total Static Force

The resultant seismic forces at the base V_{dyn} are obtained by combining the modal values (**ETABS 18**) and should not be less than 80% of the resultant seismic forces determined by the equivalent static method V_{stat} for a given fundamental period by the appropriate **formula**.

X Direction:

$$\frac{V_{\mathrm{dyn/x}}}{V_{\mathrm{stat/x}}} = \frac{12059.14}{13925.24} = 0.866$$

Y Direction:

$$\frac{V_{\mathrm{dyn/y}}}{V_{\mathrm{stat/y}}} = \frac{12791.75}{14518.77} = 0.881$$

Condition:

$$\frac{V_{\mathrm{dyn}}}{V_{\mathrm{stat}}} \geq 0.8$$

Thus:

- **X Direction:** $\dfrac{V_{\text{dyn/x}}}{V_{\text{stat/x}}} = 0.866 \geq 0.8$
- **Y Direction:** $\dfrac{V_{\text{dyn/y}}}{V_{\text{stat/y}}} = 0.881 \geq 0.8$

$\Rightarrow$ Both conditions for the resultant seismic forces in the X and Y directions are satisfied:

IV.2.5 Verification of the maximum story drift

The structure will undergo deformations in the plane (o, x, y) under horizontal seismic action. The horizontal displacement at each level k of the structure is calculated as follows:

$$\delta_k = R\delta_{ek}$$

Where:

- $\delta_{\mathbf{k}}$: Horizontal displacement at each level k of the structure
- $\delta_{\mathbf{ek}}$: Displacement due to seismic forces F_{iy} including torsion
- **R**: Structural behavior coefficient

The relative displacement at level k compared to $k-1$ is equal to:

$$\Delta_k = \delta_k - \delta_{k-1}$$

The RPA stipulates that relative displacements should not exceed 1% of the floor height (limit displacement):

$$\Delta_k^{\text{limit}} = 1\% h_e$$

Where h_e is the free height of the considered floor.

Therefore, it must be verified in both directions that:

$$\Delta_k \leq \Delta_k^{\text{limit}}$$

$$\Rightarrow \quad \text{Max story drift} = \frac{\Delta_k}{h_e} \leq 1\%$$

The following graphs illustrate the maximum story drifts (%) for the X and Y directions, compared to the story drift limit.

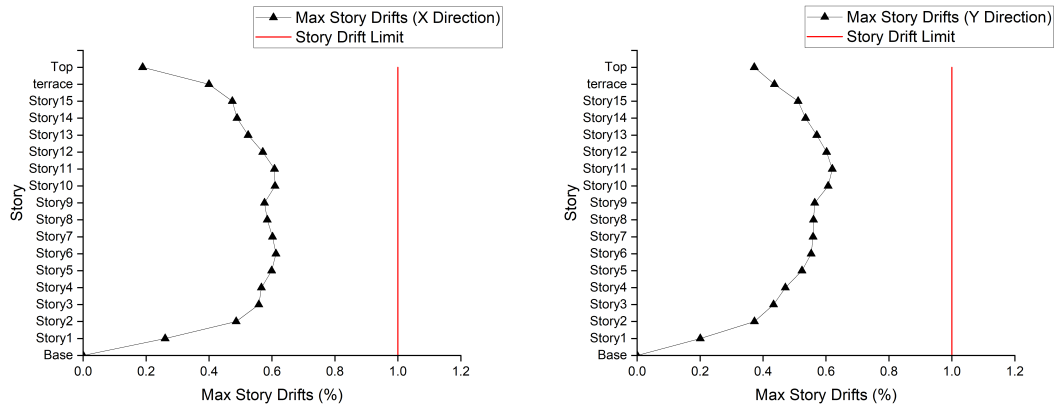

Figure 4.2: Maximum Story Drifts for X and Y directions.

The graphs of maximum story drifts in the X and Y directions indicate that the middle stories (Story 6 to Story 10) experience significant increases in drifts. However, these drifts remain below the 1% limit, indicating compliance with the RPA seismic regulations. The structural design effectively maintains the drifts within acceptable limits, ensuring the building's seismic performance meets the required standards.

IV.2.6 Conclusion

The modal spectral analysis and the equivalent static analysis showed that the structure can effectively resist seismic loads, meeting the RPA99/2003 regulations. The total static force and maximum story drifts verifications confirmed that the structure's response is within acceptable limits.

However, to fully understand the structure's capacity beyond its elastic limit under seismic demands, a nonlinear analysis is necessary. This will provide a comprehensive evaluation of the structure's performance and ensure its resilience against seismic forces.

In summary, while the linear analysis confirms the structure's ability to withstand seismic loads effectively, further nonlinear analysis is required to determine its ultimate capacity and ensure safety beyond the elastic range.

IV.3 Nonlinear Analysis

IV.3.1 Introduction

The pushover analysis is ideal for evaluating the seismic vulnerability of buildings due to its simplicity and efficiency compared to other nonlinear methods. Unlike dynamic time-history analysis, which requires significant resources and complex

modeling, pushover analysis enables a rapid assessment of lateral resistance capacities with fewer resources. It identifies plastic hinges and inelastic behaviors, which are crucial for seismic strengthening while providing detailed information on performance points. We chose pushover analysis for our study because of its simplicity, efficiency, and ability to quickly provide reliable results while being robust enough to identify potential failure mechanisms and evaluate the overall performance of the structure.

IV.3.2 Nonlinear Behavior of Construction Materials

IV.3.2.1 Concrete

The nonlinear behavior of concrete was modeled using the Mander stress-strain curve definition in ETABS. This model effectively captures the enhanced strength and ductility of confined concrete. We selected the Concrete Hysteresis type to accurately represent the cyclic behavior of concrete, including stiffness degradation and strength deterioration under repeated loading.

The resulting stress-strain relationship for both confined and unconfined concrete is depicted in the following figure.

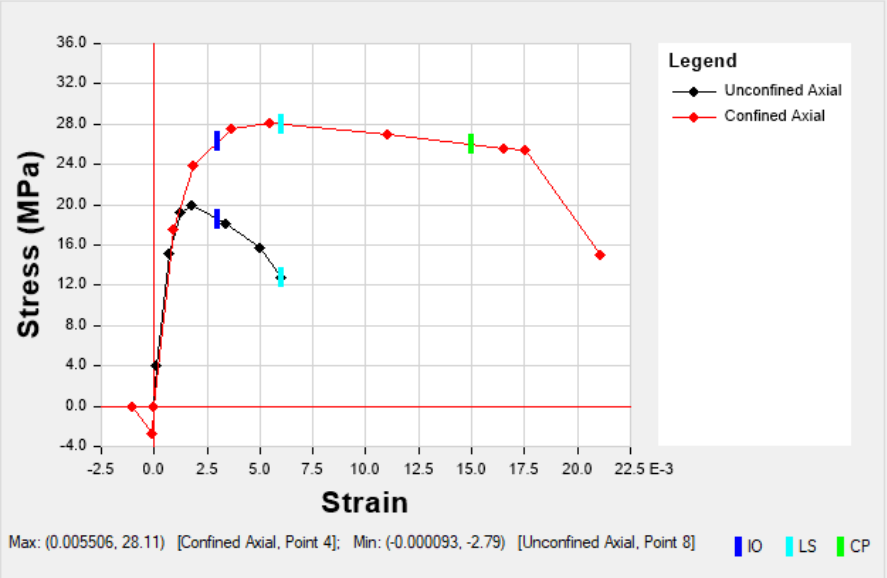

Figure 4.3: concrete behavior

IV.3.2.2 Rebar

For rebar, the Park stress-strain curve option was used in ETABS to capture the detailed behavior, including the elastic phase, yield plateau, and strain hardening region. We chose the Kinematic Hysteresis type to reflect the cyclic behavior of rebar, particularly the Bauschinger effect, which is crucial for modeling energy dissipation and inelastic deformation during seismic events.

The resulting stress-strain relationship for rebar is illustrated in the following figure.

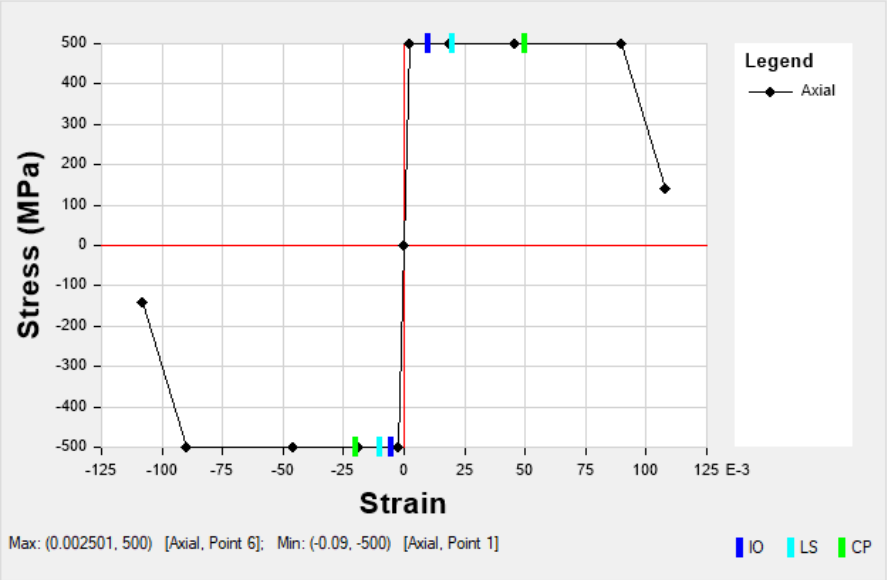

Figure 4.4: Stress-Strain Relationship for Rebar

IV.3.3 Implementation of Nonlinear Behavior in Structural Elements Using ETABS (Plastic Hinges)

- **Beams:** The M3 auto hinges were assigned to beam elements at the locations where a maximum moment is expected, typically at the ends near the beam-column joints. These hinges were placed at the relative distances of 0 and 1 along the length of the beams. ETABS automatically generates the hinge properties based on the specified ASCE 41-13 parameters.

- **Shear Walls:** Auto fiber P-M3 hinges were applied to shear walls, utilizing fiber sections to model the interaction of axial forces and flexural moments. This approach ensures a detailed simulation of the wall's nonlinear response under seismic loading.

- **Columns:** Fiber P-M2-M3 hinges were assigned to column elements at the relative distances of 0 and 1 along the length of the columns, with a hinge length of 0.5 times the column width. This configuration allows for a realistic representation of the column's behavior under combined axial and bending loads.

By incorporating these hinge definitions, the ETABS model effectively captures the nonlinear behavior of the tower's structural elements, providing a robust framework for seismic performance assessment and vulnerability analysis.

IV.3.4 Elastic Spectrum

In nonlinear analyses such as pushover analysis, the structure's inelastic behavior is directly simulated. Therefore, the behavior modification factors used in linear analyses are unnecessary, resulting in the response modification factor R being set to 1. Similarly, the quality factor Q, which accounts for redundancy, regularity, and quality control, is also set to 1. The other factors will remain the same as shown in **Table 4.2**.

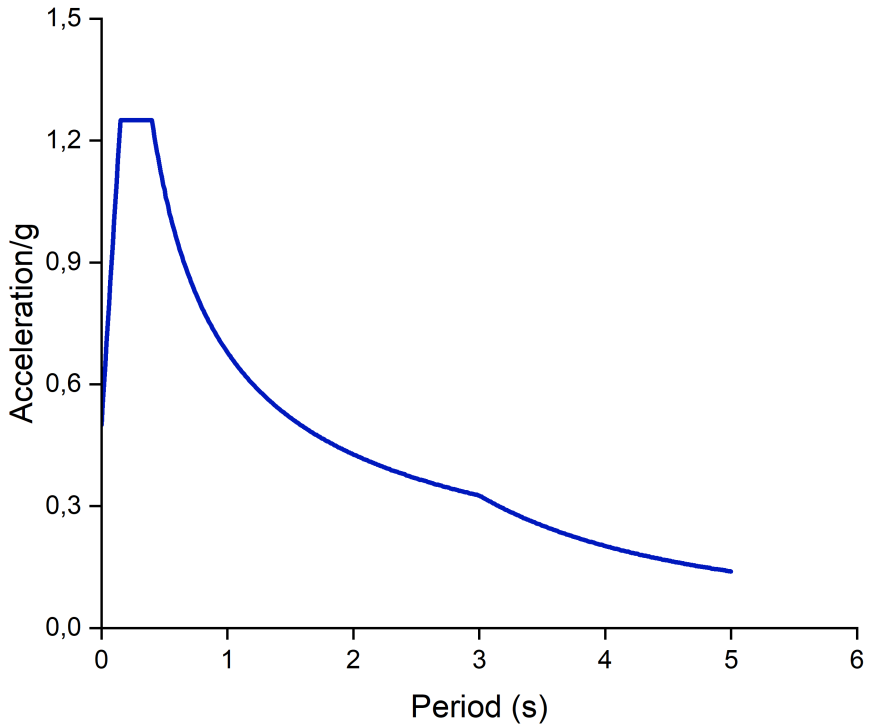

Figure 4.5: Elastic Spectrum

IV.3.5 Lateral Load Distribution

According to FEMA 356 guidelines [30], we adopted both uniform and modal distribution patterns for lateral loading in our pushover analysis. The uniform distribution applies a consistent load across all floors, simulating seismic forces in a simplified manner. The modal distribution, based on the building's fundamental vibration mode, accounts for dynamic characteristics. Using both patterns allows for a comprehensive evaluation of the building's seismic performance, identifying potential weaknesses and failure mechanisms under various loading scenarios.

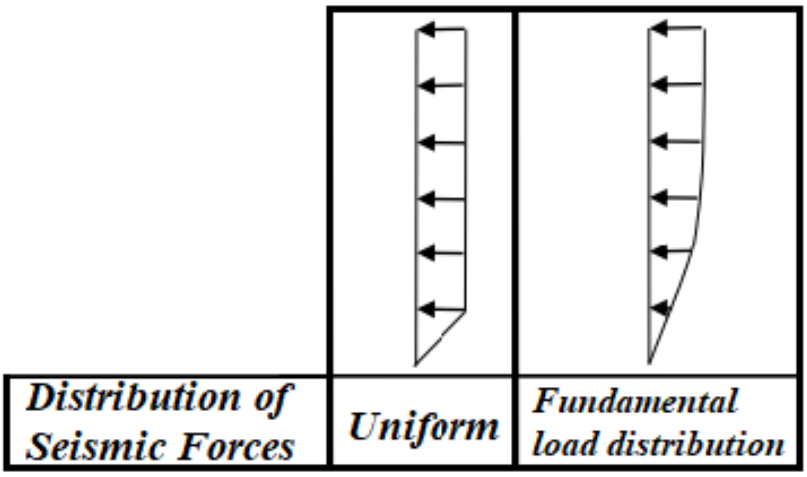

Figure 4.6: Seismic Force Distribution Patterns: Uniform and Modal

IV.3.6 Pushover Analysis Results

The pushover analysis results provide critical insights into the nonlinear behavior of the structure under seismic loading. In this section, we present the findings from the pushover analysis, focusing on capacity curves, performance points, and story drifts. The analysis is conducted for two cases of reinforcement minimal and calculated under two loading scenarios: fundamental mode loading and uniform loading.

IV.3.6.1 Fundamental Mode Distribution

IV.3.6.1.1 Capacity curves

The capacity curves under fundamental mode loading distribution illustrate the structural response to increasing lateral loads for both minimal and calculated reinforcement. These curves help identify the yield and ultimate capacities of the building.

The following figures represent the capacity curves in both the X and Y directions.

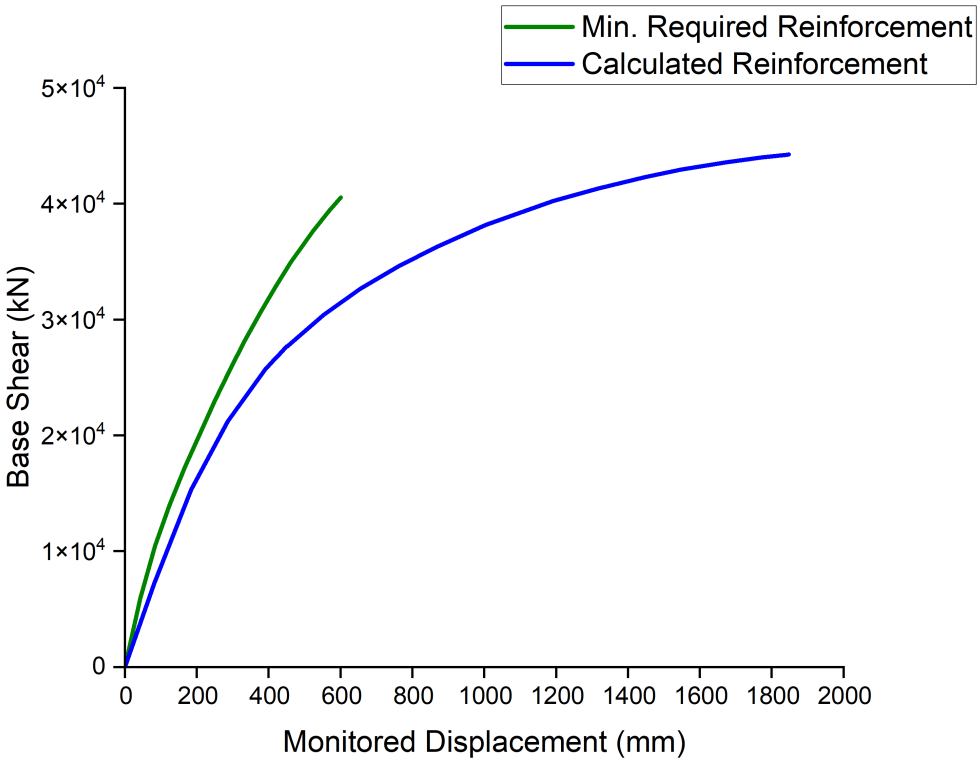

Figure 4.7: Capacity Curves Under Fundamental Mode Loading in the X-Direction

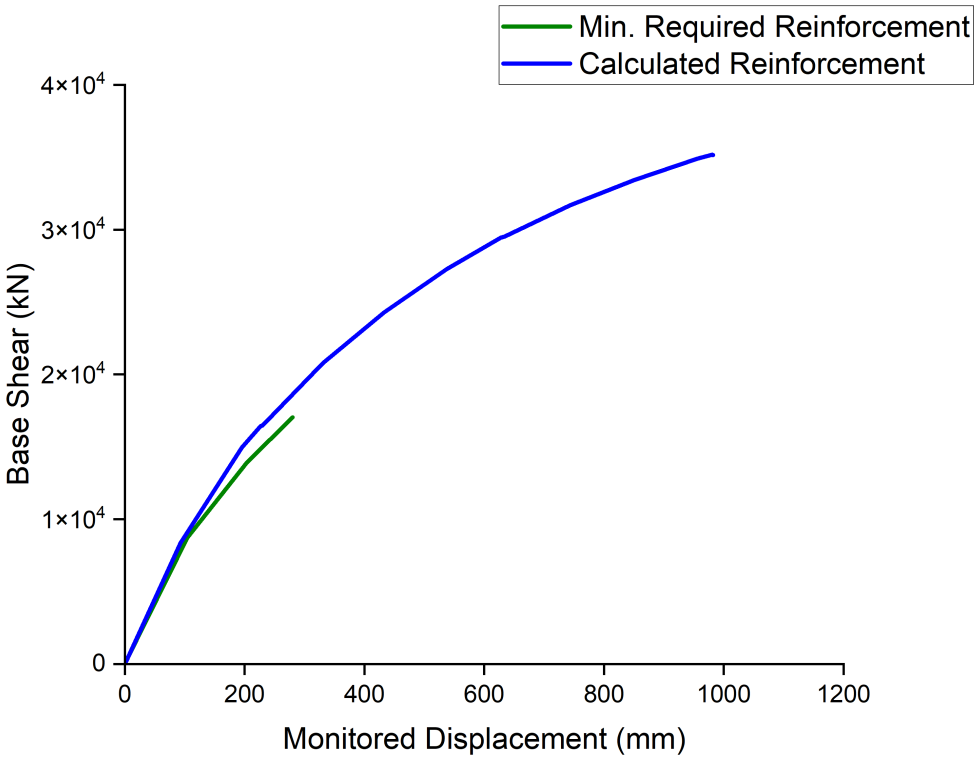

Figure 4.8: Capacity Curves Under Fundamental Mode Loading in the Y-Direction

The pushover analysis in both the X and Y directions shows that the calculated reinforcement significantly enhances the structural capacity under seismic loading compared to the minimum required reinforcement.

The interpretation of the capacity curves has provided a clear comparison of the performance between minimal and calculated reinforcement under seismic loading. Utilizing the data extracted from these graphs, we now proceed to the verification of the resultant seismic forces at the base. This step involves a thorough validation process according to established norms (RPA), ensuring that the reinforcement strategies meet the required safety standards. By linking the fundamental mode loading maximum capacity to the verification process, we can comprehensively evaluate the structural performance and confirm the adequacy of our reinforcement approaches

IV.3.6.1.2 Verification of the Resultant Seismic Forces at the Base

The following table verifies the resultant seismic forces at the base under fundamental mode loading for both minimal and calculated reinforcement types in the X and Y directions. It compares the base shear force under fundamental mode loading to the total seismic force calculated using the static equivalent method [**Paragraph IV.2.2.1.1**].

For this verification, the structural behavior coefficient (R) and the qualite factor (Q) were set to 1. This setting is based on the conservative approach to ensure the safety margin is adequate without any reduction or amplification factors.

Direction	Base Shear Force Fp (kN)	Total Seismic Force (kN)	Seismic Force Verification
Minimal Reinforcement			
X-axis	24,893.41	37,780.94	Not Verified
Y-axis	17,038.34	41,091.89	Not Verified
Calculated Reinforcement			
X-axis	44,239.19	37,799.24	Verified
Y-axis	35,164.32	41,095.08	Verified

Table 4.3: Verification of the Resultant Seismic Forces at the Base

The table indicates that the minimal reinforcements are insufficient to meet the seismic demands in both X and Y directions, failing the verification checks.

This is expected as minimal reinforcements typically provide a baseline level of structural capacity. In contrast, the calculated reinforcements successfully meet or exceed the required seismic forces, ensuring that the structure can withstand the seismic loads as per the Algerian seismic regulations.

To further understand the seismic performance, we now examine the performance points under fundamental mode loading for both cases.

IV.3.6.1.3 Performance point

As improved in FEMA-440, the **Coefficients Method** is preferred over the Capacity Spectrum and N2 Method for its simplicity and efficiency. Unlike the complex plotting and iteration required by the Capacity Spectrum Method or the detailed nonlinear analysis of the N2 Method, the Coefficient Method uses predefined coefficients to adjust response values, reducing computational effort and time. This makes it ideal for quick, routine assessments while ensuring reasonable accuracy. It aligns with design standards like FEMA-440 and adapts to different seismic hazard levels, providing a robust, practical, and accessible means of evaluating seismic performance.

In this section, we will present the results obtained using the Coefficient Method in both the X and Y directions.

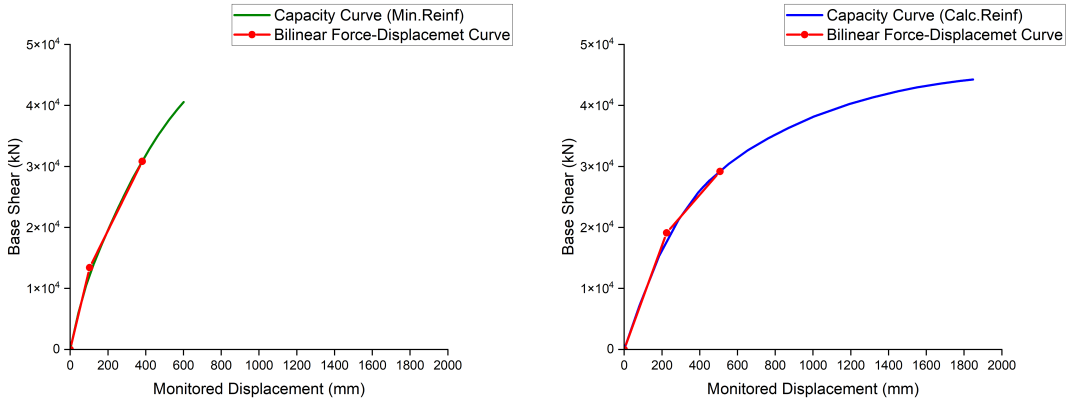

Figure 4.9: Performance points Under Fundamental Mode Loading in the X-Direction

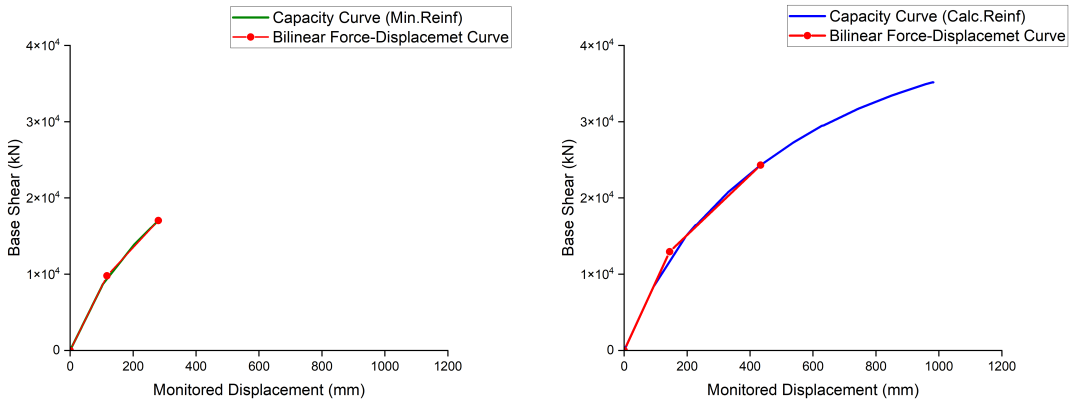

Figure 4.10: Performance points Under Fundamental Mode Loading in the Y-Direction

The calculated reinforcements show a higher capacity and performance point than the minimum required reinforcements. This indicates that the building, with calculated reinforcements, can handle more significant seismic forces and displacements. Similarly, in the Y direction, the calculated reinforcements surpass the minimum required reinforcements, showing that the calculated reinforcements offer better seismic performance.

To further quantify the additional strength provided by these reinforcements, we analyze the overstrength factors.

IV.3.6.1.4 Overstrength

The following table compares the overstrength of both minimal and calculated reinforcement types under Fundamental Mode loading conditions.

Direction	Maximum Capacity Under Fundamental Mode Loading (kN)	Performance Point (kN)	Overstrength
Minimal Reinforcement			
X-axis	30309.23	24981.41	1.22
Y-axis	17083.31	17083.31	1.0
Calculated Reinforcement			
X-axis	40219.18	27174.35	1.48
Y-axis	35154.17	24299.54	1.45

Table 4.4: Comparison of Reinforcement Types Overstregth Under Fundamental Mode Loading

The table shows that:

- The calculated reinforcements provide a significantly higher safety margin compared to the minimal reinforcements in both directions.
- In both reinforcement scenarios, the Y direction shows a lower overstrength than the X direction, suggesting that the structure is potentially more vulnerable in the Y direction under seismic loads.

These results are logical as the calculated reinforcement is designed to enhance the structure's capacity and ensure it can handle greater loads with a higher margin of safety.

IV.3.6.1.5 Maximum Story Drift

The maximum story drift results reveal the deformation patterns along the building height under fundamental mode loading for both minimal and calculated reinforcement. These patterns are crucial for identifying potential weak stories and necessary reinforcements.

The following figures illustrate the maximum story drift under fundamental mode loading in both the X and Y directions.

- **X Direction**

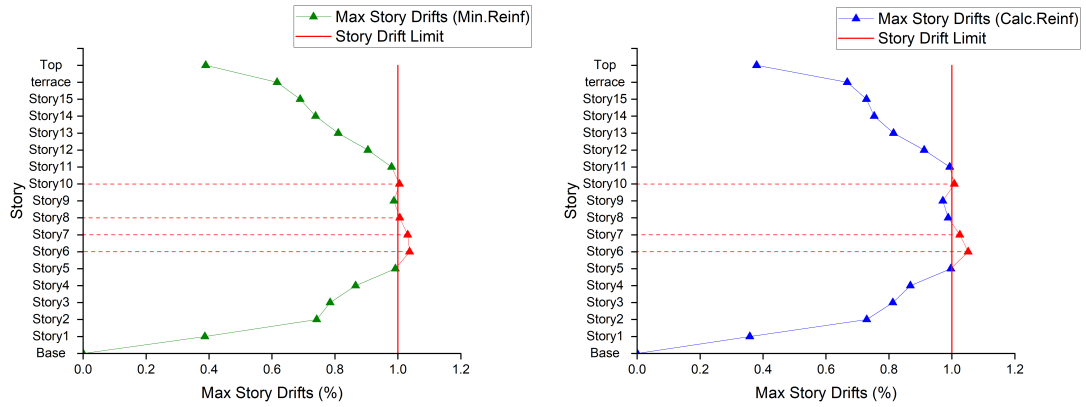

Figure 4.11: Maximum Story Drift Under Fundamental Mode Loading in the X-Direction

The graphs illustrate that both minimal and calculated reinforcement scenarios experience significant increases in story drifts within the X direction around the middle stories (Story 6 to Story 10), with several points exceeding the 1.0% drift limit. The calculated reinforcement shows some improvement over the minimal reinforcement, Given these observations, it is noteworthy that the calculated reinforcement brings the story drifts closer to the acceptable limit. Considering the precision limitations inherent in story drift assessment, the calculated reinforcement can be regarded as acceptable.

- **Y Direction**

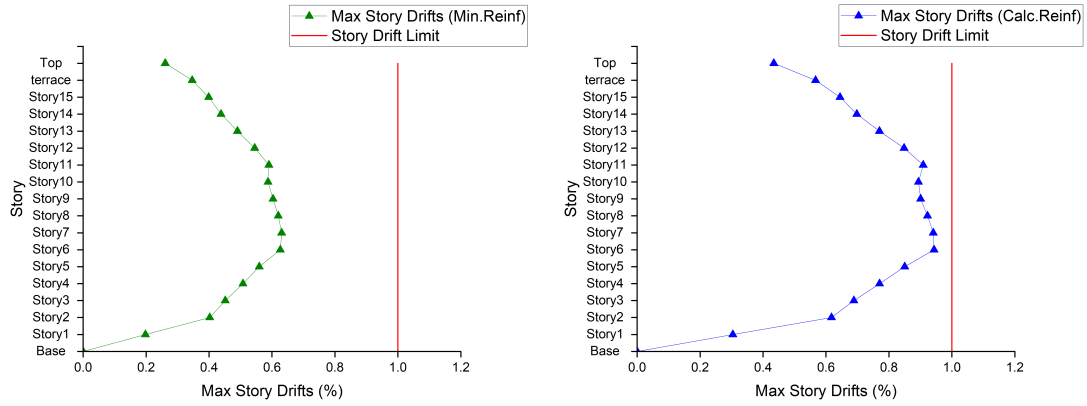

Figure 4.12: Maximum Story Drift Under Fundamental Mode Loading in the Y-Direction

The graphs of maximum story drifts in the Y direction for both minimal and calculated reinforcement scenarios indicate that the middle stories (Story 6 to Story 10) experience significant increases in drifts. However, these drifts remain below the 1.0% limit, indicating compliance with the RPA seismic regulations. Both reinforcement strategies effectively maintain the drifts within acceptable limits, ensuring the building's seismic performance meets the required standards.

The middle stories may experience larger drifts than the top or bottom stories. This is due to the structural dynamics where the flexibility and lateral displacement are often more pronounced in the middle sections of the building.

Now we turn our attention to the second loading scenario. To ensure a thorough evaluation, we will consider the capacity curves under uniform loading, which provides an alternative perspective on the building's structural response. This will help us understand how the structure behaves under a different lateral load distribution and assess the robustness of both reinforcement cases.

IV.3.6.2 Uniform Distribution

IV.3.6.2.1 Capacity curves

The capacity curves under uniform loading offer an alternative perspective on the structural response for both minimal and calculated reinforcement. This analysis helps in understanding the effects of a different lateral load distribution on the building's performance.

The following figures represent the capacity curves in both the X and Y directions.

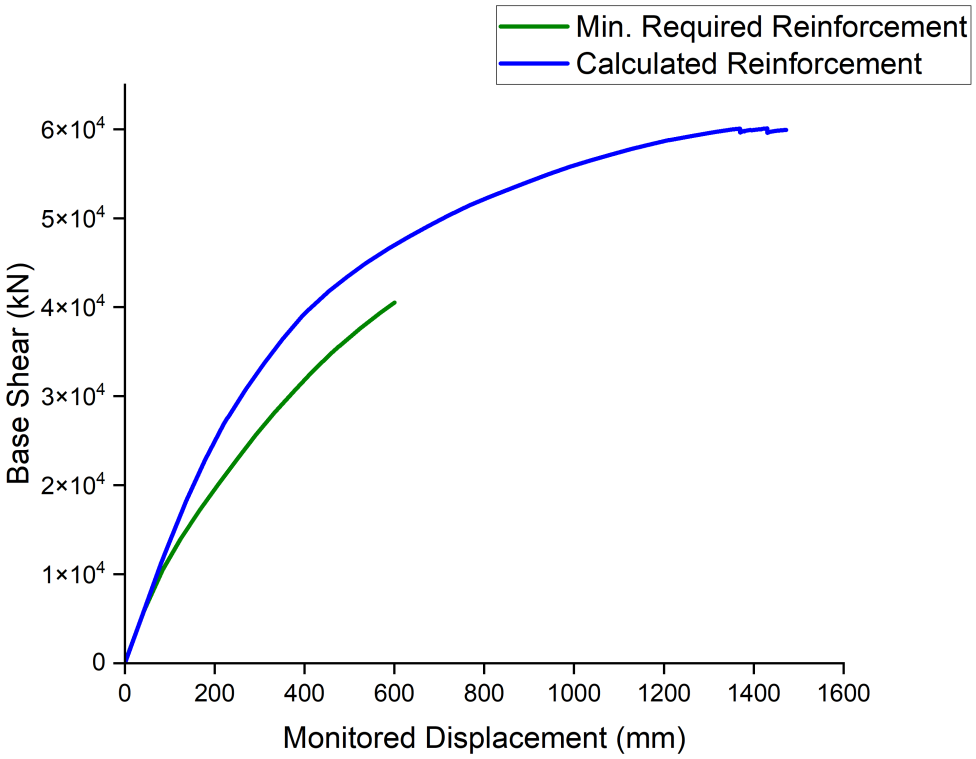

Figure 4.13: Capacity Curves Under Uniform Loading in the X-Direction

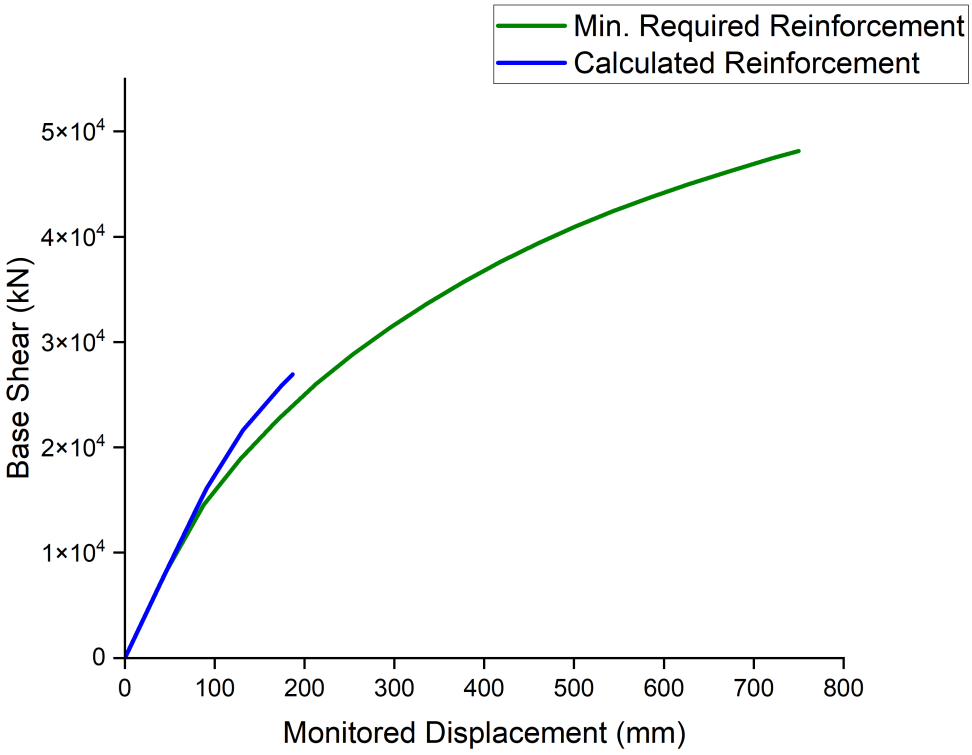

Figure 4.14: Capacity Curves Under Uniform Loading in the Y-Direction

Capacity curves in the X direction show that the calculated reinforcement significantly enhances the structural capacity under uniform loading compared to the minimum required reinforcement. This finding is consistent with the results obtained from fundamental mode loading, confirming the effectiveness of the calculated reinforcement in improving structural performance.

In contrast, the Y direction shows that the minimum required reinforcement capacity under uniform loading is far superior to the calculated reinforcement. This discrepancy is due to the pushover analysis failing in the Y direction of the calculated reinforcement model because of numerical instability.

IV.3.6.2.2 Verification of the Resultant Seismic Forces at the Base

The following table verifies the resultant seismic forces at the base under uniform loading for both minimal and calculated reinforcement types in the X and Y directions.

Direction	Base Shear Force Fp (kN)	Total Seismic Force (kN)	Seismic Force Verification
Minimal Reinforcement			
X-axis	30825.87	39135.14	Not Verified
Y-axis	32244.69	42224.75	Not Verified
Calculated Reinforcement			
X-axis	37300.78	39135.14	Verified
Y-axis	Not available	42224.75	Unknown

Table 4.5: Verification of the Resultant Seismic Forces at the Base

these results highlight that while calculated reinforcement significantly improves the structural capacity in the X direction to meet the seismic demands, the performance in the Y direction remains uncertain due to numerical instability. Conversely, minimal reinforcement fails to meet the required seismic forces in both directions.

Next, we will examine the performance points under uniform loading for both cases to complete the assessment.

IV.3.6.2.3 Performance point

In this section, we will present the results obtained using the Coefficient Method in both the X and Y directions.

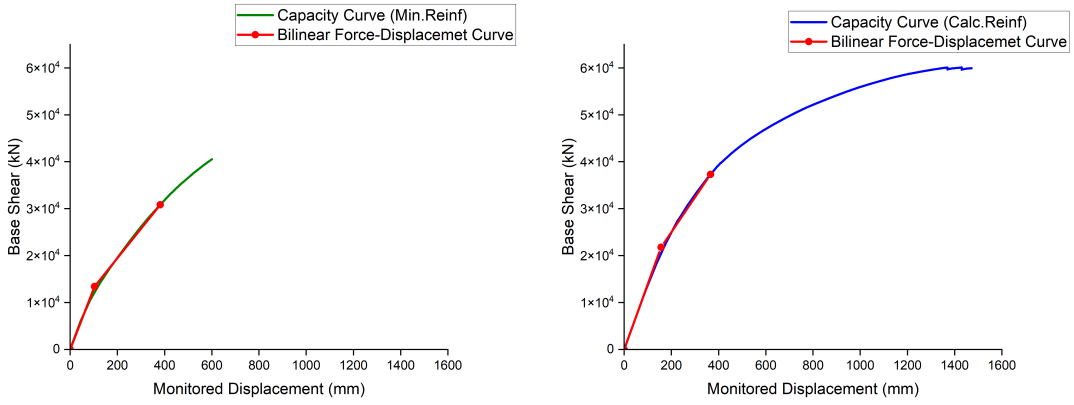

Figure 4.15: Performance points Under Uniform Loading in the X-Direction

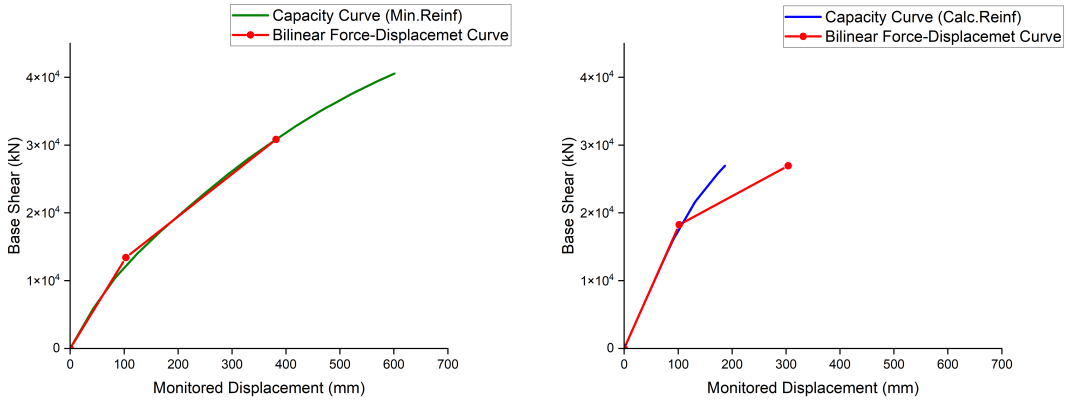

Figure 4.16: Performance point Under Uniform Loading in the Y-Direction of Minimal reinforcement

The comparison between minimal and calculated reinforcement in the X direction highlights the benefits of calculated reinforcement in enhancing seismic performance. While minimal reinforcement provides basic strength, calculated reinforcement offers significantly higher capacity and resilience, ensuring better protection against seismic forces. The performance points, represented by the peak of the red bilinear curves, clearly show the superior capacity and displacement tolerance of the structure with calculated reinforcement. This underscores the importance of using detailed, performance-based reinforcement design to achieve optimal seismic resilience.

The analysis in the Y direction with minimal reinforcement indicates that the structure has a good capacity to withstand uniform seismic loading. The comparison between the capacity curve and the bilinear force-displacement curve shows that the structure can endure significant base shear and displacement. This highlights that minimal reinforcement offers sufficient overstrength to meet seismic demands, ensuring the structure's safety and resilience under such loading conditions.

IV.3.6.2.4 Overstrength

The following table compares the overstrength of different reinforcement types under uniform loading conditions.

Direction	Maximum Capacity Under Uniform Loading (kN)	Performance Point (kN)	Overstrength
Minimal Reinforcement			
X-axis	40544.16	30825.87	1.32
Y-axis	48146.20	32244.69	1.49
Calculated Reinforcement			
X-axis	59914.62	37300.78	1.61
Y-axis	26942.74	Not available	Not available

Table 4.6: Comparison of Reinforcement Types Overstregth Under Uniform Loading

These results indicate that the calculated reinforcement substantially increases overstrength compared to minimal reinforcement in the X direction, enhancing the structural capacity under seismic loading. However, due to numerical instability in the Y direction for the calculated reinforcement, only the minimal reinforcement's performance is available, showing a higher overstrength compared to the X direction.

IV.3.6.2.5 Maximum Story Drift

he maximum story drifts under uniform loading further clarify the distribution of deformations along the building height for both minimal and calculated reinforcement. These results are crucial for validating the overall structural performance.

The following figures illustrate the maximum story drift under uniform loading in both the X and Y directions :

- **X Direction:**

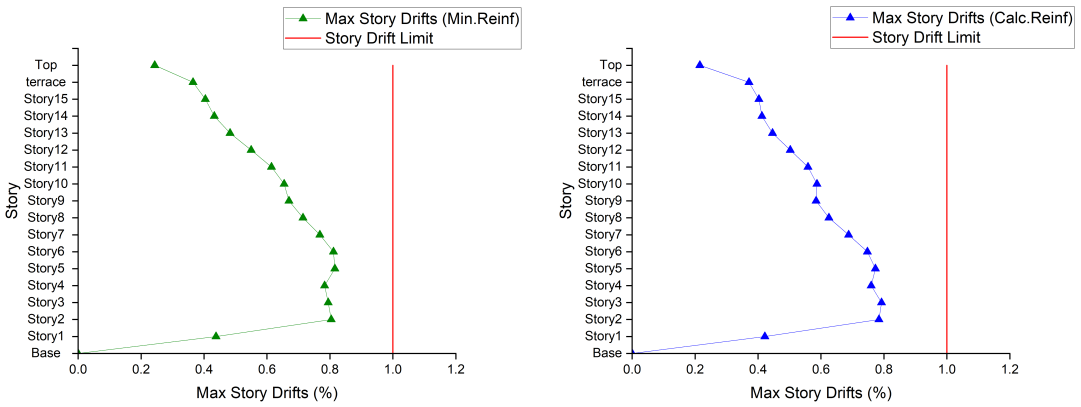

Figure 4.17: Maximum Story Drift Capacity Curve Under Uniform Loading in the X-Direction

These results suggest that both minimal and calculated reinforcements respect the 1% story drift limit, indicating that both reinforcement strategies are effective in maintaining structural integrity within acceptable limits. However, calculated reinforcement is more efficient in controlling story drifts under uniform loading, providing enhanced structural performance. Notably, the most affected stories by the drift are the lower ones (Stories 1-6) due to the uniform loading distribution.

- **Y Direction:**

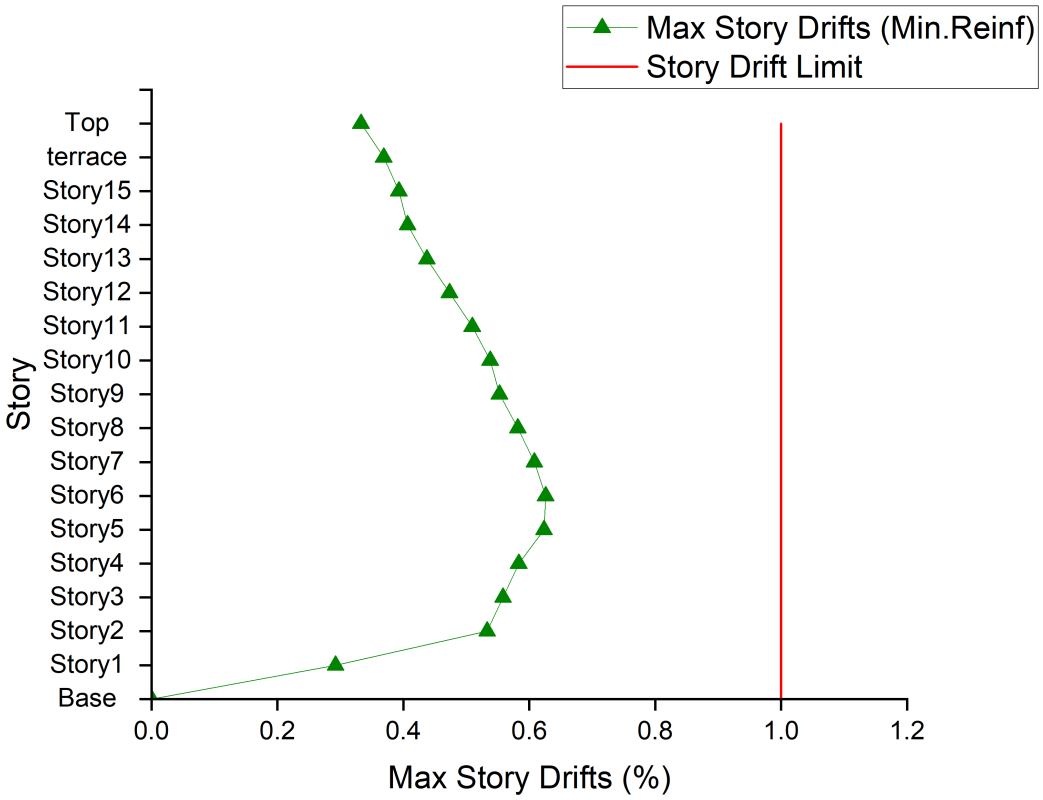

Figure 4.18: Maximum Story Drift Under Uniform Loading in the Y-Direction

All story drifts are within the 1% story drift limit, indicating that minimal reinforcement is effective in maintaining structural integrity within acceptable limits.

Again, the most affected stories by the drift are the lower ones (Stories 1-6), which is typical due to the uniform loading distribution. However, the absence of a performance point for calculated reinforcements in this direction prevents us from generating a comparative story drift graph for the calculated reinforcement. This limits our ability to fully evaluate and compare the effectiveness of the calculated reinforcement in the Y direction.

IV.3.6.3 Comparison of Base Shear and Target Displacement

The following table represents a comparison of base shear and taget displacement for minimal and calculated reinforcement under different loading conditions :

	Base Shear (kN)		**Target Displacement (mm)**	
Direction	**Minimal Reinforcement**	**Calculated Reinforcement**	**Minimal Reinforcement**	**Calculated Reinforcement**
Fundamental mode loading				
X-axis	2893.41	44239.19	527	507.495
Y-axis	17038.34	35164.32	280.15	433.349
Uniform loading				
X-axis	30825.87	37300.78	381.654	366.008
Y-axis	32244.69	Not available	311.037	Not available

Table 4.7: Comparison of Base Shear and Target Displacement for Minimal and Calculated Reinforcement

The comparison of base shear and target displacement values for minimal and calculated reinforcement highlights the following key points:

- **Increased Base Shear Capacity:** Calculated reinforcement significantly enhances the base shear capacity under both fundamental mode and uniform loading, indicating a stronger resistance to seismic forces.
- **Target Displacement:** The target displacement values vary with reinforcement scenarios. While calculated reinforcement generally improves structural stiffness (as seen with reduced displacements in some cases), it can also lead to increased flexibility in certain directions (e.g., Sens yy under fundamental mode loading).

An important observation is that minimal reinforcement results in less target displacement in the Y direction compared to the X direction. This is because the structure has reached collapse at a smaller base shear due to insufficient capacity in the Y direction, highlighting the structural vulnerabilities.

These results emphasize the importance of calculated reinforcement in improving structural performance and ensuring compliance with seismic regulations.

By comparing base shear and target displacement, we gain valuable insights into the structural behavior under different reinforcement strategies, guiding us toward optimal reinforcement designs for enhanced seismic resilience.

IV.4 Vulnerability Evaluation per EMS98:

Given that the minimal reinforcement does not yield satisfactory results, the assessment using the EMS98 method is neither necessary nor consistent. However, for the calculated reinforcement, an evaluation using EMS98 can be performed without issue. This approach allows for a more precise damage degree evaluation, which the RPA 2003 does not provide. The degradation curve is established using the target displacement as a reference, meaning the results will be provided for the most unfavorable scenario in terms of displacement. This scenario corresponds to Fundamental mode loading in the X direction **table 4.7**.

We created a Python script (check **appendices**) that takes the capacity curve, which is a function of displacement and base shear force, and transforms it into a function of spectral displacement and spectral acceleration using the formula:

$$Sa = \frac{\text{base shear force}}{(\text{ mass }).(\text{ gravity })}$$

The script also calculates a bilinear approximation using the SciPy library and then deduces the elastic limit and damage degrees per **Table 1.3**. It displays all the results in a single graph. represented by the following image :

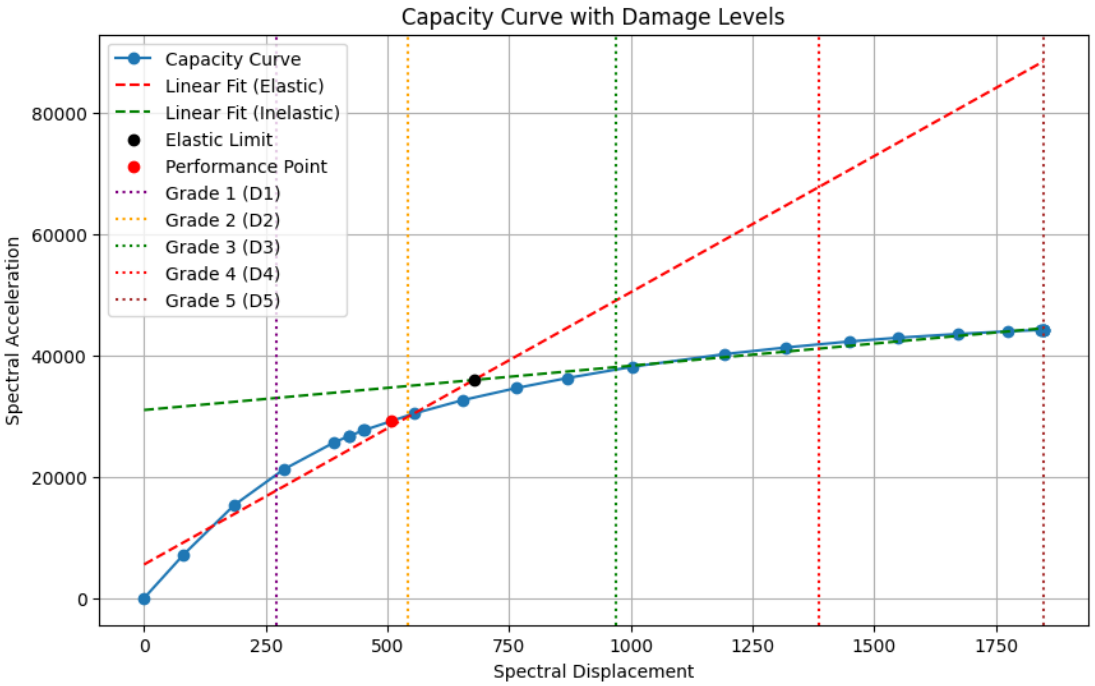

Figure 4.19: Capacity Curve with Damage Levels and Performance Analysis

The image shows that the damage degree is equal to 2 according to EMS98, which is a reasonable result considering the hypotheses adapted for our model. This result suggests that the structure, with the calculated reinforcement, can sustain moderate damage under the given seismic loading conditions, validating the effectiveness of the proposed reinforcement design in enhancing the seismic resilience of the structure.

IV.5 Conclusion

The pushover analysis was conducted on two reinforcement scenarios: minimal reinforcement, representing the most unfavorable case, and calculated reinforcement, representing the actual reinforcement in the tower. Due to the unavailability of the real reinforcement details, the reinforcement was calculated manually. The vulnerability of the tower was assessed using specific criteria from the Algerian parasismic code. The minimal reinforcement scenario did not meet these criteria, whereas the calculated reinforcement scenario did. However, the RPA does not provide further detailed criteria for assessment, necessitating the use of EMS98. Utilizing EMS98 allowed us to determine a damage degree of 2, which is considered a reasonable result given the framework of our study.

Greneral Conclusion

Greneral Conclusion

This project aimed to assess the seismic vulnerability of a reinforced concrete tower located in Zone III of Algiers using advanced analytical methods. The study combined ambient vibration experiments for dynamic characterization and detailed numerical analyses, adhering to the guidelines provided by the Algerian seismic regulation RPA99/2003.

Key Steps and Findings:

- **Ambient Vibration Analysis:** We started by conducting ambient vibration experiments to capture the tower's dynamic characteristics. The natural frequencies and vibration modes obtained from these experiments were crucial for calibrating our finite element model in ETABS.
- **Finite Element Model Calibration:** The initial finite element model was calibrated using the experimental results, ensuring that the numerical model accurately represented the tower's dynamic behavior. This step involved adjusting the model parameters to match the observed natural frequencies and mode shapes.
- **Elastic Linear Analysis:** An elastic linear analysis was performed to establish a baseline understanding of the structure's response to seismic loads. This analysis provided insights into the building's deformations, displacements, internal forces, frequencies, and natural vibration modes within the elastic range. Both minimal and calculated reinforcements passed the acceptance criteria set by the RPA during this stage.
- **Nonlinear Pushover Analysis:** The pushover analysis was conducted on two reinforcement scenarios: minimal reinforcement and calculated reinforcement. The minimal reinforcement scenario represented the most unfavorable case, while the calculated reinforcement scenario represented the real reinforcement in the tower, determined manually due to the lack of access to actual reinforcement details. The vulnerability of the tower was assessed using specific criteria from the Algerian parasismic code. The minimal reinforcement case did not pass these criteria, whereas the calculated reinforcement did.
- **EMS98 Evaluation:** Given that the RPA99 does not provide detailed dam-

age assessments, we extended our evaluation using the EMS98 method. The EMS98 evaluation determined the degree of damage as 2, a reasonable result considering the study's framework and hypotheses. This suggests that the structure, with the calculated reinforcement, can sustain moderate damage under seismic loading conditions.

The comprehensive vulnerability study confirms that the tower, with the calculated reinforcement, is adequately prepared to withstand seismic events, ensuring the safety and stability of its occupants. While the minimal reinforcement scenario highlighted potential vulnerabilities, the calculated reinforcement provided significant improvements in terms of capacity, story drift control, and overall resilience. This study underscores the importance of detailed, performance-based reinforcement design in achieving optimal seismic resilience.

The calibration of the numerical model is crucial to accurately represent the real behavior of the structure. Future studies should focus on enhancing the calibration process to ensure even greater accuracy in predicting structural responses.

The study highlights the need for enhancements to the RPA to include more detailed performance assessment criteria, similar to those in EMS98. This would allow for a more comprehensive evaluation of the structure's performance under seismic conditions, ensuring higher levels of safety and reliability.

By continuously improving our understanding of the structure's behavior under seismic loads and advocating for updates to seismic codes, we can ensure the highest levels of safety and reliability in earthquake-prone regions. This project sets a solid foundation for future seismic assessments and contributes valuable insights to the field of structural engineering.

Bibliography

[1] C. Michel, P. Guéguen, and P.Y. Bard. "Ambient Vibration Monitoring for Seismic Vulnerability Assessment of Structures." In: *Bulletin of Earthquake Engineering* 6.3 (2008), pp. 505–534.

[2] G. De Roeck, B. Peeters, and W.X. Ren. "Dynamic testing and monitoring of bridges in Belgium, an overview." In: *Proceedings of the Institution of Civil Engineers-Bridge Engineering* 11.4 (2000), pp. 223–230.

[3] B. Peeters and G. De Roeck. "One-year monitoring of the Z24-Bridge: environmental effects versus damage events." In: *Earthquake Engineering Structural Dynamics* 30.2 (2001), pp. 149–171.

[4] W.X. Ren, L. Zhang, and I.E. Harik. "Ambient vibration measurements of the Great Belt Bridge: Comparison of results." In: *Engineering Structures* 26.6 (2004), pp. 619–628.

[5] J.F. Clinton et al. "Seismic Instrumentation of Buildings (with Emphasis on Federal Buildings)." In: *U.S. Geological Survey Open-File Report* 2006-1216 (2006).

[6] M. Çelebi. "Recorded earthquake responses from the integrated seismic monitoring system of the Atwood Building, Anchorage, Alaska." In: *NISTIR* 5734 (1996).

[7] M. Çelebi and A. Sanli. "GPS in pioneering dynamic monitoring of long-period structures." In: *Earthquake Spectra* 18.1 (2002), pp. 47–61.

[8] T. Saito et al. "Dynamic properties of a historical Japanese pagoda: Field measurements and structural identification." In: *Engineering Structures* 30.1 (2008), pp. 16–28.

[9] M. Çelebi. "Seismic retrofit of buildings: case studies and guidelines." In: *NIST GCR* 6 (2006).

[10] Ali Mikael. "Évaluation des paramètres physiques des bâtiments: amortissement, fréquence et modes de comportement des structures de génie civil : approche expérimentale." NNT: 2011GRENU016. PhD thesis. Université de Grenoble, 2011.

[11] United Nations. *Risk Assessment*. New York, NY: United Nations Publications, 2002.

[12] G. Grünthal, ed. *European Macroseismic Scale 1998 (EMS-98)*. Luxembourg: Centre Européen de Géodynamique et de Séismologie, 1998.

[13] A. Kahil, B. Benmokrane, and M. Boulfiza. "État d'endommagement des structures en béton armé." In: *Revue canadienne de génie civil* 37.3 (2010), pp. 421–431. DOI: 10.1139/L10-003.

[14] P. Gulkan and M.A. Sozen. "Inelastic Responses of Reinforced Concrete Structures to Earthquake Motions." In: *American Concrete Institute Journal* 71.12 (1974), pp. 604–610.

[15] A.K. Chopra and R.K. Goel. "A modal pushover analysis procedure for estimating seismic demands for buildings." In: *Earthquake Engineering Structural Dynamics* 31.3 (2002), pp. 561–582.

[16] A. Gupta and S. Kunnath. "Adaptive Spectral Analysis (AMPA)." In: *Journal of Structural Engineering* 126.4 (2000), pp. 405–412.

[18] Applied Technology Council. *Seismic Evaluation and Retrofit of Concrete Buildings*. Redwood City, CA: ATC, 1996.

[19] Kenji Konno and Tatsuo Ohmachi. "Ground-motion characteristics estimated from spectral ratio between horizontal and vertical components of microtremor." In: *Bulletin of the Seismological Society of America* 88.1 (1998), pp. 228–241.

[20] Anil K. Chopra. *Dynamics of Structures: Theory and Applications to Earthquake Engineering*. 5th ed. Pearson, 2017.

[21] Anil K. Chopra. *Dynamics of Structures: Theory and Applications to Earthquake Engineering*. Upper Saddle River, NJ: Prentice Hall, 2001.

[22] Ministère de l'Habitat et de l'Urbanisme. *Règles Parasismiques Algériennes 1999*. Algiers, Algeria: Algerian Seismic Regulations, 2003.

[23] International Conference of Building Officials. *Uniform Building Code (UBC)*. Whittier, CA: ICBO, 1988.

[24] Clotaire Michel. "Vulnérabilité Sismique de l'échelle du bâtiment à celle de la ville : Apport des techniques expérimentales in situ. Application à Grenoble." Thèse de doctorat, Sciences de la Terre, de l'Univers et de l'Environnement. PhD thesis. Grenoble, France: Université Joseph Fourier - Grenoble I, 2007.

[25] R. A. Ibrahim. *Parametric Random Vibration*. New York: Elsevier, 1977. ISBN: 9780080305002.

[26] Federal Emergency Management Agency. *NEHRP Guidelines for the Seismic Rehabilitation of Buildings (FEMA 273)*. Washington, D.C.: FEMA, 1997.

[27] FEMA. *Evaluation of Earthquake Damaged Concrete and Masonry Wall Buildings: Basic Procedures Manual*. Federal Emergency Management Agency. 1998.

[29] Algerian Ministry of Housing and Urbanism. *DTR B.C 22: Algerian Regulations for Loads on Buildings*. Available from the Algerian Ministry of Housing and Urbanism. 2010.

[30] FEMA. *Prestandard and Commentary for the Seismic Rehabilitation of Buildings*. Federal Emergency Management Agency. 2000.

Webography

[17] Youcef Mehani, Aghiles Nekmouche, and Abdelmounaim Mechaala. *Contribution à l'introduction des méthodes capacitaires dans les futures versions du RPA. Programme d'étude, de recherche et prestations MHU/CGS Convention 2020.* Rapport de phase de projet, Centre National de Recherche Appliquée en Génie Parasismique (CGS). Projet N°1 / 2020, Phase 01: Recherche bibliographique, Simulations numériques avec les résultats préliminaires. Ministère de l'Habitat et de l'Urbanisme et de la Ville (DRC/SDR), Dec. 2021.

[28] Algerian Standards. *Standards NA 5023 and NA 5024 for Clay Bricks.* Available from Algerian Standardization Institute. 2010.

Appendices

Appendices

Geometric characteristics of the equivalent strut

The geometric characteristics of the equivalent strut for various stories and directions are summarized in the table below.

Story	Base - 3rd	Base - 3rd	4th - 8th	4th - 8th	9th - 13th	9th - 13th	14th	14th	15th	15th
story height (m)	4.42	4.42	4.08	4.08	4.08	4.08	4.08	4.08	4.08	4.08
beam height_OX (m)	0.6	0.6	0.6	0.6	0.6	0.6	0.4	0.4	0.4	0.4
beam height_OY (m)	0.8	0.8	0.8	0.8	0.8	0.8	0.8	0.8	0.4	0.4
h_column_OX (m)	4.42	4.42	4.08	4.08	4.08	4.08	4.18	4.18	4.08	4.08
h_column_OY (m)	4.42	4.42	4.08	4.08	4.08	4.08	4.08	4.08	4.28	4.28
h_infill_OX (m)	3.82	3.82	3.48	3.48	3.48	3.48	3.68	3.68	3.68	3.68
h_infill_OY (m)	3.62	3.62	3.28	3.28	3.28	3.28	3.28	3.28	3.68	3.68
column width (m)	1	1	0.8	0.8	0.6	0.6	0.4	0.4	0.4	0.4
bay length_OX (m)	4.5	4.35	4.5	4.35	4.5	4.35	4.5	4.35	4.5	4.35
bay length_OY (m)	4.85	7.4	4.85	7.4	4.85	7.4	4.85	7.4	4.85	7.4
l_infill_OX (m)	3.5	3.35	3.7	3.55	3.9	3.75	4.1	3.95	4.1	3.95
l_infill_OY (m)	3.85	6.4	4.05	6.6	4.25	6.8	4.45	7	4.45	7
Θ_OX (rad)	0.83	0.85	0.75	0.78	0.73	0.75	0.73	0.75	0.73	0.75
Θ_OY (rad)	0.75	0.51	0.68	0.46	0.66	0.45	0.64	0.44	0.69	0.48
L diagonal_OX (m)	5.18	5.08	5.08	4.97	5.23	5.12	5.51	5.40	5.51	5.40
L diagonal_OY (m)	5.28	7.35	5.21	7.37	5.37	7.55	5.53	7.73	5.77	7.91
thickness (m)	0.2	0.2	0.2	0.2	0.2	0.2	0.2	0.2	0.2	0.2
Inertia_column (m^4)	0.083333333	0.083333333	0.034133333	0.034133333	0.0108	0.0108	0.002133333	0.002133333	0.002133333	0.002133333
α_h_OX	1.58	1.58	1.86	1.86	2.48	2.48	3.76	3.77	3.67	3.68
α_h_OY	1.60	1.54	1.88	1.79	2.50	2.37	3.74	3.54	3.84	3.68
w_ds_OX (m)	0.76	0.74	0.69	0.68	0.64	0.62	0.57	0.56	0.57	0.56
w_ds_OY (m)	0.77	1.08	0.71	1.02	0.65	0.93	0.57	0.82	0.59	0.82

Table 4.8: geometric characteristics of the equivalent strut.

Data extracted from treating the Ambient Vibration signals

Tower 1	Story	Nom de fichier	f1	A1	ξ1(%)	f2	A2	ξ2(%)	f3	A3	ξ3(%)
Ministry Of Trade	Basement	120411_1324.009_N	0.723261	0.000114404	~ 7	2.72891	0.00025414	~ 9	4.06441	0.000280591	~ 4
		120411_1324.009_E	0.723261	0.000164532	~ 3	2.61075	0.000321847	~ 3	9.85054	0.000281745	~ 6
	1 st	120411_1255.008_N	0.723261	0.000410161	~ 1	2.28611	0.00075531	~ 1	4.06441	0.000962383	~ 1
		120411_1255.008_E	0.755994	0.000831935	~ 1	2.61075	0.00173908	~ 1	4.85165	0.00107938	~ 2
	3 rd	120411_1235.007_N	0.723261	0.00141246	~ 1	2.28611	0.00258665	~ 1	4.06441	0.00281347	~ 1
		120411_1235.007_E	0.755994	0.00239681	~ 1	2.61075	0.00452987	~ 1	4.85165	0.00249367	~ 1
	5 th	120411_1215.006_N	0.723261	0.00501234	~ 1	2.28611	0.00672348	~ 1	4.06441	0.00404843	~ 2
		120411_1215.006_E	0.755994	0.00712784	~ 1	2.61075	0.00773415	~ 1	4.85165	0.00234069	~ 2
	7 th	120411_1155.005_N	0.723261	0.009836	~ 1	2.28611	0.0113306	~ 1	6.05348	0.00150563	~ 2
		120411_1155.005_E	0.755994	0.0133228	~ 1	2.61075	0.0134042	~ 1	7.226	0.00122594	~ 2
	9 th	120411_1135.004_N	0.723261	0.0126008	~ 1	2.28611	0.00980361	~ 1	4.06441	0.00377872	~ 1
		120411_1135.004_E	0.755994	0.018099	~ 1	2.61075	0.0108538	~ 1	4.85165	0.00296946	~ 1
	11 th	120411_1113.003_N	0.723261	0.0137329	~ 1	2.38957	0.00248627	~ 1	4.06441	0.00451823	~ 1
		120411_1113.003_E	0.755994	0.0157923	~ 1	2.61075	0.00235018	~ 1	4.85165	0.0033419	~ 1
	13 th	120411_1051.002_N	0.723261	0.0197401	~ 1	2.28611	0.00552355	~ 1	4.06441	0.00144746	~ 2
		120411_1051.002_E	0.755994	0.0283514	~ 1	2.61075	0.00768855	~ 1	7.226	0.000810265	~ 2
	15 th	120411_1022.001_N	0.723261	0.0275576	~ 1	2.28611	0.013947	~ 1	4.06441	0.00521551	~ 1
		120411_1022.001_E	0.755994	0.0322315	~ 1	2.61075	0.0166656	~ 1	4.64159	0.00379666	~ 4
	Natural Frequencies of the Structure	Longitudinale	0.723261			2.28611			4.06441		
		Transversale	0.755994			2.61075			4.64159		

Figure 4.20: Data extracted from treating the Ambient Vibration signals.

Excel sheet developed to automatically identify the peaks and the natural frequency of any provided ambient vibration signals

h	0.03
T	0.93
Sampling	33.333
Sampling	31

1N

Serch rai	index	Peaks	Frequency	A/2	A/sqrt(2)
0	25	0.0276	0.7233	0.0137788	0.019486166
31	51	0.0139	2.2861	0.0069735	0.009862018
62	64	0.0052	4.0644	0.002607755	0.003687922

2N

Serch rai	index	Peaks	Frequency	A/2	A/sqrt(2)
0	25	0.0197	0.7233	0.00987005	0.013958359
31	51	0.0055	2.2861	0.002761775	0.00390574
62	64	0.0014	4.0644	0.00072373	0.001023509

3N

Serch rai	index	Peaks	Frequency	A/2	A/sqrt(2)
0	25	0.0137	0.7233	0.00686645	0.009710627
31	52	0.0025	2.3896	0.001243135	0.001758058
62	64	0.0045	4.0644	0.002259115	0.003194871

4N

Serch rai	index	Peaks	Frequency	A/2	A/sqrt(2)
0	25	0.0126	0.7233	0.0063004	0.008910111
31	51	0.0098	2.2861	0.004901805	0.006932199
62	64	0.0038	4.0644	0.00188936	0.002671959

5N

Serch rai	index	Peaks	Frequency	A/2	A/sqrt(2)
0	25	0.0098	0.7233	0.004918	0.006955102
31	51	0.0113	2.2861	0.0056653	0.008011944
62	73	0.0015	6.0535	0.000752815	0.001064641

6N

Serch rai	index	Peaks	Frequency	A/2	A/sqrt(2)
0	25	0.005	0.7233	0.00250617	0.00354426
31	51	0.0067	2.2861	0.00336174	0.004754218
62	64	0.004	4.0644	0.002024215	0.002862672

7N

Serch rai	index	Peaks	Frequency	A/2	A/sqrt(2)
0	25	0.0014	0.7233	0.00070623	0.00099876
31	51	0.0026	2.2861	0.001293325	0.001829038
62	64	0.0028	4.0644	0.001406735	0.001989424

8N

Serch rai	index	Peaks	Frequency	A/2	A/sqrt(2)
0	25	0.0004	0.7233	0.000205081	0.000290028
31	51	0.0008	2.2861	0.000377655	0.000534085
62	64	0.001	4.0644	0.000481192	0.000680508

9N

Serch rai	index	Peaks	Frequency	A/2	A/sqrt(2)
0	25	0.0001	0.7233	0.000057202	8.08958E-05
31	55	0.0003	2.7289	0.00012707	0.000179704
62	64	0.0003	4.0644	0.000140296	0.000198408

Figure 4.21: Extracted peaks and natural frequencies L direction.

h	0.03
T	#####
Samplin	33.333
Samplin	33.333

1E

Serch rai	index	Peaks	Frequency	A/2	A/sqrt(2)
0	26	0.0322	0.756	0.01611575	0.022791112
33.333	54.333	0.0167	2.6108	0.0083328	0.011784359
66.667	67.667	0.0038	4.6416	0.00189833	0.002684644

2E

Serch rai	index	Peaks	Frequency	A/2	A/sqrt(2)
0	26	0.0284	0.756	0.0141757	0.020047467
33.333	54.333	0.0077	2.6108	0.003844275	0.005436626
66.667	77.667	0.0008	7.226	0.000405133	0.000572944

3E

Serch rai	index	Peaks	Frequency	A/2	A/sqrt(2)
0	26	0.0158	0.756	0.00789615	0.011166842
33.333	54.333	0.0024	2.6108	0.00117509	0.001661828
66.667	68.667	0.0033	4.8517	0.00167095	0.00236308

4E

Serch rai	index	Peaks	Frequency	A/2	A/sqrt(2)
0	26	0.0181	0.756	0.0090495	0.012797926
33.333	54.333	0.0109	2.6108	0.0054269	0.007674796
66.667	68.667	0.003	4.8517	0.00148473	0.002099725

5E

Serch rai	index	Peaks	Frequency	A/2	A/sqrt(2)
0	26	0.0133	0.756	0.0066614	0.009420642
33.333	54.333	0.0134	2.6108	0.0067021	0.009478201
66.667	77.667	0.0012	7.226	0.00061297	0.00086687

6E

Serch rai	index	Peaks	Frequency	A/2	A/sqrt(2)
0	26	0.0071	0.756	0.00356392	0.005040144
33.333	54.333	0.0077	2.6108	0.003867075	0.00546887
66.667	68.667	0.0023	4.8517	0.001170345	0.001655118

7E

Serch rai	index	Peaks	Frequency	A/2	A/sqrt(2)
0	26	0.0024	0.756	0.001198405	0.001694801
33.333	54.333	0.0045	2.6108	0.002264935	0.003203102
66.667	68.667	0.0025	4.8517	0.001246835	0.001763291

8E

Serch rai	index	Peaks	Frequency	A/2	A/sqrt(2)
0	26	0.0008	0.756	0.000415968	0.000588267
33.333	54.333	0.0017	2.6108	0.00086954	0.001229715
66.667	68.667	0.0011	4.8517	0.00053969	0.000763237

9E

Serch rai	index	Peaks	Frequency	A/2	A/sqrt(2)
0	25	0.0002	0.7233	0.000082266	0.000116342
33.333	54.333	0.0003	2.6108	0.000160924	0.00022758
66.667	84.667	0.0003	9.8505	0.000140873	0.000199224

Figure 4.22: Extracted peaks and natural frequencies T direction.

Elements sections

Story	Ground floor	1	2	3	4	5	6	7	8	9	10	11	12	13	14	15	Terrace	Top
Story Height	4.42	4.42	4.42	4.42	4.08	4.08	4.08	4.08	4.08	4.08	4.08	4.08	4.08	4.08	4.08	4.08	4.08	3
Floor Thickness	20	20	20	20	15	15	15	15	15	15	15	15	15	15	15	15	15	15
Columns	100 x 100	100 x 100	100 x 100	100 x 100	100 x 100	80 x 80	80 x 80	80 x 80	80 x 80	80 x 80	60 x 60	60 x 60	60 x 60	60 x 60	60 x 60	40 x 40	40 x 40	40 x 40
Secondary Beams	60 x 60	60 x 80	60 x 80	60 x 80	60 x 80	50 x 80	50 x 80	50 x 80	50 x 80	50 x 80	40 x 80	40 x 80	40 x 80	40 x 80	40 x 80	40 x 80	40 x 80	40 x 80
Principal Beams	60 x 60	60 x 60	60 x 60	60 x 60	60 x 60	50 x 60	50 x 60	50 x 60	50 x 60	50 x 60	40 x 60	40 x 60	40 x 60	40 x 60	40 x 60	40 x 40	40 x 40	40 x 40
Shear Walls	170 x 40 (X direction) & 4x400 (Y direction)																	
Staires	20																	

Figure 4.23: Elements sections.

Seismic Vulnerability Assessment Script

The following Python script was developed to perform a comprehensive seismic vulnerability assessment of a reinforced concrete tower. The script includes the steps for calculating the mass, converting base shear to spectral acceleration, performing a bi-linear approximation, calculating damage levels according to the EMS-98 scale, and plotting the results.

```
import numpy as np
import pandas as pd
import matplotlib.pyplot as plt
from scipy import stats

# Constants
g = 9.81  # Acceleration due to gravity (m/s^2)
weight = 128946.6431  # Total weight of the structure (kN)

# Convert weight to mass (m = W / g)
mass = weight * 1000 / g  # Convert kN to N

# New provided data representing the capacity curve (Base Shear vs. Roof Displacement)
data = {
    'Displacement': [0, 81.237, 184.686, 286.61, 390.704, 422.172, 422.172, 451.185, 451.591, 553.976, 655.458, 763.878, 868.849, 1004.75, 1192.25, 1317.25, 1448.5, 1548.5, 1673.5, 1773.5, 1843.22, 1843.268, 1847.659, 1847.728, 1847.728, 1847.731],
    'Base_Shear': [0, 7184.9864, 15306.1162, 21210.861, 25680.8045, 26762.3876, 26739.5983, 27683.9996, 27672.9998, 30422.9849, 32660.2038, 34619.9531, 36277.9016, 38171.4985, 40230.0771, 41317.4985, 42309.7424, 42933.9715, 43561.391, 43986.1848, 44222.3832, 44222.6972, 44239.0538, 44239.1907, 44239.1903, 44239.1767]
}

# Convert to DataFrame
df = pd.DataFrame(data)

# Convert Base Shear to Spectral Acceleration (Sa)
```

```
df['Spectral_Acceleration'] = df['Base_Shear'] / (mass * g)

# New performance point coordinates (Roof Displacement, Base Shear)
performance_point = (507.495, 29174.5522)

# Convert Performance point to Spectral Acceleration and Spectral Displacement
performance_spectral_displacement = performance_point[0]
performance_spectral_acceleration = performance_point[1] / (mass * g)

def bi_linear_approximation(df):
    # Split data into two segments for linear fitting
    split_index = 12  # Assume the elastic limit is near this index for demonstration
    # Linear fit for the initial linear portion
    slope1, intercept1, _, _, _ = stats.linregress(df['Displacement'][:split_index], df['Base_Shear'][:split_index])
    # Linear fit for the inelastic portion
    slope2, intercept2, _, _, _ = stats.linregress(df['Displacement'][split_index:], df['Base_Shear'][split_index:])
    # Calculate intersection point (Elastic limit)
    intersection_x = (intercept2 - intercept1) / (slope1 - slope2)
    intersection_y = slope1 * intersection_x + intercept1
    return (slope1, intercept1, slope2, intercept2, intersection_x, intersection_y)

def calculate_damage_level(intersection_x, intersection_y, performance_spectral_displacement, ultimate_displacement):
    Sdy = intersection_x
    Sdu = ultimate_displacement
    Sd_d1 = 0.4 * Sdy
    Sd_d2 = 0.8 * Sdy
    Sd_d3 = Sdy + 0.25 * (Sdu - Sdy)
    Sd_d4 = 0.75 * Sdu
    Sd_d5 = Sdu
    Sd_performance = performance_spectral_displacement
    if Sd_performance <= Sd_d1:
        damage_degree = 'D1'
    elif Sd_performance <= Sd_d2:
        damage_degree = 'D2'
    elif Sd_performance <= Sd_d3:
        damage_degree = 'D3'
    elif Sd_performance <= Sd_d4:
        damage_degree = 'D4'
    else:
        damage_degree = 'D5'
    return damage_degree, Sd_d1, Sd_d2, Sd_d3, Sd_d4, Sd_d5

def plot_capacity_curve_with_damage_levels(df, slopes_intercepts, performance_spectral_displacement, Sd_d1, Sd_d2, Sd_d3, Sd_d4, Sd_d5):
    slope1, intercept1, slope2, intercept2, intersection_x, intersection_y = slopes_intercepts
    # Plot the capacity curve and the bi-linear approximation
    plt.figure(figsize=(10, 6))
```

```
    plt.plot(df['Displacement'], df['Base_Shear'], label='Capacity Curve', marker='o')
    plt.plot(df['Displacement'], slope1 * df['Displacement'] + intercept1, 'r--', label='Linear Fit (Elastic)')
    plt.plot(df['Displacement'], slope2 * df['Displacement'] + intercept2, 'g--', label='Linear Fit (Inelastic)')
    plt.scatter([intersection_x], [intersection_y], color='blue', zorder=5)
    plt.text(intersection_x, intersection_y, f'Elastic Limit\n({intersection_x:.2f}, {intersection_y:.2f})', fontsize=12, ha='right')
    plt.scatter([performance_spectral_displacement], [performance_spectral_acceleration * mass * g], color='black', zorder=5)
    plt.text(performance_spectral_displacement, performance_spectral_acceleration * mass * g, f'Performance Point\n({performance_spectral_displacement}, {performance_spectral_acceleration * mass * g})', fontsize=12, ha='left')

    # Adding EMS-98 Damage Grades
    plt.axvline(x=Sd_d1, color='purple', linestyle=':', label='Grade 1 (D1)')
    plt.axvline(x=Sd_d2, color='orange', linestyle=':', label='Grade 2 (D2)')
    plt.axvline(x=Sd_d3, color='green', linestyle=':', label='Grade 3 (D3)')
    plt.axvline(x=Sd_d4, color='red', linestyle=':', label='Grade 4 (D4)')
    plt.axvline(x=Sd_d5, color='brown', linestyle=':', label='Grade 5 (D5)')
    plt.xlabel('Spectral Displacement')
    plt.ylabel('Spectral Acceleration')
    plt.title('Capacity Curve with Damage Levels')
    plt.legend()
    plt.grid(True)
    plt.show()

# Perform bi-linear approximation
slopes_intercepts = bi_linear_approximation(df)

# Assume ultimate displacement (Sdu) is the maximum displacement from the data
ultimate_displacement = max(df['Displacement'])

# Calculate damage levels
damage_degree, Sd_d1, Sd_d2, Sd_d3, Sd_d4, Sd_d5 = calculate_damage_level(slopes_intercepts[4], slopes_intercepts[5], performance_spectral_displacement, ultimate_displacement)

# Plot and display the results
plot_capacity_curve_with_damage_levels(df, slopes_intercepts, performance_spectral_displacement, Sd_d1, Sd_d2, Sd_d3, Sd_d4, Sd_d5)

```

```
# Print the damage degree
print(f"Damage Degree: {damage_degree}")
```

API Script

This C script uses the ETABS API to automate the process of creating a brace (strut) with predetermined coordinates. It includes functions to attach to a running instance of ETABS or start a new instance, open an existing model, create points and frames, set moment releases, and save the model.

```
using System;
using System.Windows.Forms;

namespace WindowsFormsApplication1
{
    public partial class Form1 : Form
    {
        public Form1()
        {
            InitializeComponent();
        }

        private void button1_Click(object sender, EventArgs e)
        {
            // Set flags for attaching to an instance and specifying the path
            bool AttachToInstance = false;
            bool SpecifyPath = false;

            // Specify the path to the ETABS executable if needed
            string ProgramPath = "C:\\Program Files\\Computers and Structures\\ETABS 21\\ETABS.exe";

            // Full path to the model
            string ModelPath = "C:\\Users\\Ayoub\\Desktop\\Model\\test.edb";

            // Dimension the ETABS Object as cOAPI type
            ETABSv1.cOAPI myETABSObject = null;

            // Use ret to check if functions return successfully (ret = 0) or fail (ret = nonzero)
            int ret = 0;

            if (AttachToInstance)
            {
                // Attach to a running instance of ETABS
                try
                {
                    // Get the active ETABS object
```

```
37                  myETABSObject = (ETABSv1.cOAPI)System.Runtime.
    InteropServices.Marshal.GetActiveObject("CSI.ETABS.API.ETABSObject
    ");
38              }
39              catch (Exception ex)
40              {
41                  MessageBox.Show("No running instance of the
    program found or failed to attach.");
42                  return;
43              }
44          }
45          else
46          {
47              // Create API helper object
48              ETABSv1.cHelper myHelper;
49              try
50              {
51                  myHelper = new ETABSv1.Helper();
52              }
53              catch (Exception ex)
54              {
55                  MessageBox.Show("Cannot create an instance of the
     Helper object");
56                  return;
57              }
58
59              if (SpecifyPath)
60              {
61                  // Create an instance of the ETABS object from
    the specified path
62                  try
63                  {
64                      myETABSObject = myHelper.CreateObject(
    ProgramPath);
65                  }
66                  catch (Exception ex)
67                  {
68                      MessageBox.Show("Cannot start a new instance
    of the program from " + ProgramPath);
69                      return;
70                  }
71              }
72              else
73              {
74                  // Create an instance of the ETABS object from
    the latest installed ETABS
75                  try
76                  {
77                      myETABSObject = myHelper.CreateObjectProgID("
    CSI.ETABS.API.ETABSObject");
78                  }
79                  catch (Exception ex)
80                  {
81                      MessageBox.Show("Cannot start a new instance
    of the program.");
```

```
                        return;
                    }
                }
                // Start ETABS application
                ret = myETABSObject.ApplicationStart();
            }

            // Get a reference to cSapModel to access all API classes and functions
            ETABSv1.cSapModel mySapModel = default(ETABSv1.cSapModel);
            mySapModel = myETABSObject.SapModel;

            // Open the existing model
            ret = mySapModel.File.OpenFile(ModelPath);
            if (ret != 0)
            {
                MessageBox.Show("Failed to open the model file.");
                return;
            }

            // Set units to meters
            ret = mySapModel.SetPresentUnits(ETABSv1.eUnits.kN_m_C);
            if (ret != 0)
            {
                MessageBox.Show("Failed to set units to kN, meters, Celsius.");
                return;
            }

            // Define the brace using coordinates
            string FrameName = "";
            double x1 = 0.0, y1 = 0.0, z1 = 0.0; // Coordinates for (A,1,Base)
            double x2 = 0.0, y2 = 4.0, z2 = 3.5; // Coordinates for (A,2,Story1)

            // Create the points if they do not exist
            string Point1 = "", Point2 = "";
            ret = mySapModel.PointObj.AddCartesian(x1, y1, z1, ref Point1);
            if (ret != 0)
            {
                MessageBox.Show("Failed to create the start point.");
                return;
            }

            ret = mySapModel.PointObj.AddCartesian(x2, y2, z2, ref Point2);
            if (ret != 0)
            {
                MessageBox.Show("Failed to create the end point.");
                return;
            }

```

```
            // Add frame object between unique points
            ret = mySapModel.FrameObj.AddByPoint(Point1, Point2, ref
    FrameName, "Strut OY_Base-3rd_S", "Bracing");
            if (ret != 0)
            {
                MessageBox.Show("Failed to add the frame object
    between points.");
                return;
            }

            // Set moment releases (pinned)
            bool[] iEndReleases = new bool[6] { true, true, true,
    true, true, true };
            bool[] jEndReleases = new bool[6] { true, true, true,
    true, true, true };
            double[] iEndValues = new double[6] { 0, 0, 0, 0, 0, 0 };
            double[] jEndValues = new double[6] { 0, 0, 0, 0, 0, 0 };
            ret = mySapModel.FrameObj.SetReleases(FrameName, ref
    iEndReleases, ref jEndReleases, ref iEndValues, ref jEndValues,
    ETABSv1.eItemType.Objects);
            if (ret != 0)
            {
                MessageBox.Show("Failed to set releases for the frame
     object.");
                return;
            }

            // Save the model
            ret = mySapModel.File.Save(ModelPath);
            if (ret != 0)
            {
                MessageBox.Show("Failed to save the model file.");
                return;
            }

            MessageBox.Show("API script completed successfully.");

            // Clean up variables
            mySapModel = null;
            myETABSObject = null;
        }
    }
}
```

Listing IV.1: C# Code for Modifying ETABS Model